Aus der Abteilung für Klinische Pharmakologie

Direktor: Prof. Dr. med. S. Endres

Medizinische Klinik und Poliklinik IV

Klinikum der Universität

Ludwig-Maximilians-Universität München

Direktor: Prof. Dr. med. M. Reincke

Myeloid-derived suppressor cells (MDSC) in murine pancreatic cancer: Role of IRF4 in development and function of MDSC in RIG-I-like helicase-based immunotherapy

Dissertation

zum Erwerb des Doctor of Philosophy (Ph.D.)

an der Medizinischen Fakultät der

Ludwig-Maximilians-Universität zu München

vorgelegt von

Philipp Metzger

aus Dahn

2019

Mit Genehmigung der Medizinischen Fakultät

der Universität München

1. Berichterstatter:	Prof. Dr. med. Max Schnurr
2. Berichterstatterin:	Prof. Dr. med. Marion Subklewe
Mitberichterstatter:	Prof. Dr. rer. nat. Wolfgang Zimmermann
	Prof. Dr. med. Stefan Böck
Mitbetreuung durch die promovierten Mitarbeiter:	PD Dr. rer. biol. hum. Peter Düwell
Dekan:	Prof. Dr. med. dent. Reinhard Hickel
Tag der mündlichen Prüfung:	27.06.2019

Meinen Eltern

Table of Content

1. Introduction

1.1 Pancreatic ductal adenocarcinoma (PDAC)

1.1.1 Clinical and pathological aspects of PDAC

The pancreas is a central organ in the digestive system with an exocrine function that comprises secretion of digestive enzymes and an endocrine function that controls the blood sugar level. Most neoplasms in the pancreas develop from ductal or acinar cells of the exocrine part and are called pancreatic ductal adenocarcinoma (PDAC). In the Western world, PDAC is the fourth-leading cause of cancer-associated death and the five year survival rate is only eight percent [1]. The global burden of PDAC is expected to increase in the next decade and it is estimated that PDAC will be the second-leading cause of cancer death in 2030 [2]. Recent modeling confirmed this estimation for Germany [3]. One reason for the poor prognosis is the late time of diagnosis, when most of the primary tumors (> 80%) have already metastasized regionally or distantly [4]. Patients with distant metastasis have the worst prognosis with a five-year survival rate of three percent [1] and a median survival of 3-4 months [5].

Smoking, excessive alcohol consumption, overweight and chronic pancreatitis are known risk factors for PDAC [6, 7]. A small proportion of pancreatic cancer patients have elevated inherited risk due to a germline mutation of the DNA damage repair components Breast Cancer 1, early-onset (BRCA1) and BRCA2 [8]. Under inflammatory or stress conditions, acinar cells of the exocrine pancreas transdifferentiate into ductal-like cells and acquire progenitor-like characteristics in a process called acinar-to-ductal metaplasia (ACM). Those highly plastic cells are prone to develop into tumors if they acquire additional oncogenic hits. Over 90% of PDAC patients acquire activating mutations in the proto-oncogene *KRAS*. Furthermore, the *KRAS* locus is frequently amplified, which was recently associated with early tumor development and metastasis [9]. In addition to the activation of the proto-oncogene *KRAS*, several tumor suppressors including *TP53*, cyclin dependent kinase inhibitor 2A *(CDKN2A)* and MAD-Homolog 4 (*SMAD4)* are frequently inactivated in patients with pancreatic cancer.

Several whole genome and transcriptome sequencing approaches have defined four distinct subgroups of pancreatic cancer: 1) squamous subtype, 2) aberrantly differentiated endocrine/exocrine (ADEX) subtype, 3) pancreatic progenitor subtype, and 4) immunogenic subtype [10-12]. Recent studies confirmed this classification and

defined histological markers such as keratin 81 (*KRT81*) and hepatocyte nuclear factor 1A (*HNF1A*) for routine classification of patients with pancreatic cancer [13].

1.1.2 Tumor microenvironment of PDAC

The tumor microenvironment of PDAC is characterized by dense infiltration of various non-neoplastic cells including pancreatic stellate cells (PSC), cancer-associated fibroblasts (CAF) and immune cells. Already early in tumorigenesis, there is a close cross-talk between transformed pancreatic cells and surrounding bystander cells. During inflammation, PSC are pathologically activated and produce large amounts of extracellular matrix (ECM) deposits [14]. Recent data suggest that focal adhesion kinase 1 (*FAK1*) activity of early transformed neoplastic cells mediates the stromal-rich microenvironment and FAK1 inhibition leads to stromal remodeling [15]. High stromal content is described to be one driver of therapy resistance. Stromal matrix stiffness reduces drug delivery and stromal cells have been described to increase the pro-inflammatory cytokine milieu [16] .

Other key components of the tumor microenvironment in PDAC are immune cells such as macrophages, monocytes and granulocytes. Macrophages are polarized into a M2 pro-tumoral and pro-angiogenic state. Tumor-associated M2 macrophages (TAM) suppress T cell responses against tumor cells and increase the tumor-initiating capability of pancreatic tumor cells by activating tumor intrinsic signal transducer and activator of transcription 3 (*STAT3*) signaling. Furthermore, high macrophage and low $CD8^+$ T cell infiltration as well as high STAT3 phosphorylation correlates with a poor prognosis in patients with pancreatic cancer [17]. Monocytes and granulocytes are frequently enriched and exhibit immunosuppressive functions. The pathological activation of those cells changes their function. Therefore, such monocytes are called monocytic myeloid-derived suppressor cells (M-MDSC) and granulocytes are called polymorphonuclear MDSC (PMN-MDSC) [18]. Tumor-derived CC-chemokine ligand 2 (CCL2) and CXC-chemokine ligand 1 (CXCL1) recruit M-MDSC and PMN-MDSC into the tumor microenvironment, respectively [19]. In mouse studies, it has been shown that individual CXCL1-secreting tumor cells are capable of recruiting PMN-MDSC and thereby creating an immunosuppressive microenvironment which is characterized by low T cell infiltration and impaired T cell function [20]. In mouse models, antibody-mediated depletion of PMN-MDSC increased the frequency of intratumoral T cell and induced tumor cell apoptosis [21].

1.1.3 Current therapy of PDAC

In contrast to other tumor entities, the survival of patients suffering from PDAC has not been considerably improved over the last decades. The standard treatment for resectable PDAC is surgery followed by chemotherapy. Patients with locally advanced or metastasized PDAC are treated with chemotherapy or in some cases with radiochemotherapy [22]. New, very aggressive poly-chemotherapy regimens such as folinic acid, 5-FU, irinotecan plus oxaliplatin (FOLFIRINOX) or gemcitabine plus nab-paclitaxel have been recently introduced and have changed the first-line treatment options. However, both chemotherapies improved the overall survival of PDAC patients by a few months only and the harsh treatment is frequently associated with dose-limiting toxicity [23, 24]. The FOLFIRINOX treatment can only be offered to patients with an excellent performance status [23]. All trials testing targeted therapy modalities including multikinase inhibitors and anti-angiogenic treatment strategies did not show major clinical benefit [25, 26]. Only the treatment with epidermal growth factor receptor (EGFR) inhibitor showed minor clinical improvement, which lead to the approval for patients with metastatic PDAC [27].

1.1.4. Immunotherapeutic approaches in PDAC

During the last decade, immunotherapy revolutionized the treatment of many tumor types. Several approaches that showed clinical benefit in other cancer types have been tested in clinical trials for pancreatic cancer. However, no immunotherapy has been approved for PDAC so far. The causes for the failure in clinical trials are believed to be low frequency of neo-antigens due to low mutational burden and the strong immune suppression in the tumor microenvironment. Patients with better neo-antigen quality and high frequency of $CD8^+$ T cells have prolonged survival [28, 29]. Immune checkpoint inhibitors such as anti-cytotoxic T-lymphocyte-associated protein 4 (CTLA4) and anti-programmed cell death protein 1 (PD-1) antibodies have shown efficacy in melanoma [30], non-small cell lung cancer [31] and head and neck cancer [32] and other solid tumors. However, monotherapeutic approaches did not show any benefit in the majority of PDAC patients [33, 34]. In melanoma, high T cell infiltration and T cell activation prior to therapy correlate with better treatment response to checkpoint blockade. Other prognostic factors are currently on the horizon [35]. In contrast to melanoma, PDAC is poorly infiltrated by T cells [36]. A very small group (approximately 2%) of pancreatic cancer patients with microsatellite instability (MSI) has shown responses to anti-PD-1 treatment [37]. In 2017, anti-PD-1 therapy was approved by the American Food and Drug Administration (FDA) for MSI^{high} cancer patients, including patients with PDAC [38].

Patients with instable microsatellites have a higher neo-antigen load and it is believed that this is the reason why MSI^{high} tumors have a higher chance to respond to checkpoint blockade [39, 40].

To induce tumor antigen-specific T cells, several cancer vaccination strategies using recombinant peptides [41], whole cell lysates [42] or vector-based vaccines [43] have been tested in clinical trials. Several trials demonstrated a considerable induction of immune responses against the vaccinated antigens. However, no significant improvement in survival was convincingly demonstrated to date. Another strategy to improve anti-tumor immunity is the treatment with a CD40 agonistic antibody, which activates dendritic cells (DC) and polarizes macrophages in an anti-tumoral M1 state [44]. Clinical trials testing CD40 agonist in combination with chemotherapy and checkpoint blockade are currently ongoing [45]. Studies from our group in preclinical models of pancreatic cancer showed that ligands for cytosolic RNA sensors, called retinoic acid-inducible gene I (RIG-I)-like helicases (RLH), induce an immunogenic form of tumor cell death and improve antigen uptake and presentation by DC [46, 47]. RIG-I ligands are currently tested in clinical phase I-II studies for therapy of solid tumors (https://clinicaltrials.gov/ct2/results?term=RGT100). Oncolytic viruses that most likely activate similar immune mechanisms are also currently tested in clinical trials [48].

As described above, one key hurdle in the treatment of pancreatic cancer is the immunosuppressive, stroma-rich microenvironment. In pre-clinical models of PDAC, the recruitment of suppressive PMN-MDSC or M-MDSC was reduced by blockade of CXCL2 or CCL2 respectively [49]. Initial phase I trials showed promising results for CCL2 blockade in combination with chemotherapy [50, 51]. One key component of the stroma is hyaluronic acid. Treatment with hyaluronidase, an enzyme degrading hyaluronic acid, in combination with chemotherapy showed clinical benefit in a phase II trial [52]. However, two groups using different strategies to deplete the tumor stroma in mouse models of PDAC questioned the pro-tumoral role of the stroma recently [53, 54].

1.1.5 Mouse models of PDAC

To study pancreatic cancer in mice, several mouse models have been established. Mice have been genetically engineered by introducing genetic alterations, which are frequently found in human PDAC. For example, in the classical KPC model, mutated $Kras^{G12D}$ and mutated $P53^{R172H}$ are introduced specifically in pancreatic precursor cells using the Cre-lox system. KPC mice spontaneously develop multiple neoplasms specifically in the pancreas. Tumors from KPC mice resemble the stroma-rich histology

of human PDAC and KPC mice have a short median survival of approximately five months [55]. Many other genetically engineered mouse models (GEMM) with pancreas-specific tumor drivers have been established. In addition, tumor cells from GEMM have been isolated and cell lines have been generated. Cell lines can be implanted subcutaneously or orthotopically in the pancreas of C57BL/6 mice. A frequently studied syngenic mouse model is the Panc02 model. The Panc02 cell line has been generated by applying the cancerogen 3-methylcholanthrene (3-MCA) to the pancreas of wild-type mice. Previous work from our group showed that the orthotopically transplanted KPC-derived cell line T110299, which is used in this study, reflects more closely the histology of primary tumors in the KPC mouse and also of human PDAC, as compared to the Panc02 model [56].

1.2 Myeloid-derived suppressor cells (MDSC)

1.2.1 Origin and nomenclature of MDSC

During the past 15 years, there is increasing evidence that myeloid cells acquire suppressive capacity during cancerogenesis and are functionally different compared to myeloid cells in healthy controls. In 2007, Gabrilovich et al. introduced the term myeloid-derived suppressor cells (MDSC) to harmonize the research area [57]. Increased frequency of myeloid cells in the tumor microenvironment is associated with poor prognosis across most cancer types. [58]. A recent meta-analysis showed that a high neutrophil-to-lymphocyte ratio is a poor prognostic factor for patients with pancreatic cancer [59].

MDSC develop from myeloid precursors in the bone marrow. Under physiological conditions, myeloid cells differentiate from hematopoietic stem cells (HSC) via the common myeloid precursor (CMP) and the granulocyte macrophage precursor (GMP) to the terminally differentiated effector cells. The tumor alters the myelopoiesis and induces the differentiation of MDSC (Fig. 1)[60]. Two subtypes have been identified in both mouse and humans [61]. On the one hand, there are polymorphonuclear MDSC (PMN-MDSC), which develop from granulocyte precursor cells. Formerly, PMN-MDSC have been called granulocytic MDSC (G-MDSC). However, due to fact that these cells have a very low number of granules, this term is misleading and the term PMN-MDSC describes them better. Nevertheless, the terms PMN-MDSC and G-MDSC are interchangeable [18]. On the other hand, there are monocytic MDSC (M-MDSC), which derive from monocytic precursors. PMN-MDSC are terminally differentiated, whereas M-MDSC have the capability to differentiate into macrophages or PMN-MDSC [61].

The tumor induces a chronic, systemic, mild inflammation by secreting two classes of factors that manipulate the myelopoiesis and lead to the development of MDSC. Firstly, the tumor secretes factors such as GM-CSF, G-CSF and IL-6 which induce the expansion of the myeloid compartment and the accelerated release of myeloid cells from the bone marrow into the periphery (Fig. 1). Secondly, factors such as interferon (IFN) γ, tumor necrosis factor (TNF), interleukin (IL)-1β and IL-6 are released and induce a pathological activation of myeloid cells [62].

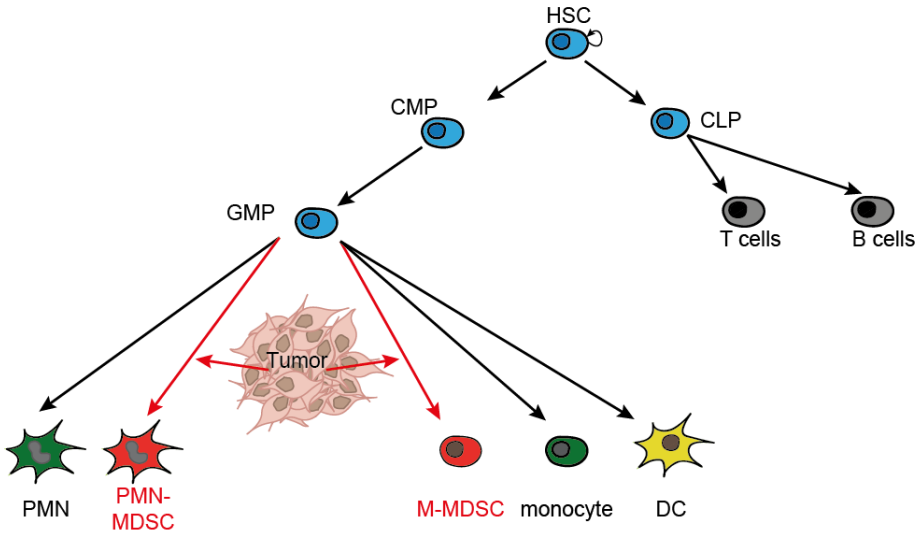

Figure 1: Origin of myeloid-derived suppressor cells (MDSC)

Myeloid cells develop from the hematopoietic stem cells (HSC) via the common myeloid progenitor (CMP) to the granulocyte macrophage progenitor (GMP). Under physiological conditions GMP differentiate into granulocytes (PMN), monocytes or dendritic cells (DC). In case of a tumor, the myelopoiesis is altered and PMN-MDSC and M-MDSC develop from GMP. Adapted from Gabrilovich (2017) [60]

Recently, lectin-type oxidized LDL receptor-1 (LOX1) has been identified as a marker to distinguish PMN-MDSC from granulocytes in humans [63]. However, in mice *Lox1* is not associated with PMN-MDSC. To date, no marker has been identified to distinguish murine PMN-MDSC from granulocytes and M-MDSC from monocytes. Bronte et al. defined a three-step classification to define MDSC: Firstly, the myeloid compartment has to be expanded. Secondly, both PMN-MDSC and M-MDSC have to express the cell defining surface markers (assessed by flow cytometry). Thirdly, suppressive activity has to be demonstrated [18].

1.2.2 Function of MDSC

The suppressive mechanisms of MDSC are influenced by tumor and host-derived factors and differ between tumor types as well as individuals. One important mechanism is the depletion of the essential amino acids arginine and tryptophan by arginase 1 (ARG1) and indoleamine 2,3-dioxygenase 1 (IDO1), respectively. Amino acid deprivation induces T cell proliferation arrest and apoptosis [64]. Furthermore, MDSC secrete immunosuppressive cytokines, such as transforming growth factor (TGF)-β and IL-10, which lead to the induction of regulatory T cells, M2 polarization of macrophages and inhibition of NK cells [65]. MDSC express inducible nitric oxide synthases (iNOS) and nicotinamide adenine dinucleotide phosphate oxidase (NOX), which catalyze the generation of reactive oxygen species (ROS) and nitrogen species (NOS). ROS and NOS nitrosylate the T cell receptor leading to proliferation arrest and T cell dysfunction [66]. Furthermore, MDSC secrete chemokines that attract other immunosuppressive cells [61] and express surface molecules such as PD-L1 that suppress T cells in a contact dependent manner [67] (Fig. 2).

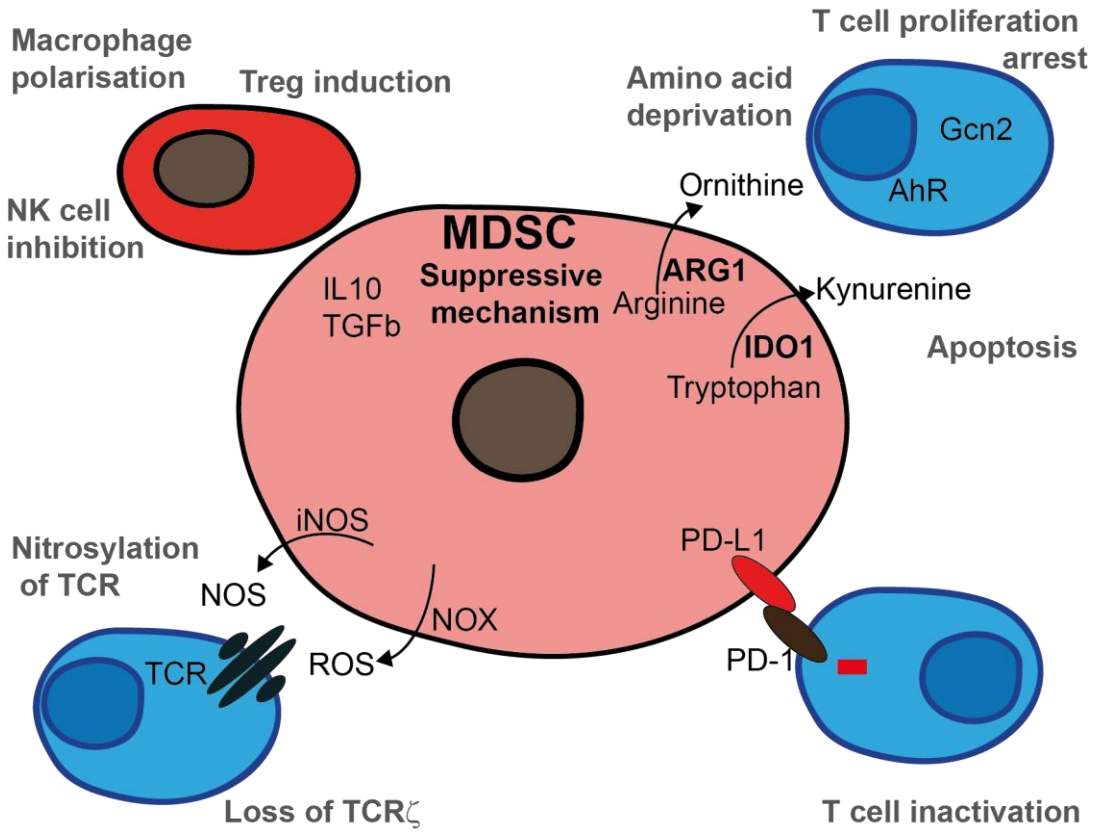

Figure 2: Suppressive mechanisms of MDSC
MDSC suppress immune responses via distinct mechanisms: Firstly, enzymes such as arginase 1 (ARG-1) and indoleamine 2,3-dioxygenase 1 (IDO-1) degrade essential amino acids. Secondly, suppressive cytokines such as IL-10 or TGF-β remodel immune cells. Thirdly, reactive oxygen and nitrogen species (ROS and NOS) are produced inducing T cell dysfunction. Fourthly, immunological checkpoints such as PD-L1 are expressed, binding to T cells via PD-1 and thereby inhibition T cell function. Adapted from de Haas et al. (2016) [68].

1.3 RIG-I-like helicases (RLH)

1.3.1 Physiological role of RLH

Under physiological conditions, the cytoplasm of healthy cells contains only modified RNA (e.g. 5'-capped mRNA). Upon virus infection, unmodified viral RNA is present in the cytoplasm and this RNA is sensed by RNA binding proteins including retinoic acid-inducible gene I (RIG-I) and melanoma differentiation-associated antigen 5 (MDA5). RIG-I and MDA5 are members of the RIG-I-like helicases (RLH) family. MDA5 recognizes long double-stranded RNA molecules and RIG-I recognizes the 5'-triphosphate moiety of unmodified viral RNA [69, 70]. Both receptors signal via mitochondrial antiviral-signaling protein (MAVS) and induce a type I IFN response and pro-inflammatory cytokine secretion. Thereby, virus-infected cells induce in an auto- and paracrine manner antiviral programs including immune activation and induction of antigen presentation. Depending on the viral load, RLH signaling is also capable of inducing cell death via caspase activation [71] (Fig. 3).

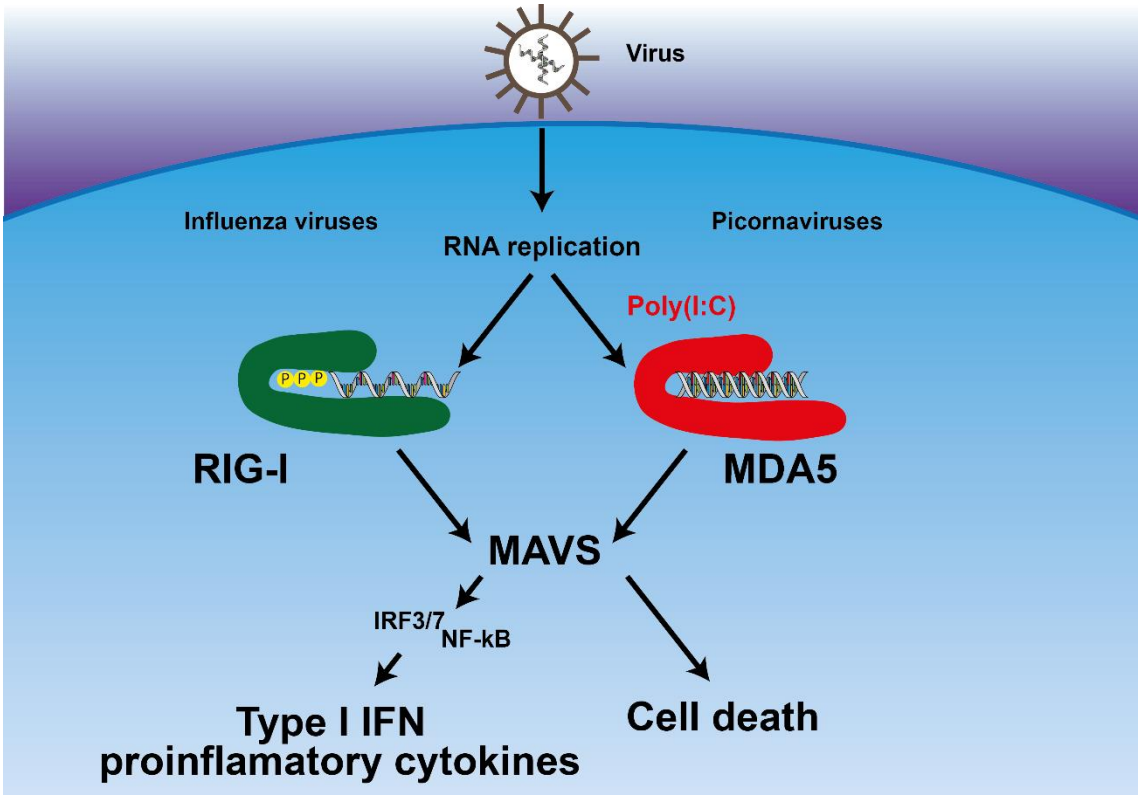

Figure 3: RIG-I-like helicase signaling
Viral RNA is sensed by RIG-I through the 5'-triphosphate moiety or by MDA5 due to the double stranded nature of the RNA. Both receptors signal via the mitochondrial adaptor protein MAVS, which leads to type I IFN and pro-inflammatory cytokine production, as well as cell death induction.

1.3.2 RLH-based tumor immunotherapy

The helicases MDA5 and RIG-I can be activated by synthetic RNA ligands such as polyinosinic:polycytidylic acid (poly(I:C)) and *in vitro* transcribed 5'-triphosphate RNA (ppp-RNA), respectively. Both, poly(I:C) and ppp-RNA can form complexes with polyethylenimine (PEI), which ensures intracellular delivery via transfection. Treatment of pancreatic cancer cells with poly(I:C) or ppp-RNA induces immunogenic cell death and secretion of pro-inflammatory cytokines [46]. *In vivo*, treatment with RLH ligands activates the immune system, induces a systemic type I IFN response and increases survival of mice with pancreatic cancer [47, 72].

1.3.3 Role of type I IFN in cancer

Type I IFN such as IFN-α and IFN-β play dichotomous roles in cancer. They are produced and sensed by tumor cells as well as non-tumor cells via the type I IFN receptor (IFNAR) [73]. On the one hand, type I IFN induce MHC class I expression on the surface of tumor cells and enhance their antigen presentation [74]. On the other hand, type I IFN has been described to facilitate metastasis and induce stem cell properties in tumor cells [75]. In addition, type I IFN increases the expression of immunosuppressive markers such as PD-L1 [76]. In immune cells, acute type I IFN has many beneficial functions by increasing antigen-presentation of DC and by activating natural killer (NK) cells as well as cytotoxic T cells [73]. However, during chronic type I IFN stimulation, suppressive mechanisms are induced [77]. There is increasing evidence that, in addition to PD-L1, the expression of PD-1 on MDSC is induced under inflammatory conditions [78, 79].

1.4 Interferon regulatory factor 4 (IRF4)

1.4.1 Family of IFN regulatory factors (IRF)

IRF4 is one of nine members of the IFN regulatory factors (IRF) family. All IRF proteins share a conserved N-terminal DNA binding domain that recognizes IFN-stimulated response elements (ISRE) and thereby regulate transcription. The C-terminal region varies between the different members. Initially, IRF proteins have been described to regulate IFN signaling. In the past decade, more and more functions of IRF proteins in immune system processes have been discovered, making IRF proteins important regulators of immune cell differentiation and function. In addition, IRF protein functions have been linked to oncogenesis and metabolism. In general, IRF proteins are key regulators of the pattern recognition receptor (PRR) signaling and the induction of pro-

inflammatory cytokines. In contrast to all other IRF proteins, IRF4 is a negative regulator of toll-like receptor (TLR)-induced cytokine induction [80].

IRF5 mediates pro-inflammatory cytokine induction upon TLR activation by binding to myeloid differentiation primary response 88 (MyD88) and activates *Irf4* transcription. IRF4 competes for the same MyD88 binding site as IRF5, but does not induce pro-inflammatory cytokines und thereby limits the inflammatory response [81].

The binding affinity of IRF4 alone to DNA is low. The recruitment to the DNA binding site relies on its interaction with other transcription factors including PU.1 and PR domain zinc finger protein 1 (BLIMP1, encoded by the *Prdm1* gene) which influence the binding affinity to IRSE or AP1 elements [82]. Thereby, the different complexes regulate the development and function of lymphoid as well as myeloid cells.

1.4.2 Role of IRF4 in lymphoid cells

IRF4 and IRF8 share redundant functions in the early development of B cells. IRF4 is crucial during later stages of B cell maturation. IRF4 regulates the isotype switching during the plasma cell differentiation by transcriptional induction of activation-induced cytidine deaminase (*Aid*) and *Blimp1* [83, 84]. Therefore, IRF4-deficient mice have physiological numbers of mature B cells, however, the concentration of high affinity immunoglobulin G (IgG) antibodies is dramatically reduced [80].

T cells play a central role in adaptive immunity. $CD4^+$ T helper cell subsets regulate B cell and macrophage function, whereas $CD8^+$ T cells kill infected or transformed target cells. IRF4 plays a pivotal role in T cells. Under physiological, uninfected conditions, T cell frequency is not altered in IRF4-deficient mice and IRF4 is dispensable for early T cell development. However, IRF4 is induced upon T cell receptor (TCR) engagement and is an essential transcriptional regulator of the induction of cytolytic activity [85], metabolic reprograming [86] as well as the induction of activation-induced expansion of $CD8^+$ T cells [87, 88]. IRF4-deficient mice are more susceptible to virus infections [88] and to infections by intracellular pathogens [85] due to the lack of functional $CD8^+$ T cells as well as B cells.

$CD4^+$ T helper (Th) cells differentiate into different subsets such as Th1, Th2, Th9, Th17 cells depending on the cytokine milieu during antigen-specific stimulation [89]. IL-4 differentiates naïve T cells (Th0) to Th2 cells by inducing IRF4 expression, which cooperates with NFAT transcription factors in inducing the GATA3-dependent Th2

differentiation program [90]. Therefore, IRF4-deficient $CD4^+$ T cells fail to differentiate into functional Th2 cells [91]. Moreover, IRF4 is involved in the differentiation of Th9 by regulating the expression of IL-9 [92]. Furthermore, IRF4 is pivotal for the differentiation of naïve $CD4^+$ T cell into Th17 cells [93]. Under Th17 polarizing conditions, IRF4 is phosphorylated and subsequently regulates the transcription of RAR-related orphan receptor (RORγt), the Th17 fate-defining transcription factor [94]. IRF4-deficient mice are resistant to the Th17-mediated disease experimental autoimmune encephalomyelitis (EAE) [95]. In addition, IRF4 controls effector function of regulatory T cells (Treg) by regulating IL-10 expression [96] (Fig. 4).

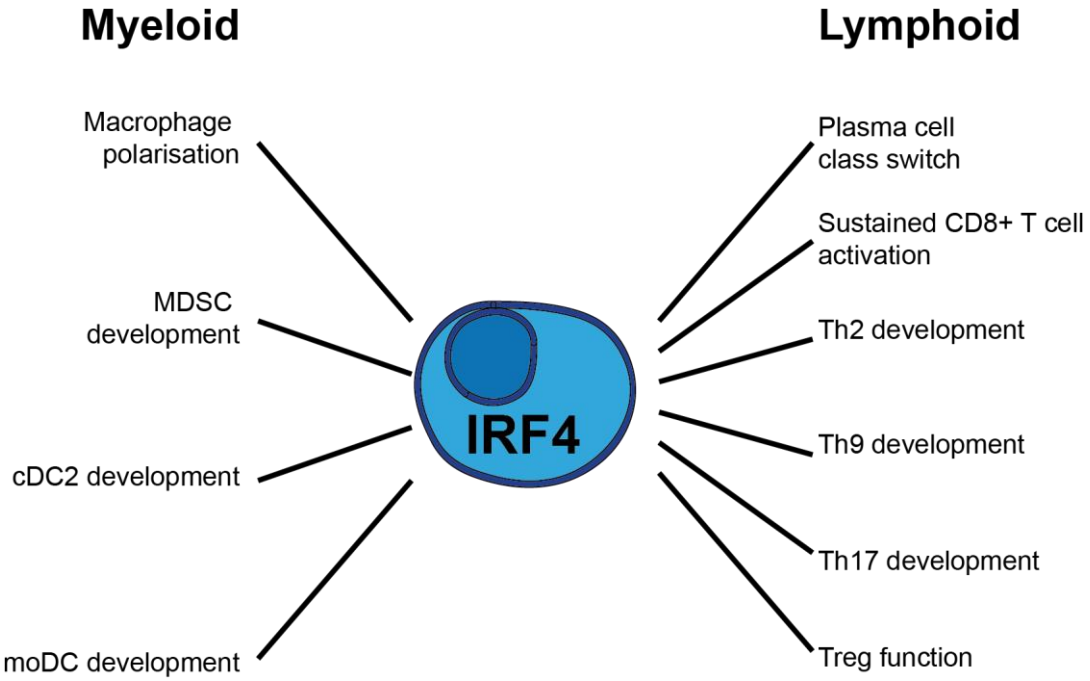

Figure 4: IRF4 function in immune cell subsets
IRF4 is expressed by myeloid and lymphoid immune cells. IRF4 regulates M2 macrophage polarization, MDSC development, cDC2 development and moDC development. IRF4 is the key transcription factor for the class switch of plasma cells, for effective $CD8^+$ T cell function, Th2, Th9 and Th17 development, as well as Treg function.

1.4.3 Role of IRF4 in myeloid cells

Myeloid cells consist of monocytes, macrophages, granulocytes and DC and derive from the hematopoietic stem cells and the common myeloid progenitor cells (CMP). IRF4 and IRF8 share structural and functional characteristics and are described to play a critical role in myelopoiesis. Initially, it has been described that both, IRF8 and to a lesser extent IRF4, are expressed in granulocyte-macrophage progenitors (GMP), common myeloid progenitor (CMP), macrophages, granulocytes and DC. IRF4-deficient mice have only a minor change in the frequency of myeloid cells, whereas the number of granulocytes is

dramatically increased, and the frequency of macrophages is reduced in IRF8-deficient mice [97]. Recent data challenge the expression of IRF4 in myeloid progenitor cells [98].

There are four main groups of dendritic cells (DC): monocyte-derived DC (moDC), plasmacytoid DC (pDC), conventional type1 DC (cDC1) and conventional type2 DC (cDC2) [99]. cDC1 represent a migratory cross-presenting subtype which is essential for effective anti-tumoral T cell response. The role of cDC2 in cancer is still unclear. cDC2 take up antigens in the tumor microenvironment and migrate to the draining lymph node, however, cDC2 are dispensable for the induction of T cell responses [100]. In the development of conventional DC, IRF4 and IRF8 play opposing roles. IRF4 is one of the linage-defining transcription factors in the differentiation of cDC2. However, it is dispensable for cDC1 differentiation. In contrast, IRF8 is pivotal for the differentiation of cDC1 [99]. IRF4-deficient mice have dramatically reduced numbers of cDC2 in lung and spleen whereas cDC1 are unaffected [101]. Recently, it has been shown, that differentiation of $Ly6C^+$ monocytes to moDC, which are capable of cross-presenting antigens, requires IRF4 [102].

Macrophages can be polarized into a classically activated pro-inflammatory M1 or an alternatively activated anti-inflammatory M2 state. IL-4 and IL-13 induce M2 macrophage polarization by activation of the epigenetic regulator jumonji domain containing protein D3 (JMJD3). JMJD3 removes inhibitory methyl marks on histone H3 Lys 27 (H3K27) of the *Irf4* promoter region and thereby facilitates IRF4 expression. Subsequently, expression of suppressive proteins such as ARG1 is transcriptionally regulated by IRF4. JMJD3-deficient mice fail to mount a M2 immune response against helminths [103]. Tumor-associated macrophages are M2 polarized with immune suppressive and vascular remodeling potential.

The role of IRF4 in granulocytes is still unclear. Ectopic expression or induction by IL-4 or by the drug simvastatin blocked the differentiation of granulocytes *in vitro* [104]. The expression of IRF4 is gradually down-regulated in PMN-MDSC in a model of 4T1 breast cancer, accompanied by an induction of ARG1 and an increase in suppressive capacity [104] (Fig 4).

1.5 Objective

PDAC is characterized by potent resistance mechanisms against conventional tumor therapies, such as chemotherapy, targeted therapy and radiation therapy. Despite intensive research, survival of patients suffering of PDAC has barely improved over the last decades. In several tumor entities immunotherapy has shown efficacy and is on the verge to become standard of care. However, in PDAC a potent immunosuppressive microenvironment is found with expansion of myeloid cells such as MDSC, opposing effective immune responses. A profound understanding of the regulation and function of MDSC in pancreatic cancer may help to develop novel immune-mediated treatment strategies for PDAC.

This study aims at improving the understanding of the role of the myeloid cell compartment in pancreatic cancer in murine PDAC. The specific objectives are:

1) To characterize the immune cell composition and specifically MDSC recruitment in a KPC-derived PDAC model
2) To investigate functional properties of MDSC as targets of RLH-based immunotherapy of PDAC
3) To characterize the role of IRF4 in MDSC differentiation and function in PDAC

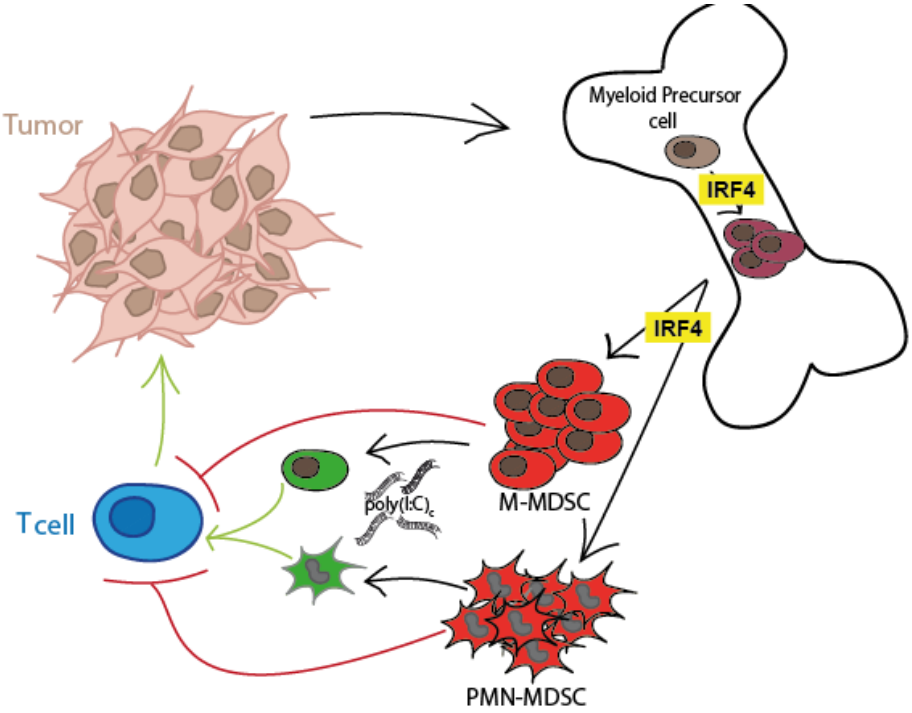

Figure 5: Working model
Tumor-derived factors alter the development of myeloid cells by inducing immune suppressive cells such as MDSC. In this study the impact of MDA5-targeting immunotherapy on MDSC and the role of IRF4 in MDSC in development and function was analyzed.

2. Material and methods

2.1 Material

2.1.1 Technical equipment

Name	Company
Bioanalyzer 2100	Agilent, USA
Cell culture CO_2 incubator (BD 6220)	Heraeus, Germany
Cell culture Laminar Flow	Thermo Scientific, Germany
Centrifuge (Multifuge 3L-R)	Thermo Scientific, Germany
Centrifuge (5424 and 5415R)	Eppendorf, Germany
ChemiDoc™ Imaging Systems	Bio-Rad, Germany
Multi plate reader (Mithras LB940)	Berthold Technologies, Germany
FACSCanto II	BD Bioscience, Germany
FACS Fortessa	BD Bioscience, Germany
Gel electrophoresis system	peqlab, Germany
gentleMACS Dissociator	Miltenyi Biotec
NextSeq 500 Sequencer	Illmuina, USA
LightCycler® 480 II	Roche, Germany
Microscope Axiovert25 and Axiovert200M	Zeiss, Germany
NanoDrop® 2000c	Thermo Scientific, Germany
pH meter	WTW, Germany
Thermocycler T3	Biometra, Germany

2.1.2 Chemicals and reagents

Name	Company
7-Aminoactinomycin D	Sigma-Aldrich, USA
3,3-Diaminobenzidine (DAB)	Dako, US
Bovine serum albumin	Roth, Germany
Chloroform	Roth, Germany
DC Protein Assay (Bradford)	Bio-Rad, Germany
Dimethyl sulfoxide	Roth, Germany
Dulbecco’s PBS	Lonza, Belgium
Ethanol	Sigma-Aldrich, Germany
Ethylenediaminetetraacetic acid (EDTA)	Sigma-Aldrich, Germany
Elisa Substrate Reagent A/B	BD Pharmingen, USA
Fixable viability Dye (FVD)	life technologies, Germany
Geneticin (G418)	ThermoFisher, Germany
Heparin-Natrium Braun	Rathiopharm, Germany
Isopropanol	Applichem, Germany
KAPA PROBE FAST Universal qPCR Master Mix	peqlab, Germany
Lipofectamine	life technologies, Germany
Lipofectamine RNAiMax	life technologies, Germany
Novagen Genejuice® transfection	Merck, Germany

Pharmlyse	BD Bioscience, Germany
Phenol-chlorofrom isoamyl alcohol	Sigma-Aldrich, Germany
Primer-probe mix, 10x conc.	Roche, Germany
Propidium iodide	Sigma-Aldrich, Germany
Sodium azide (NaN_3)	Sigma-Aldrich, Germany
Sulfuric acid (H_2SO_4, 2N)	Pharmacy, LMU Munich, Germany
TMB Substrate Reagent Set	BD Bioscience, Germany
Trypan blue	Sigma-Aldrich, Germany
Trypsin-EDTA(10x)	PAA, Austria
Tween® 20	Roth, Germany

2.1.3 Antibodies

The following antibodies were used for flow cytometry:

Specificity	Fluoro-chrome	Species/isotype	Clone	Concen-tration	Company
CD3	APC	hamster/IgG_1	145-2C11	1:100	BD Bioscience
CD3	PB	rat/IgG_{2b}	17A2	1:200	BioLegend
CD4	PB	rat/IgG_{2a}	RM4-5	1:200	BioLegend
CD4	FITC	rat/IgG_{2a}	RM4-5	1:200	BioLegend
CD4	PE-Cy7	rat/IgG_{2a}	RM4-5	1:200	BioLegend
CD4	PerCP	rat/IgG_{2a}	RM4-5	1:200	BioLegend
CD8a	APC-Cy7	rat/IgG_{2a}	53-6.7	1:200	BioLegend
CD8a	PB	rat/IgG_{2a}	53-6.7	1:200	BioLegend
CD8a	PerCP	rat/IgG_{2a}	53-6.7	1:200	BioLegend
CD8a	BV786	rat/IgG_{2a}	53-6.7	1:200	BioLegend
CD11c	APC	hamster/IgG	N418	1:200	BioLegend
CD11c	BV605	hamster/IgG	N418	1:200	BioLegend
CD19	PE-Cy7	rat/IgG_{2a}	6D5	1:200	BioLegend
CD45R/ B220	PE-Cy7	rat/IgG_{2a}	RA3-6B2	1:200	BioLegend
CD69	FITC	hamster/IgG_1	H1.2F3	1:100	BD Pharmingen
CD69	APC	hamster/IgG_1	H1.2F3	1:100	Biolegend
CD86	PE-Cy7	rat/IgG_{2a}	GL-1	1:100	BioLegend
Ly6G	BV786	rat/IgG2a, κ	1A8	1:200	BioLegend
Ly6C	FITC	rat/IgG2c, κ	HK1.4	1:200	BioLegend
Ly6C	PB	rat/IgG2c, κ	HK1.4	1:200	BioLegend
CD11b	PerCP	rat/IgG2b, κ	M1/70	1:200	BioLegend
PD-1	PE	rat/IgG2a, κ	29F1A12	1:200	BioLegend
PD-1	APC	rat/IgG2a, κ	29F1A12	1:200	BioLegend
PD-L1	PE	rat/IgG_{2a}	10F.9G2	1:200	eBioscience
CD45	AF700	rat/IgG2b, κ	30-F11	1:200	BioLegend
NK1.1	PerCP	mouse/IgG_{2a}	PK136	1:200	BioLegend
NK1.1	BV605	mouse/IgG_{2a}	PK136	1:200	BioLegend
MHC-I	FITC	mouse/IgG_{2a}	AF6-88.5	1:200	BioLegend
MHC-II	FITC	mouse/IgG_{2a}	AF6-120.1	1:200	BD Pharmingen

MHC-II	PB	mouse/IgG_{2a}	AF6-120.1	1:200	Biolegend
IRF4	AF647	rat/IgG1, κ	IRF4.3E4	1:100	Biolegend
Gr1	PE	rat/IgG2b, κ	RB6-8C5	1:200	Biolegend
Isotype Ctrl.	AF647	rat/IgG1, κ	RTK2071	1:100	Biolegend
Isotype Ctrl.	PE	rat/IgG2, κ	RTK2758	1:200	Biolegend
Isotype Ctrl.	FITC	Armenian Hamster IgG	HTK888	1:200	Biolegend
Isotype Ctrl.	APC	Armenian Hamster IgG	HTK888	1:200	Biolegend
Isotype Ctrl.	PE-Cy7	rat/IgG2, κ	RTK2758	1:200	Biolegend

Table 1: Antibodies for flow cytometry

2.1.4 Assay kits

Name	**Company**
Mouse GM-CSF DuoSet ELISA	R&D Systems, USA
Mouse G-CSF DuoSet ELISA	R&D Systems, USA
Mouse IL-6 DuoSet ELISA	R&D Systems, USA
Mouse CXCL10/IP-10/CRG-2 DuoSet ELISA	R&D Systems, USA
FAM-FLICA® Caspase-8 Assay Kit	ImmunoChemistry Techn, USA
eBioscience™ Foxp3 / Transcription Factor Staining Buffer Set	Thermo Fisher, Germany
Tumor Dissociation Kit®	Miltenyi, Germany
Myeloid-derived suppressor cell (MDSC) isolation Kit	Miltenyi, Germany
Pan T cell isolation Kit II, mouse	Miltenyi, Germany
QIAzol Kit	QIAGEN, Germany
RNeasy Kit,	QIAGEN, Germany
Agilent RNA 6000 Pico Kit	Agilent, USA
Agilent DNA 1000 Kit	Agilent, USA
SMARTer® Stranded Total RNA-Seq Kit v2 - Pico-input mammalian total RNA kit	Takara, Japan
NextSeq® 500/550 High Output Kit v2 (150 cycle)	Illumina

2.1.5 Cell lines

Murine pancreatic cancer cell lines that were isolated from spontaneous genetically engineered mouse models (GEMM) were obtained from Prof. Saur (Innere Medizin II, Klinikum der Technischen Universität (TU) Munich) and Prof. Siveke (West German Cancer Center, University Hospital Essen). All cell lines were tested positive for cytokeratin 18 and negative for fibroblast activation protein (FAP). Genetic background of mice, of which the cell lines have been generated from, are listed in table 2.

Splenocytes from PD-1 knockout mice (B6.Cg-*Pdcd1*$^{tm1.1Shr}$/J) were a kind gift from Dr. Festag and Prof. Protzer (Institute of Virology, TU Munich)

Cell line name	**Detailed genotype**
8024	p48-Cre +/-, LSL-Kras +/-
8025	p48-Cre +/-, LSL-Kras +/-
R254	p48-Cre +/-, LSL-Kras +/-, LSL-Trp53R172H
8028	p48-Cre +/-, LSL-Kras +/-
8305	p48-Cre +/-, LSL-Kras +/-
8661	p48-Cre +/-, LSL-Kras +/-
9203	p48-Cre +/-, LSL-Kras +/-
13871	Low-Cre +/-, LSL-Kras +/-, p53 lox/lox
MG 846	Pdx1-Cre +/-, LSL- Kras +/-, p53 lox/+
T110299	Ptf1aCre +/-, LSL-KrasG12D, p53fl/R172H

Table 2: Pancreatic tumor cell lines

2.1.6 Cell culture, supplements and cytokines

Name	**Company**
β-mercaptoethanol	Sigma-Aldrich, Germany
Dulbecco's modified Eagls's medium (DMEM), high glucose	Sigma-Aldrich, Germany
Dynabeads® Mouse T activator CD3/CD28	life technologies, Germany
Fetal bovine serum (FBS)	life technologies, Germany
L-glutamine (200 mM)	Sigma-Aldrich, Germany
MEM-NEAA (non-essential amino acids)	life technologies, Germany
Penicillin/Streptomycin (100 x)	Lonza, Germany
Opti-MEM	life technologies, Germany
$OVA_{257-264}$ peptide (SIINFEKL)	InvivoGen, USA
OVA protein	Sigma-Aldrich, Germany
Roswell Parl Memorial Institute (RPMI) 1640 medium	Sigma-Aldrich, Germany
Sodium pyruvate	Sigma-Aldrich, Germany
Recombinant murine GM-CSF	Peprotech, Germany
Recombinant murine IL-4	Peprotech, Germany
Recombinant murine IL-13	Peprotech, Germany

2.1.7 Material animal experiments

Name	**Company**
Sodium chloride, pyrogen-free (NaCl 0.9%)	Baxter, UK
Buprenovet (Buprenorphin)	Bayer, Germany
Midazolam-hameln (Benzodiazepin)	hameln, Germany
Dorbene vet (Medetomidin)	zoetis, Germany
Flumazenil Hikma (Benzodiazepin-Antagonist)	Hikma, Germany
Alzane (Atipamezol)	Pfizer, USA

In vivo-JetPEI™	Polyplus transfection, USA
Isoflurane-CP®	CP-Pharma, Germany
Bepanthen (Augen und Nasensalbe)	Bayer, Germany
Aqua ad injectabilia	Braun AG, Melsungen, DE
Poly(I:C)-HMW (high molecular weight), vaccigrade	Invivogen, USA
Surgery and dissecting set, autoclaved	RSG, Germany
Capillary tube, heparinized	Hirschmann, Germany
Insulin U-100 0.3 ml	BD Microfine, Germany
Scalpel (No. 22)	Feather, Japan
SurgiproTM II P-13 5-0	Covidien, Ireland

Anesthesia:

Drug	Stock concentration	amout for injection mix	Vol for injection mix
Dorbene	1 mg/ml	0.5 mg	500 µl
Midazolam	5 mg/ml	5 mg	1 ml
NaCl (0,9%)			1 ml
Buprenorphin	0.324 mg/6 ml	0.0675 mg	1.25 ml

➔ 150 µl/mouse

Antidote:

Drug	Stock concentration	amout for injection mix	Vol for injection mix
Flumazenil	0.1 mg/ml	0.5 mg	5 ml
Alzane	5 mg/ml	2.5 mg	500 µl

➔ 110 µl/mouse

2.1.8 Buffer compositions

DNA isolation buffer for genotyping:
Lysis buffer: 25 mM NaOH, 0.2 mM EDTA in H_2O
Neutralization buffer: 40 mM Tris-HCl in H_2O

FACS buffer:
2 mM EDTA
2 % FBS
0.1 % NaN_3
in PBS

MACS buffer:
2 mM EDTA
5% BSA
in PBS

2.1.9 Primer and oligonucleotide sequences

Name	**Sequence 5`->3`**
Ly6G_wt_ctrl_fwd	GAGACTCTGGCTACTCATCC
Ly6G_wt_ctrl_rev	CCTTCAGCAAGAGCTGGGGAC
Ly6G_Cre_1_fwd	GGTTTTATCTGTGCAGCCC
Ly6G_Cre_rev	GAGGTCCAAGAGACTTTCTGG
Ly6G_Cre_2_fwd	ACGTCCAGACACAGCATAGG

Irf4-fl_geno1_fw	TGGGCACCTCTACTGTCTGG
Irf4-fl_geno2_rv	CTCTGGGGACATCAGTCCT
Irf4-fl_geno3_rv	CGACCTGCAGCCAATAAGC
FLP_tg_geno1_fw	TGCCGGTCCTATTTACTCGT
FLP_tg_geno1_rv	TACTTCTTTAGCGCAAGGGGTAG
FLP_wt_geno1_fw	CTAGGCCACAGAATTGAAAGATCT
FLP_wt_geno1_rv	GTAGGTGGAAATTCTAGCATCATCC
LysM_geno1_fw	CCCAGAAATGCCAGATTACG
LysM_geno_rv	CTTGGGCTGCCAGAATTTCTC
LysM_geno2_fw	TTACAGTCGGCCAGGCTGAC
IRF4-wt-for-A2	TGCCTTTGGGACGGATGCTC
IRF4-wt-rev-B2	CTTCTAGCTGACCACTAAGAAC
IRF4-Δfrt-rev-D	AATCAAGTGTGGGCAAGACTG
pOVA_fwd	TCCTCAACCAAATCACC
pOVA_rev	AGACAATGGCATTAACC

Table 3: Primers for PCR

Name	**Sequence 5`->3`**	**Probe No**
Cytokeratin8_fw	AGTTCGCCTCCTTCATTGAC	67
Cytokeratin8_rv	GCTGCAACAGGCTCCACT	67
Cytokeratin18_fw	AGATGACACCAACATCACAAGG	78
Cytokeratin18_rv	TCCAGACCTTGGACTTCCTC	78
Cytokeratin19_fw	AGTCCCAGCTCAGCATGAA	97
Cytokeratin19_rv	TAACGGGCCTCCGTCTCT	97
FAP_fw	CGTGTATCGAAAACTGGGTGT	100
FAP_rv	AAACCCATTTCTATGAATTTTCTGAC	100
beta-actin_fw	CTA AGG CCA ACC GGG AAA AG	64
beta-actin_rv	ACC AGA GGC ATA CAG GGA CA	64

Table 4: Primers for quantitative PCR

Name	**Sequence 5`->3`**[1]
sgRNA1_fwd	GTCGTCTCCCACCG**AGCCCCTCGCCCAAACCAGA**GTTTCGAGACGTG
sgRNA1_rev	CACGTCTCGAAAC**TCTGGTTTGGGCGAGGGGCT**CGGTGGGAGACGAC
sgRNA2_fwd	GTCGTCTCCCACCG**CGGAGGATCTTATGCTGAAC**GTTTCGAGACGTG
sgRNA2_rev	CACGTCTCGAAAC**GTTCAGCATAAGATCCTCCG**CGGTGGGAGACGAC

Table 5: Oligonucleotids for molecular cloning

[1] sgRNA targeting sequence are indicated with bold and underlined letters

2.1.10 Consumables

Name	Company
Cryo`s™ Greiner	Frickenhausen, Germany
1.5 ml reaction tubes	Eppendorf, Hamburg, DE
Polystyrene round-bottom tubes	Dickinson, San Jose, USA
PCR-Tubes Biozym	Hess, Germany
MACS® SmartStrainers (30 µm, 70 µm, 100 µm)	Miltenyi Biotec, Germany
Cell scraper	Sarstedt, Germany
1 ml disposable syringe Norm-Ject	Henke Sass Wolf, Germany
Syringe (5 ml, 20 ml)	Becton Dickinson, USA
Injection needle (27 G 3/4 0.4x19 mm)	Becton Dickinson, USA
Cell culture flasks (175 cm^3, 75 cm^3)	Greiner, Germany
6-well cell culture plate	Becton Dickinson, USA
96-well cell culture plate round bottom	Greiner, Germany

2.2 Methods

2.2.1 Cell biological methods

2.2.1.1 Cell culture

Tumor cells were cultured in DMEM supplemented with 10 % fetal bovine serum (FBS), 2 mM L-glutamine, 100 U/l penicillin and 100 µg/ml streptomycin. Primary cells were cultured in RPMI-1640 medium supplemented with 10 % FBS, 2 mM L-glutamine, 100 U/l penicillin, 0.1 mg/ml streptomycin, 100 mM non-essential amino acids, 1 mM sodium pyruvate and 50 mM 2-mercaptoethanol. All cells were cultured in a humidified incubator at 37 °C with 5 % CO_2. All cells were frequently tested for mycoplasma contamination.

2.2.1.2 Generation of tumor-conditioned medium

2×10^5 tumor cells per 2 ml medium were seeded in a 6-well plate. After 48 h, supernatant was harvested, and cells were removed by centrifugation (400 x g, 5 min). Tumor conditioned medium was stored at -20 °C until usage.

2.2.1.3 Bone marrow-derived cell culture

Bone marrow cells were isolated by flushing femur and tibia. 2×10^6 cells per 10 ml were seeded in a 10 cm cell culture round plate in primary cell medium supplemented with 20 ng/ml GM-CSF. 25 % tumor-conditioned medium was added as indicated. Three days later, 10 ml primary cell medium with the above-mentioned supplements was added. Five days after cell isolation, 66 % of the medium with the respective supplements was exchanged.

2.2.1.4 Flow cytometry

Single cell suspension was washed in FACS buffer. Subsequently, cells were stained with primary fluorochrome-conjugated antibodies, with dilutions as indicated in Table 1. After 30 min incubation on ice, cells were washed with FACS buffer and resuspended in 100 to 300 µl FACS buffer. Intracellular antigens were stained using the transcription factor staining buffer set, according to manufacturer's protocol. In brief, after extracellular antigen staining, cells were fixed and permeabilized for 30 min at 4 °C. Subsequently, cells were washed with permeabilization buffer, incubated for 30 min at 4 °C with antibodies against respective intracellular antigens, and washed with permeabilization buffer. Samples were resuspended in FACS buffer and analyzed on a Canto II or LSRFortessa flow cytometer.

Measurement of caspase activity in MDSC was done using the FAM FLICA™ Caspase 8 kit, according to manufacturer's protocol. Briefly, splenic MDSC were incubated for 1 hour with the FLICA reagent at 37 °C. Cells were washed and surface antigens were stained. Finally, cells were washed again and resuspended in FACS buffer. Samples were analyzed on a Canto II flow cytometer.

2.2.1.5 T cell isolation and CFSE labeling

Splenic T cells were isolated by negative selection using the Pan T Cell Isolation Kit II. Purity was controlled by flow cytometry and reached > 95 %. T cells were labeled with 2.5 µM CFSE in 10 ml PBS by incubating 4 min at RT. Subsequently, staining reaction was stopped by adding 20 ml FBS. T cells were isolated by centrifugation (400 x g, 5 min) and resuspended in primary cell medium.

2.2.1.6 T cell suppression assay

CFSE-labeled wild-type T cells were transferred into a 96-well plate, at 5 x 10^4 cells per well. Suppressive effector cells were isolated as described (see 2.2.2.6 MDSC isolation and 2.2.1.7 FACSorting). A serial dilution of suppressive effector cells (5 x 10^4, 2.5 x 10^4, 1.25 x 10^4, 0.625 x 10^4 or 0.3125 x 10^4) was added to CFSE-labeled T cells. Anti-CD3/anti-CD28 beads were washed once in PBS and subsequently resuspended in primary cell medium. 1 µl beads was added to each well. CFSE-labeled T cell controls, either with or without anti-CD3/anti-CD28 beads, were included. Cells were incubated for 72 h and CFSE-dilution of proliferating $CD4^+$ and $CD8^+$ T cells was analyzed by flow

cytometry. CFSE-labeled T cells without stimulation were used to set the $CFSE^{low}$ T cell proliferation threshold.

2.2.1.7 FACSorting

Bone marrow cells were isolated by FACSorting for T cell suppression assays as well as splenic and tumor-derived MDSC for RNA isolation. FACSorting was performed by PD Hristov on a BD Aria III flow cytometer. Cell preparation was performed as described (see 2.2.2.6 MDSC isolation) and cells were stained as described (see 2.2.1.4 Flow cytometry). PMN-MDSC and M-MDSC were sorted using following marker set: FVD^-, $CD45^+$, $CD11b^+$, $Ly6G^+$, $Ly6C^{int}$ (PMN-MDSC) and FVD^-, $CD45^+$, $CD11b^+$, $Ly6G^-$, $Ly6C^{high}$ (M-MDSC), respectively. Post sort quality was controlled by flow cytometry.

2.2.1.8 Generation of OVA overexpressing T110299

An ovalbumin (OVA) overexpressing T110299 tumor cell line (T110299-OVA) was generated by PD Düwell. Briefly, cells were transiently transfected with the pAc-Neo-OVA plasmid [105] using the Novagen Genejuice® transfection reagent, according to the manufacturer's instructions. Cells were maintained in tumor cell medium, supplemented with G418 (geneticin) as selection reagent. OVA expression was confirmed by PCR.

2.2.1.9 Antigen presentation assay

Splenic OVA-specific transgenic OT-I T cells (C57BL/6-$Tg^{(TcraTcrb)1100Mjb}$/J) were isolated and CFSE-labeled as described before (see 2.2.1.5 T cell isolation and CFSE labeling). 5 x 10^4 CFSE-labeled OT-I T cells per well were transferred into a 96-well plate. MDSC as potential antigen presenting effector cells were isolated as described before (see 2.2.2.6 MDSC isolation). A serial dilution of T110299-OVA tumor-derived MDSC (5 x 10^4, 2.5 x 10^4, 1.25 x 10^4, 0.625 x 10^4 and 0.3125 x 10^4) were added to CFSE-labeled OT-I T cells, without stimulating beads. Splenic MDSC were either loaded with SIINFEKL peptide at indicated concentrations or were incubated over night at 37°C with 1 µg/ml OVA protein. Subsequently, OVA antigen treated MDSC were washed, resuspended in primary cell medium, diluted and seeded as described above. Cells were incubated for 72 h at 37° C and CFSE-dilution of proliferated $CD8^+$ OT-I T cells was analyzed by flow cytometry. CFSE-labeled OT-I T cells without stimulation were used to set the threshold for proliferated T cells ($CFSE^{low}$).

2.2.1.10 CRISPR knockout generation

Pdcd1 (PD-1/CD279) knockout B3Z T cell lines were generated using a lentiviral CRISPR/Cas9 approach as described [106, 107]. *Pdcd1-targeting* sgRNA sequences were retrieved from the GeCKOv2 mouse library (http://genome-engineering.org/gecko/). A BsmBI restriction overhang was added as described [107]. The DNA sequence was ordered by eurofins genomics (see Table 5) and cloned into a pLentiCRISPRv2_ccdB_Cas9-P2A-Puro vector (kind gift from Prof. Schmidt-Supprian, III. Medizinische Klinik, TU Munich). HEK-293T cells were transfected with the CRISPR/Cas9 plasmid as well as with plasmids encoding the viral envelop proteins (pcMV_dR8-74 and pVSVG) using Lipofectamine® 2000. After 2 days, the lentivirus-containing supernatant was transferred to B3Z cells. After additional 48 h, cells were treated with puromycin for positive selection. PD-1-negative B3Z cells were single-cell sorted into a 96-well plate using a BD FACSAria™ III cell sorter.

2.2.2 Animal experiments

All animal experiments were approved by the local authority (Regierung von Oberbayern, Munich, Germany; animal protocol number 55.2-1-54-2532-175-12). All experiments were done in the animal facility Tierhaltung Ziemssenstr. 1 (THZ) under specific pathogen-free (SPF) conditions. Sentinel mice were sent for health status monitoring to MFD diagnostics (Wendelsheim, Germany) quarterly.

2.2.2.1 Mouse strains

C57BL/6 wild-type mice were purchased from Janvier, France. Irf4^{flox} mice (B6.129S1-*Irf4*^{tm1Rdf}/J) were a kind gift from Prof. Bopp (Institute of Immunology, Universitätsmedizin Mainz), Ly6G^{Cre} mice (C57BL/6-*Ly6g*$^{tm2621(Cre\text{-}tdTomato)}$Arte) were a kind gift from Prof. Gunzer (Institute for Experimental Immunology and Imaging, University of Duisburg-Essen), LysM^{Cre} mice (B6.129P2-*Lyz2*$^{tm1(cre)Ifo}$/J) were a kind gift from PD Lech, (Institute of Clinical Biochemistry, Klinikum der Universität München). *Ifnar*$^{-/-}$ (B6.129S2-*Ifnar1*^{tm1Agt}) were a kind gift from Prof. Rothenfußer (Division of Clinical Pharmacology, Klinikum der Universität München) and OT-I mice (C57BL/6-Tg$^{(TcraTcrb)1100Mjb}$/J) were a kind gift from PD Kobold (Division of Clinical Pharmacology, Klinikum der Universität München). FLP1 recombinase expressing FLPe mice (B6;SJL-Tg$^{(ACTFLPe)9205Dym}$/J) were purchased from Jackson Laboratory (Sulzfeld, Germany).

LysM^{Cre} were cross-bred with IRF4^{flox} mice to obtain LysM^{Cre}Irf4^{flox} and Ly6G^{Cre} were cross-bred with Irf4^{flox} mice to obtain Ly6G^{Cre}Irf4^{flox}. Both mouse strains were kept on

homozygous *Irf4$^{fl/fl}$ background*. Exon 4 of *Irf4* in B6.129S1-*Irf4^{tm1Rdf}*/J mice harbors two FRT sites, of which one is located upstream and one downstream of exon 4. To generate global IRF4-deficient mice, FLPe mice were cross-bred with B6.129S1-*Irf4^{tm1Rdf}*/J mice and *Irf4$^{-/-}$* mice were obtained. IRF4 sufficient mice originating from those breedings were used as littermate controls. Genotypes of all mice were routinely analyzed by PCR as described below (see 2.2.3.3 Genotyping PCR).

2.2.2.3 Orthotopic tumor induction

T110299 tumor cells were passaged at a 1:2 ratio the day prior surgery to ensure optimal growth behavior at the day of injection. The next day, tumor cells were washed three times with PBS to remove residing FBS completely. The surgery was performed under general anesthesia as well as analgesia applied intraperitoneally (i.p.) and eyes were protected from exsiccation using eye cream. The fur was disinfected and the skin as well as the peritoneal cavity was opened with an approximately 1 cm cut. Pancreatic tissue was carefully dislocated and 2 x 10^5 tumor cells in 25 µl PBS were injected into the tail of the pancreas. Organs were carefully relocated, and cuts were sewed. To antagonize general anesthesia, the antidote (see 2.1.7 Material animal experiments) was administered and the mice were kept under warming light. Mice were administered analgesia during the following 24 h and distressed mice were sacrificed.

2.2.2.4 Treatment

For *in vivo* treatment, high molecular weight poly(I:C) was complexed with invivo-jetPEI at a N/P ratio[2] of 6, in 5 % glucose solution (Poly(I:C)$_c$). Mice were treated i.v. with 50 µg poly(I:C)$_c$ or 5 % glucose solution (control) at day 18 and 20 after tumor induction. Mice were sacrificed at day 21.

2.2.2.5 Survival

For survival, health status of mice (body weight, general condition, spontaneous behavior and clinical status) was evaluated daily following the EU-severity assessment and according to the animal protocol´s score sheet. Mice were sacrificed as soon as they reached a severity score of three or higher.

[2] N/P ratio is the ratio of positively charged amino groups of PEI to negatively charged phosphate groups of the RNA molecule

2.2.2.6 MDSC isolation

To isolate MDSC from the spleen, splenocytes were flushed out with a syringe and red blood cells were lyzed using BD PharmLyse. To isolate tumor-derived MDSC, tumors were cut into 1 to 2 mm^2 pieces and mechanically dissociated with the gentleMACS device (program imptumor2_2), in the presence of digestion enzymes by using the Tumor Dissociation Kit®.

For functional assays, MDSC were isolated using MDSC MACS isolation. In brief, PMN-MDSC were isolated with anti-Ly6G microbeads. Subsequently, M-MDSC were isolated from the negative fraction using anti-Gr1 microbeads. Purity was analyzed by flow cytometry. The purity of PMN-MDSC was > 90% and the purity of M-MDSC was > 70%. For RNA isolation, MDSC were enriched using $CD11b^+$ MACS positive selection kit, followed by FACSorting (see 2.2.1.7 FACSorting).

2.2.3 Molecular biology methods

2.2.3.1 Enzyme-linked immunosorbent assay (ELISA)

The concentration of G-CSF, GM-CSF, IL-6 and CXCL10 in serum or tumor-conditioned cell culture medium was measured by ELISA, according to manufacturer's protocol. Briefly, 96-well plates were coated over night with capture antibody diluted in PBS and unspecific binding was blocked with 1 % BSA. Samples were added and incubated for 2 h. After a washing step, biotinylated detection antibodies and streptavidin-coupled horse radish peroxidase (HRP) were added. HRP-mediated conversion of the tetramethylbenzidine (TMB) substrate was measured as absorbance at 450 nm with wavelength correction 570 nm by a multi-plate reader.

2.2.3.2 DNA isolation for mouse genotyping

DNA from ear or tail biopsies was extracted and analyzed as described before [108]. Briefly, biopsies were incubated in 75 µl alkaline lysis buffer for 30 min at 95°C and reaction was stopped by adding 75 µl neutralization buffer. Supernatant containing genomic DNA was subsequently used for genotyping.

2.2.3.3 Genotyping PCR

For genotyping of mice, isolated DNA was analyzed using locus specific primer pairs listed in Table 3, by using genotype-specific cycling programs, as summarized in Table 6.

Locus	Initial Denaturation	Denaturation	Annealing	Elongation	Number of cycles	Final elongation
$IRF4^{flox}$	94 °C, 5 min	94 °C, 30 sec	60 °C, 30 sec	72 °C, 30 sec	35	72 °C, 5 min
$IRF4^{-/-}$	95 °C, 5 min	95 °C, 15 sec	62 °C, 30 sec	72 °C, 60 sec	30	72 °C, 5 min
$LysM^{Cre}$	94 °C, 5 min	94 °C, 20 sec	60 °C, 15 sec	72 °C, 15 sec	25	72 °C, 2 min
$Ly6G^{Cre}$	94 °C, 5 min	94 °C, 30 sec	60 °C, 30 sec	72 °C, 60 sec	35	72 °C, 10 min
$Ly6G^{WT}$	94 °C, 5 min	94 °C, 30 sec	60 °C, 30 sec	72 °C, 60 sec	35	72 °C, 10 min
FLP1	94 °C, 5 min	94 °C, 20 sec	60 °C, 15 sec	72 °C, 15 sec	25	72 °C, 2 min
OT-I	94 °C, 5 min	94 °C, 30 sec	60 °C, 30 sec	72 °C, 60 sec	35	72 °C, 10 min

Table 6: PCR cycling conditions for genotyping PCR

2.2.3.4 RNA isolation

For RNA sequencing, MDSC were isolated in a combined $CD11b^+$ MACSorting and FACSorting approach. MDSC RNA was isolated using the QIAzol kit. In brief, cells were lyzed in trizol reagent. RNA was isolated by adding chloroform and was extracted using RNeasy RNA binding columns (RNeasy Kit, Qiagen). RNA concentration and rRNA integrity was measured using the Pico 6000 assay on a bioanalyzer 2100.

2.2.3.5 RNA-Seq sample preparation and next generation sequencing

The SMARTer® Stranded Total RNA-Seq Kit v2 - Pico-input mammalian total RNA kit was used to prepare the cDNA library for next generation sequencing. The library was prepared according to manufacturer's protocol. In brief, after confirming high integrity of the RNA using the Agilent RNA 6000 Pico Kit on a Bioanalyzer 2100 (RIN > 7), RNA was fragmented for the maximum time frame (4 min at 94°C). Next, first-strand cDNA synthesis was performed using supplied random primers. Subsequently, Illumina adapters and indexes were added in a PCR step. The cDNA library was isolated for next generation sequencing using AMPure beads, and ribosomal sequences were depleted using ZapRv2 and R-Probes v2. Finally, the RNA-Seq library was amplified in 13 PCR

cycles and isolated using AMPure beads. cDNA fragment length and concentration were analyzed on the bioanalyzer 2100 using the Agilent DNA 1000 Kit. The library was loaded on an Illumina NextSeq® 500/550 High Output Kit v2 and analyzed on an Illmuina NextSeq sequenzer. Library loading and sequencing were performed by Dr. Rohlf (Care-for-Rare Laboratories at the Dr. von Haunerschen Kinderspital, LMU, Munich).

2.2.3.5 Complementary DNA (cDNA) synthesis

cDNA was synthesized from RNA by RevertAID™ first strand cDNA synthesis kit according to manufacturer's protocol. In brief, master mix summarized in Table 7 was incubated for 1 h at 42°C, followed by a 5 min inactivation step at 70° C.

	Stock concentration	1x reaction
RNA		1000 ng
Oligo(dT)$_{18}$	10 µM	1 µl
Ribolock™	20 U/µl	1 µl
dNTP	10 mM	2 µl
RevertAid™	200 U/µl	1 µl
5x Reaction buffer		4 µl
H_2O		up to 12 µl

Table 7: Mastermix for cDNA synthesis

2.2.3.6 Quantitative PCR (qPCR)

Messenger RNA (mRNA) expression levels were analyzed by quantitative PCR (qPCR) using the Roche Universal probe library according to manufacturer's protocol. In brief, the master mix summarized in Table 8 was mixed and subsequently analyzed on the Roche LightCycler 480 II using the program summarized in Table 9.

	Stock concentration	1x reaction
cDNA		3 µl
Forward primer	10 µM	0.2 µl
Reverse primer	10 µM	0.2 µl
Probe		0.1 µl
Kapa probe fast universal qPCR master mix (2x)		5 µl
H_2O		up to 10 µl

Table 8: Mastermix for qPCR

	Temperature	Time	Quantification	
Pre-incubation	95 °C	10 min	None	

Denaturation	95 °C	15 sec	None	40 Cycles
Elongation	60 °C	60 sec	Yes	
Cooling	40 °C	oo	None	

Table 9: Cycling program of LightCycler

2.3 Computational analysis

2.3.1 Statistical analysis

Data are displayed as mean and standard deviation (SD) or standard error of the mean (SEM) as indicated in the figure legend. Generally, data with individual mice are shown as mean and SEM. To detect statistically significant differences between two groups, Mann Whitney U test was used. To compare more than two groups, we applied Kruskal-Wallis test followed by posthoc tests between selected samples. To compare the influence of two independent variables e.g. treatment and genotype two-way analysis of variance (ANOVA) was conducted, followed by posthoc tests between selected samples. Spearman correlation analyses were performed to explore associations between potential influencing factors. To analyze differences in the survival, Mantel-Cox test was conducted.

2.3.2 Bioinformatics analysis

Whole transcriptomic sequencing results were kindly analyzed by Michael Kluge and Prof. Friedel (Institute for Informatics, Ludwig-Maximilians-Universität Munich) using the following procedure: Quality of sequencing reads was assessed using fastQC [109]. Reads were mapped against the mouse genome (mm10) and mouse rRNA sequences using ContextMap version 2.7.9 [110] (using BWA [111] as short read aligner and default parameters). Number of read fragments per gene were determined strand-specific from the mapped RNA-Seq reads using featureCounts [112] and Gencode (v16) annotations. Differential gene expression analysis was performed using DEseq2 [113]. P-values were adjusted for multiple testing using the method by Benjamini and Hochberg [114] and genes with an adjusted p-value <0.001 were considered significantly differentially expressed. The RNA-Seq analysis workflow was implemented and run using the workflow management system Watchdog [115]. Results were visualized using the online tool ClustVis [116]. Functional annotation was performed using DAVID Bioinformatics Resources 6.8 [117].

2.4 Software

Name	Company
Adobe Illustrator CS6	Adobe Systems, USA
EndNote X8	Thomson Reuters, USA
FACSDiva	BD Bioscience, Germany
FlowJo V10	Tree Star, USA
Graphpad Prism 7.0	Graphpad Software, USA
LightCycler 480 SW 1.5	Roche, Germany
ClustVis 1.0	https://biit.cs.ut.ee/clustvis/
DAVID 6.8	https://david.ncifcrf.gov/

3. Results

3.1 Induction of suppressive myeloid cells in a KPC-derived orthotopic model

3.1.1 PDAC induce systemic myeloid cell expansion

The tumor growth and immune cell composition of an orthotopic PDAC model using the KPC-derived pancreatic tumor cell line T110299 was characterized *in vivo*. T110299 tumors were induced in the pancreas of C57BL/6 wild-type mice and organ weights as well as immune cell infiltrates were monitored (Fig. 6A). One week after tumor induction small tumors were detectable macroscopically. After three weeks, mice developed tumors with an average weight of 990 mg (Fig. 6B). Concordant to tumor growth, spleen weight increased without any sign of tumor cell metastasis into the spleen (Fig. 6B). Tumor and spleen weight correlated significantly ($r = 0.78$ $p = 0.0001$) (Fig. 6C).

In the tumor tissue, PMN-MDSC ($CD11b^+Ly6G^+Ly6C^{low}$, Fig. 6A) frequency increased during tumor progression ($p = 0.001$) (Fig. 6D). M-MDSC ($CD11b^+Ly6G^-Ly6C^{high}$, Fig. 6A) infiltrated the tumor initially; however the frequency dropped the following two weeks ($p = 0.0005$) (Fig. 6D). Gating strategy is depicted in Figure S1 and S2. $CD4^+$ and $CD8^+$ T cell frequency was significantly elevated at day 14 ($CD4^+$ $p = 0.02$, $CD8^+$ $p < 0.0001$) (Fig. 6D). The relative frequency of intratumoral immune cells 7, 14 and 21 days after tumor induction is summarized in Fig. 1J.

With increased tumor weight during tumor progress, the frequencies of both PMN-MDSC and M-MDSC were elevated in the spleen three weeks after tumor induction ($p = 0.006$, $p = 0.003$, respectively) (Fig. 6E). In contrast, $CD8^+$ and $CD4^+$ T cell frequency in the spleen decreased during tumor progression ($p = 0.008$, $p = 0.003$, respectively) (Fig. 6E). The frequency of both MDSC subpopulations in the blood increased during tumor growth (PMN-MDSC $p = 0.009$, M-MDSC $p = 0.01$), whereas the $CD4^+$ and $CD8^+$ T cell frequency remained constant (Fig. 6F).

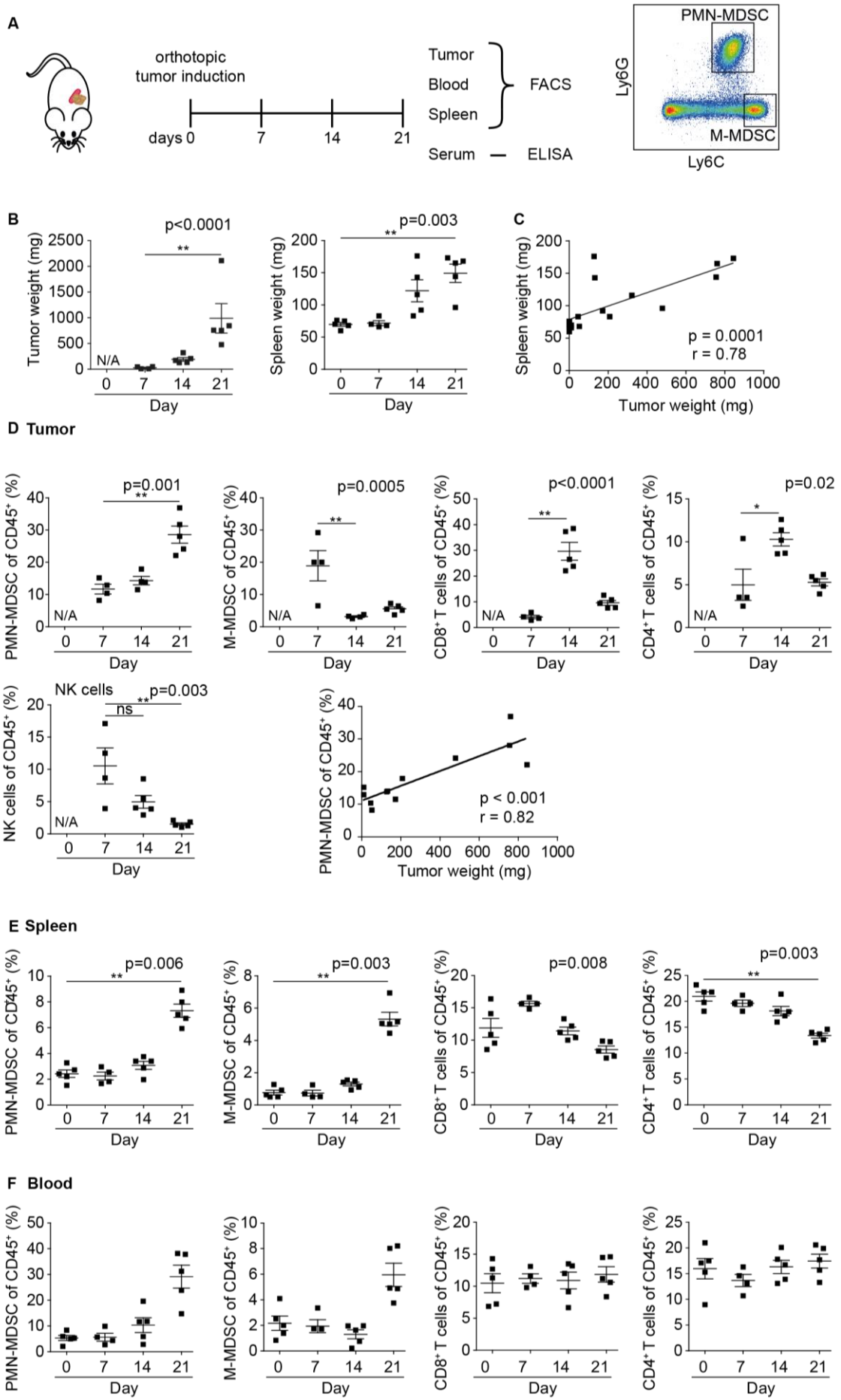

Figure 6: (continued)

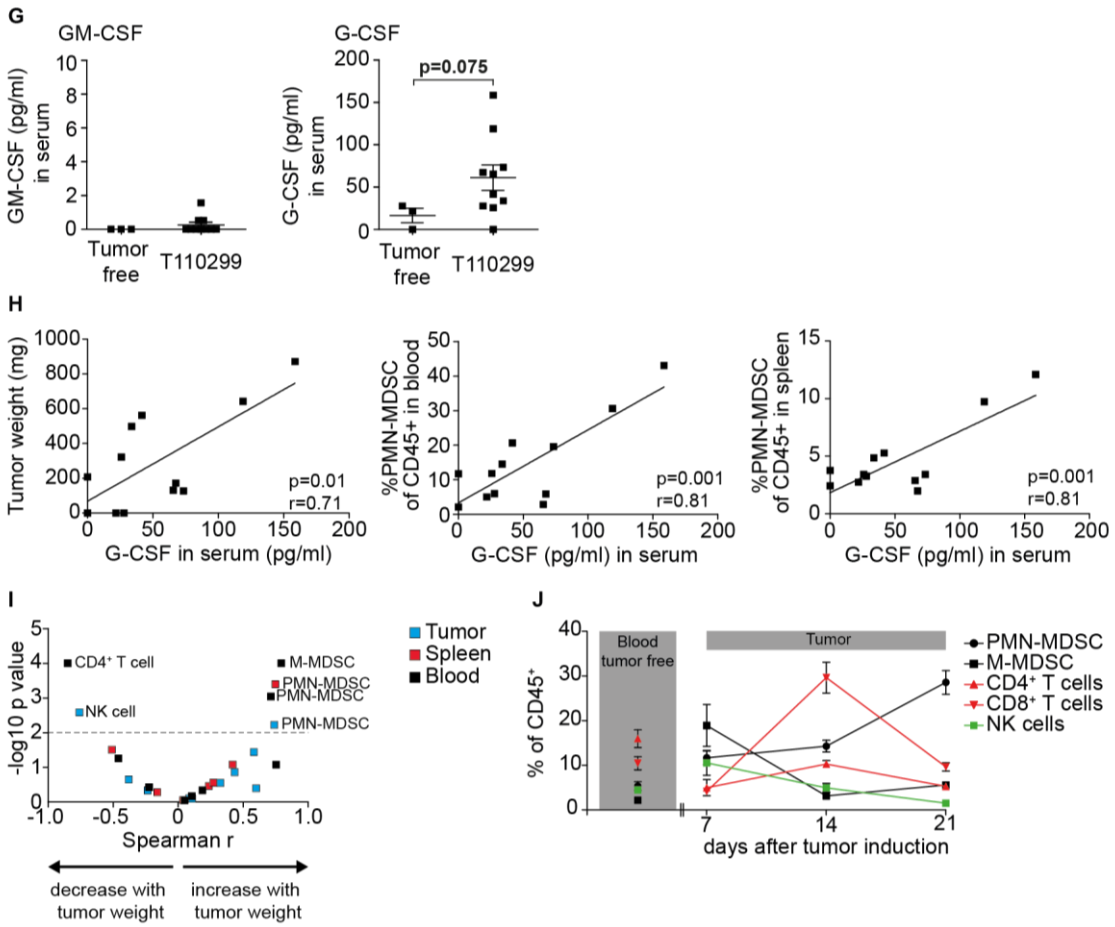

Figure 6: KPC-derived PDAC induce systemic expansion of the myeloid compartment.

A) Experimental design: T110299 tumors were induced orthotopically in C57BL/6 mice. Organ weight (B) and immune cell frequency were measured by flow cytometry 0, 7, 14 and 21 days after tumor induction (D-F, I, J), and serum cytokine levels by ELISA 14 and 21 days after tumor induction (G). Tumor weight was correlated to spleen weight (C) and frequency of PMN-MDSC in the tumor (D). H) G-CSF serum levels were correlated to tumor weight and PMN-MDSC frequency in blood and spleen 14 and 21 days after tumor induction. I) Spearman correlation results of immune cell frequency ($CD4^+$ T cells, $CD8^+$ T cells, NK cells, NKT cells, PMN-MDSC, M-MDSC, Macrophages and B cells) in organ (tumor - blue, spleen - red, blood - black) with tumor weight. Statistical analysis was performed using Kruskal Wallis test, followed by Dunn's multiple comparisons test between selected days (B, D-F) and spearman correlation (C, H) and unpaired student's t-test (G). P values of Kruskal Wallis test and significant results of Dunn's test are shown in each graph. n=4-5, error bars represent mean +/- SEM. Asterisks indicate * $p < 0.05$, ** $p < 0.01$. N/A = not applicable.

Myeloid cell stimulating cytokines such as GM-CSF and G-CSF have been described to mediate MDSC expansion [118, 119]. Interestingly, GM-CSF levels were not detectable in the serum of T110299 tumor bearing mice two and three weeks after tumor induction (Fig. 6G). In contrast, G-CSF levels were elevated in the serum of PDAC bearing mice ($p = 0.075$) (Fig. 6G). G-CSF concentration in the serum correlated significantly with tumor weight ($p = 0.01$, $r = 0.71$). Moreover, PMN-MDSC frequencies in both spleen and blood correlated significantly with G-CSF concentration in the serum ($p = 0.001$, $r = 0.81$) (Fig. 6H). To analyze the impact of the tumor weight on the immune cell composition,

PMN-MDSC, M-MDSC, macrophage, DC, T cell and B cell frequency in blood, spleen and tumor was correlated to tumor weight. As shown in Fig. 1I, PMN-MDSC frequency in all three compartments and M-MDSC frequency in the spleen correlated positively with the tumor weight ($p < 0.01$). $CD4^+$ T cell frequency in the spleen and NK cell frequency in the tumor correlated inversely with tumor weight ($p < 0.01$) (Fig. 6I).

3.1.2 KPC-derived PDAC induce suppressive capacity in MDSC

The PD-1/PD-L1 axis contributes to the immunosuppressive tumor microenvironment in many cancer entities [120]. PD-L1 expression was significantly elevated in the tumor microenvironment of both PMN-MDSC and M-MDSC compared to their splenic counterpart ($p = 0.0001$ and $p = 0.0001$, respectively; Fig. 7A). Similarly, PD-1 expression of $CD4^+$ and $CD8^+$ T cells was low in the spleen and was significantly increased in the tumor ($p = 0.0003$ and $p = 0.0002$, respectively; Fig. 7B).

The hallmark of MDSC in the context of tumors is their suppressive capacity. Both MDSC subtypes were isolated by MACS and co-cultured with anti-CD3/anti-CD28 stimulated T cells. T cell suppressive capacity of MDSC was measured by tracing T cell proliferation. Polymorphonuclear cells from the spleen of tumor-free hosts (granulocytes[3]) did not suppress $CD8^+$ T cell proliferation (Fig. 7C). PMN-MDSC from tumor-bearing hosts showed dose-dependently $CD8^+$ T cell suppressive capacity. Tumor-derived PMN-MDSC were the most potent T cell suppressors (Fig. 7C).

Similar effects were revealed for M-MDSC: Monocytes[3] from the spleen of tumor-free mice were not T cell suppressive whereas their counterparts from tumor-bearing hosts suppressed $CD8^+$ T cell proliferation. Again, M-MDSC isolated from the tumor tissue showed a tendency towards higher suppressive capacity. Furthermore, both MDSC subtypes suppressed $CD4^+$ T cell proliferation comparable to the inhibition of $CD8^+$ T cells (Fig. 7D).

Taken together, these data suggest that PDAC development modulates the immune system by systemic expansion of MDSC and induction of suppressive function in these cells.

[3] Granulocytes and PMN-MDSC as well as monocytes and M-MDSC are not distinguishable by flow cytometry. By definition PMN-MDSC and M-MDSC exist only under pathological conditions such as cancer and infection [18].

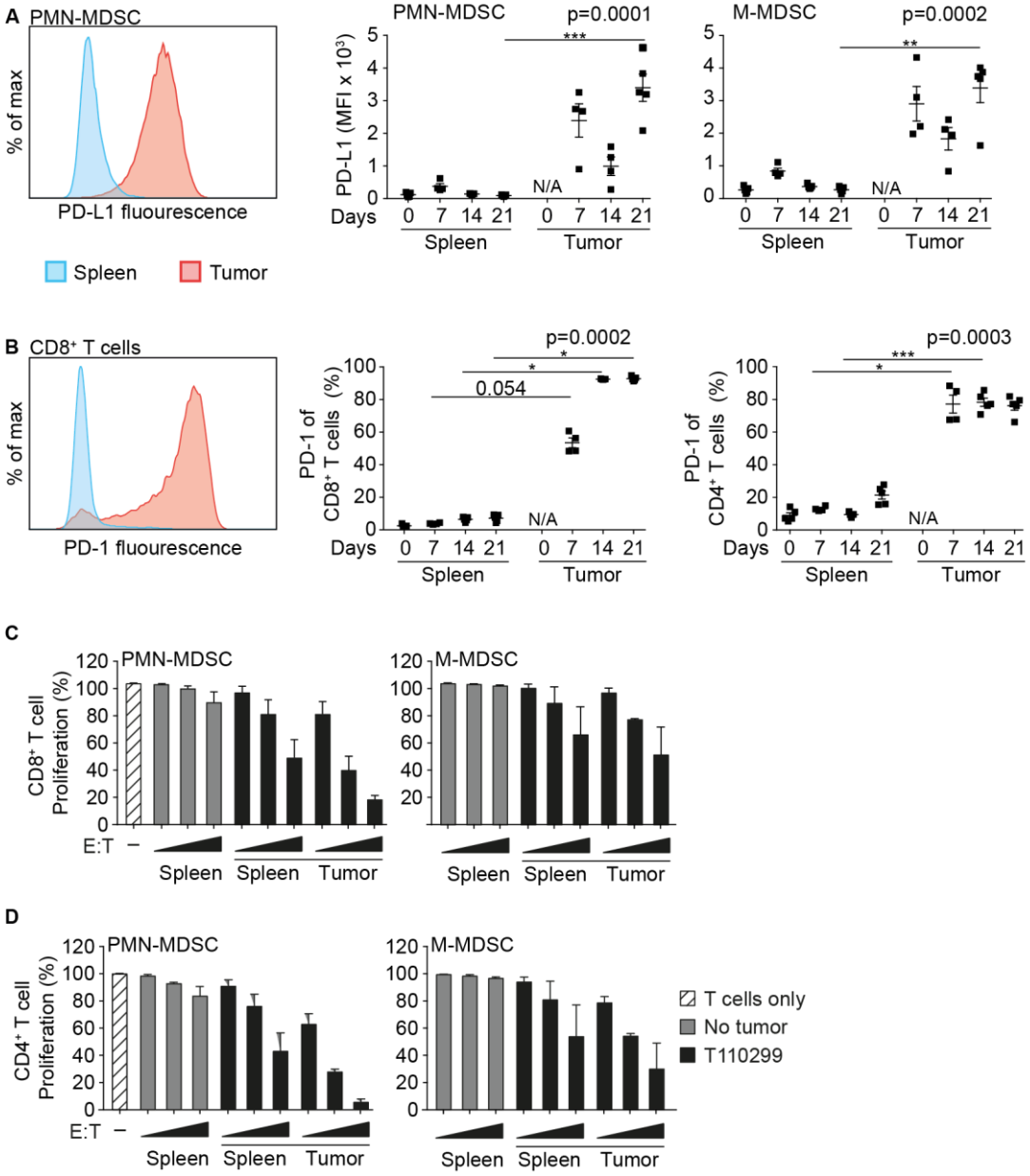

Figure 7: KPC-derived PDAC induce T cell suppressive function in MDSC.
PD-L1 expression of MDSC (A) and proportion of PD-1⁺ T cells (B) was analyzed by flow cytometry 0, 7, 14 and 21 days after orthotopic T110299 tumor induction. C-D) Three weeks after tumor induction, MDSC were isolated from tumor and spleen. Subsequently, MDSC were co-cultured with CFSE-labeled T cells. The MDSC to T cell ratio was 0.25:1, 0.5:1 and.1:1. Proportion of proliferated $CFSE^{low}$ $CD8^+$ (C) and $CD4^+$ (D) T cells was analyzed by flow cytometry. Statistical analysis was performed using Kruskal Wallis test, followed by Dunn's multiple comparisons test between selected days (A, B) n = 4-5. Figures C & D are representative graphs of three replicates with n = 4 mice per group, error bars represent mean +/- SEM. Asterisks indicate * $p < 0.05$, ** $p < 0.01$.

3.2 Characterization of PD-1 expression by MDSC

3.2.1 Viable MDSC lack PD-1 expression

There is increasing evidence, that not only PD-L1 but also its receptor PD-1 is expressed on myeloid cells including MDSC, and that intrinsic PD-1 signaling modifies cellular function [78, 121]. Thus, PD-1 expression was analyzed in MDSC in PDAC bearing mice. Anti-PD-1 staining was detectable in a subset of $Gr1^+$ MDSC by flow cytometry. However, $PD\text{-}1^+$ cells were smaller in size ($FSC\text{-}A^{low}$) and stained positive for the dead cell marker fixable viability dye (FVD) (Fig. 8A). This finding was confirmed with two additional dead cell markers, 7-AAD and cleavage of a caspase 8 substrate, which use different principles to define dead cells (Fig. 8B, C). To rule out unspecific binding of the antibody, an isotype staining control was used. Neither viable nor dead cell marker positive cells stained with the isotype control (Fig. 8B, right panel).

3.2.2. Anti-PD-1 antibody binds to an unknown antigen in PD-1-deficient cells

To analyze whether the anti-PD-1 antibody clone binds to another antigen than PD-1, wild-type and PD-1-deficient splenocytes were cultured for 48 h in the presence or absence of anti-CD3/anti-CD28 T cell stimulating beads. As expected, stimulation induced PD-1 expression on wild-type $CD4^+$ T cells. No PD-1 staining was detectable on viable PD-1-deficient cells. However, in PD-1-deficient T cells, dead cell marker-positive cells stained positive for PD-1, indicating that the antibody binds to an antigen distinct from PD-1 in these cells (Fig. 8D).

To confirm this finding, *Pdcd1* was knocked-out in a T cell myeloma hybrid cell line (B3Z), which expresses PD-1 at high levels. Single cell clones were generated, and anti-PD-1 staining was analyzed. To increase the proportion of dead cells, B3Z cells were treated with the apoptosis inducing agent staurosporine. Scrambled guideRNA-treated (B3ZsgScr) control cells were, as expected, highly positive for anti-PD-1 staining. In PD-1-deficent B3Z cells (B3ZsgPdcd1) only dead cell marker-positive cells stained positive for PD-1 (Fig. 8E).

Together, the data show that the anti-PD-1 antibody clone 29F1A12 specifically recognizes PD-1 in viable cells but binds additionally to an unknown antigen in dead cells.

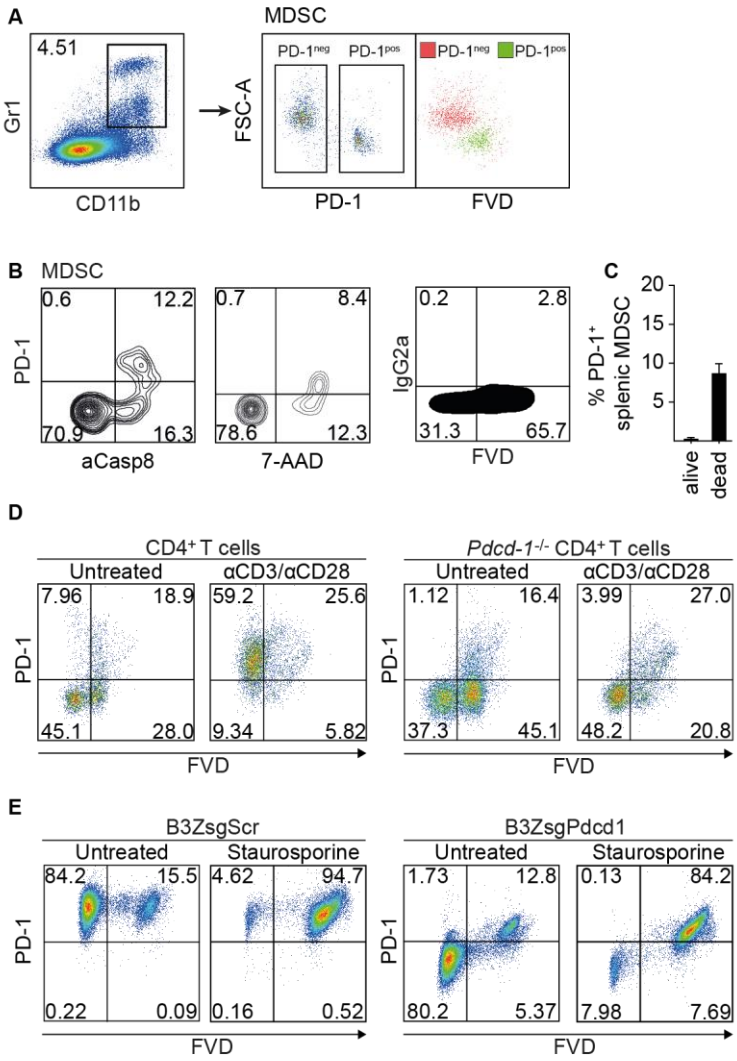

Figure 8: Anti-PD-1 antibody 29F1A12 binds to an unknown antigen in dead cells
Anti-PD-1 staining of splenic MDSC was analyzed by flow cytometry. Fixable viability dye (FVD) (A), caspase 8 activity (aCasp8) and 7-AAD (B) were used to identify dead or dying cells. Proportion of PD-1$^+$ MDSC was quantified by flow cytometry (C). Splenocytes from wild-type and PD-1-deficient mice were cultured in the presence or absence of anti-CD3/anti-CD28 beads and anti-PD-1 staining was analyzed by flow cytometry (D). Wild-type and PD-1-deficient B3Z cells were treated with staurosporine or left untreated. Anti-PD-1 staining was measured by flow cytometry (E) A, B, E). One out of three independent experiments is shown.

3.3 Bone marrow model to study MDSC differentiation and function *in vitro*

3.3.1. Tumor-derived factors induce expansion of MDSC-like cells *in vitro*

Myeloid precursor cell can be isolated from the bone marrow and cultured in the presence of GM-CSF to generate bone marrow-derived DC (BMDC) [122]. To study the influence of tumor-derived factors on myeloid precursor cells *in vitro*, GM-CSF-stimulated bone marrow cell cultures were cultivated in the presence and absence of tumor-conditioned medium (CM) generated from different KPC-derived pancreatic tumor cell lines (Fig. 9A).

MDSC-like[4] cell frequency was elevated in the presence of tumor CM. In contrast, BMDC frequency was reduced. Some CM induced a more M-MDSC-pronounced phenotype (e.g. 13871), whereas other CM favored the differentiation of PMN-MDSC-like cells (e.g. 8025, 8661) (Fig. 9B, C). Both GM-CSF and G-CSF were secreted by most of the KPC-derived tumor cell lines (Fig. 9D). Interestingly, the two cell lines, 8025 and 8661, with the highest G-CSF secretion induced the highest PMN-MDSC-like cell expansion *in vitro*. PMN-MDSC-like cell frequency correlated with the G-CSF concentration in the conditioned medium of the different tumor cell lines ($p = 0.0006$, $R^2 = 0.746$), whereas BMDC frequency correlated inversely ($p = 0.01$, $R^2 = 0.577$) (Fig. 9E).

[4] *In vitro* generated suppressive myeloid cells are not as clearly defined as MDSC *in vivo.* Therefore, in this study *in vitro* generated bone marrow-derived suppressive myeloid cells are called MDSC-like cells. PMN-MDSC and PMN-MDSC-like as well as M-MDSC and M-MDSC-like cells are defined by the same surface markers using flow cytometry.

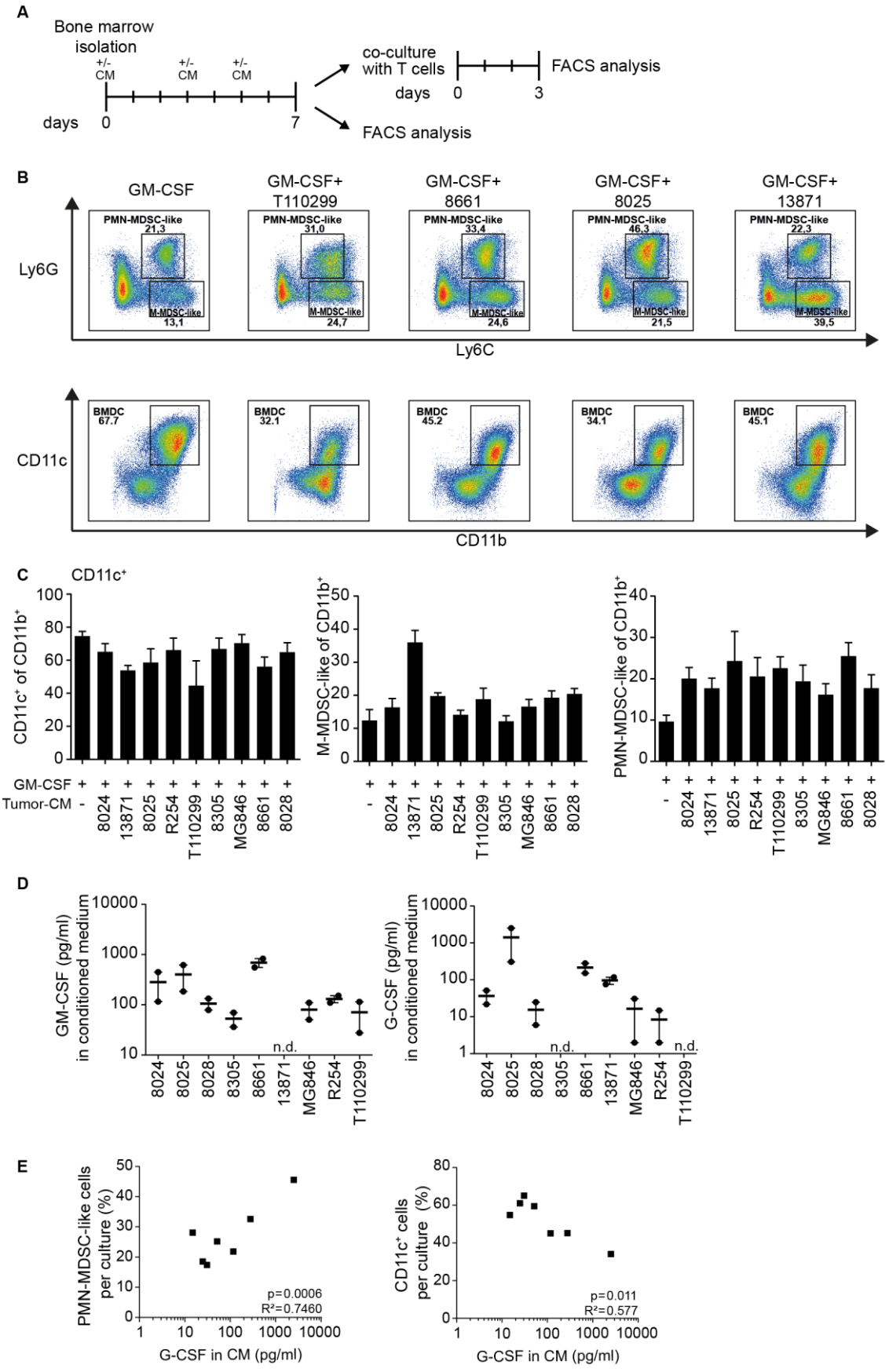

Figure 9: Tumor-derived factors increase MDSC-like cell frequency in bone marrow culture. (continued)

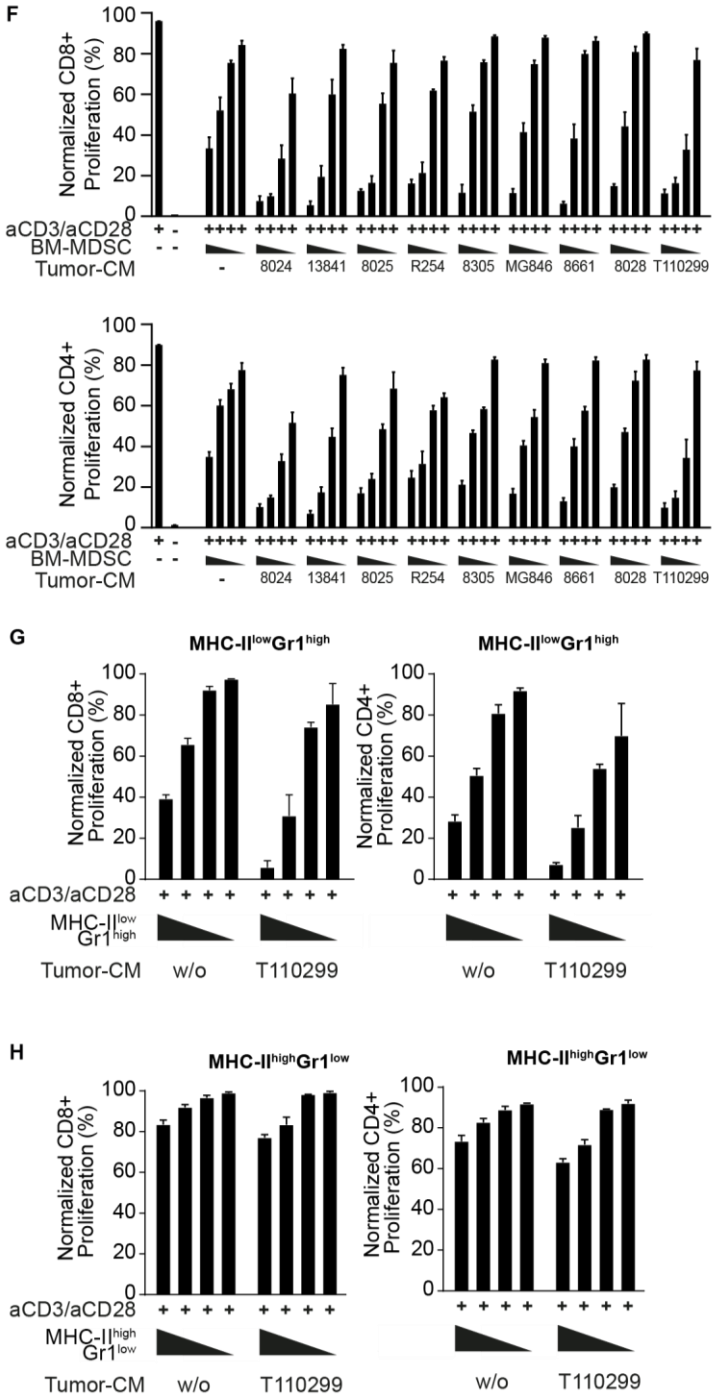

Figure 9: Tumor-derived factors increase MDSC-like cell frequency in bone marrow culture.

Bone marrow cells from C57BL/6 mice were cultured for 7 days in medium supplemented with GM-CSF and tumor-conditioned medium (CM) derived from pancreatic cancer cell lines (A). After 7 days, cells were analyzed by flow cytometry (B, C). Cytokine concentration in CM was measured by ELISA (D). G-CSF concentration in CM was correlated to MDSC and BMDC frequency in bone marrow culture (E). 7-days cultured bone marrow cells were co-cultured with CFSE-labeled T cells and the proportion of proliferated $CFSE^{low}$ $CD8^{+}$ and $CD4^{+}$ T cells was analyzed by flow cytometry (F). After 7 days in culture, MHC-II^{low} $Gr1^{high}$ (G) and MHC-II^{high} $Gr1^{low}$ (H) cells were sorted by FACS and co-cultured with CFSE-labeled T cells. T cell proliferation was monitored. Statistical analysis was performed using spearman correlation (E). Representative graphs of two independent experiments with n=2, error bar represent mean +/- SD. n.d. not detectable.

3.3.2. Tumor-derived factors induce suppressive capacity of MDSC-like cells

To investigate the suppressive capacity of *in vitro* generated MDSC-like cells, cells from whole bone marrow cultures were co-cultured with anti-CD3/anti-CD28 beads-stimulated T cells. Bone marrow cells that were differentiated in the presence of tumor CM had a higher $CD4^+$ and $CD8^+$ T cell suppressive capacity as compared to controls (Fig. 9F).

As the frequency and composition of MDSC-like cells differs depending on the tumor-derived factors, $Gr1^{high}$MHC-II^{low} MDSC-like cells were isolated by FACsorting. As a control $Gr1^{low}$ MHC-II^{high} BMDC were isolated. As expected, MDSC-like cells had a higher suppressive capacity as compared to BMDC controls. MDSC-like cells cultured with T110299 CM showed the highest suppressive capacity (Fig. 9G, H).

In summary, GM-CSF-driven bone marrow culture recapitulates MDSC development and the suppression phenotype *in vitro*. Tumor-derived factors, such as G-CSF expand PMN-MDSC-like cells and induce a suppressive program in MDSC-like cells.

3.4 Therapeutic reprograming of MDSC via MDA5-based immunotherapy

RIG-I-like helicases (RLH) such as MDA5 and RIG-I are promising targets for the immunotherapy of pancreatic cancer as they induce immunogenic tumor cell death and activate the immune system [46, 47]. Little is known about the effect of the MDA5 ligand poly(I:C) on MDSC. As PMN-MDSC are highly enriched in T110299 tumor-bearing mice, the effect of systemic poly(I:C) treatment on MDSC was investigated.

3.4.1 Therapy with poly(I:C)$_c$ activates immune cells

KPC-derived T110299 tumors were induced orthotopically in C57BL/6 mice; 18 and 20 days later mice were treated with 50 µg poly(I:C) complexed with polyethylenimine (PEI) (poly(I:C)$_c$) intravenously (Fig. 10A). Poly(I:C)$_c$ treatment induced a significant reduction of the tumor weight ($p < 0.01$; Fig. 10B). PMN-MDSC frequency was reduced by the treatment. In contrast, the M-MDSC frequency increased in both tumor ($p < 0.01$) und spleen ($p < 0.05$) after two treatments (Fig. 10C and Fig. 13D). In the spleen, poly(I:C)$_c$ treatment induced MHC class I expression on both MDSC populations. A similar induction was seen for PMN-MDSC in the tumor microenvironment. In contrast, the expression of MHC class I of M-MDSC was already elevated in the tumor prior to therapy and no further induction was measured (Fig. 10D). Similarly, PD-L1 expression on

MDSC in the spleen was induced upon poly(I:C)$_c$ treatment. As shown before, PD-L1 levels of MDSC in tumor are elevated and no further induction was seen (Fig. 10E).

No significant change in the frequency of CD4$^+$ and CD8$^+$ T cells was observed in both spleen and tumor (Fig. 10F, G). However, expression of the early activation marker CD69 was significantly increased in both T cell subsets in both tumor and spleen (Fig. 10F, G). The frequency of PD-1-expressing T cells was not influenced by the treatment at this time point (Fig. 10H).

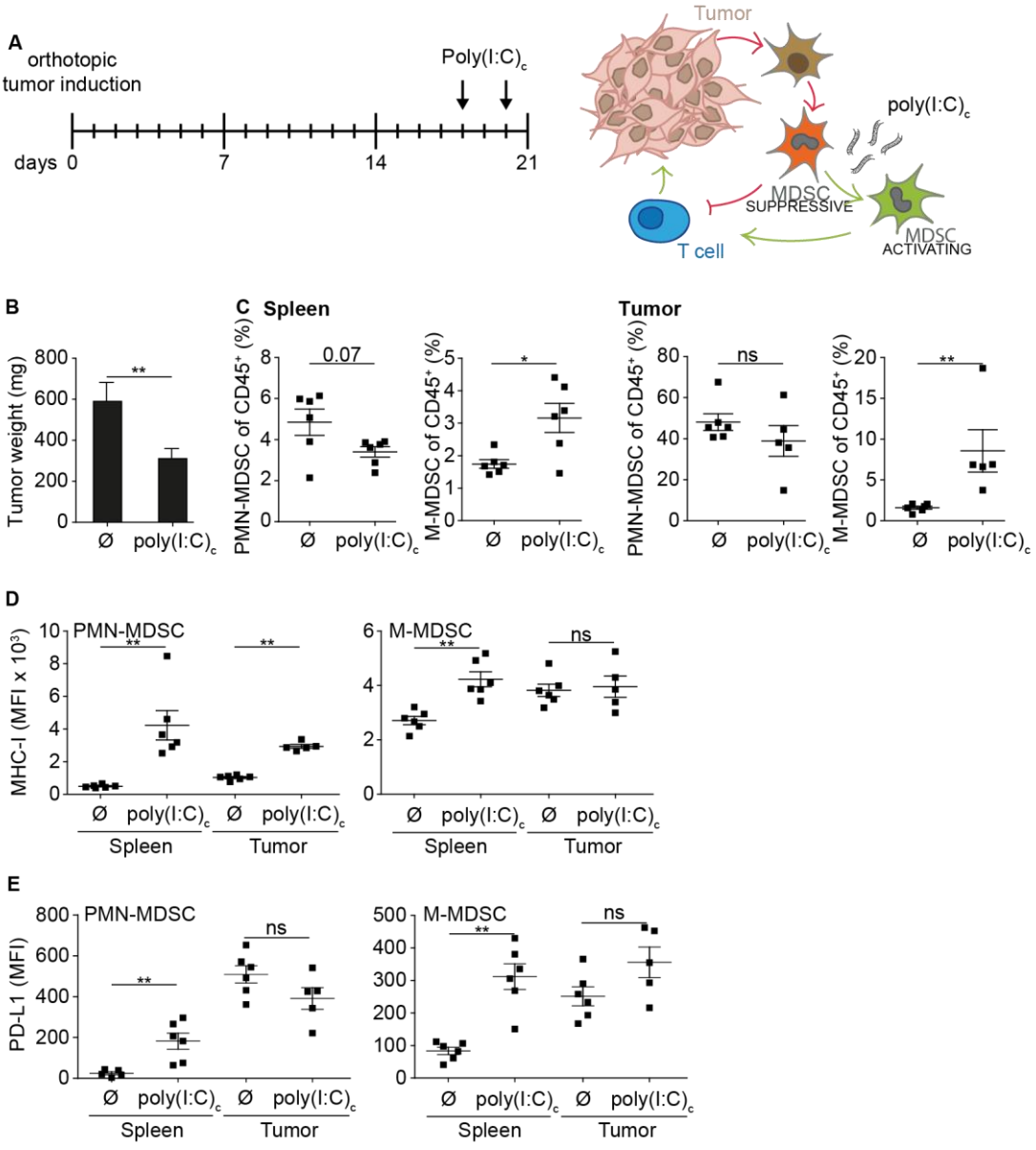

Figure 10: MDA5-targeted immunotherapy induces immune cell activation and tumor regression in PDAC-bearing mice (continued)

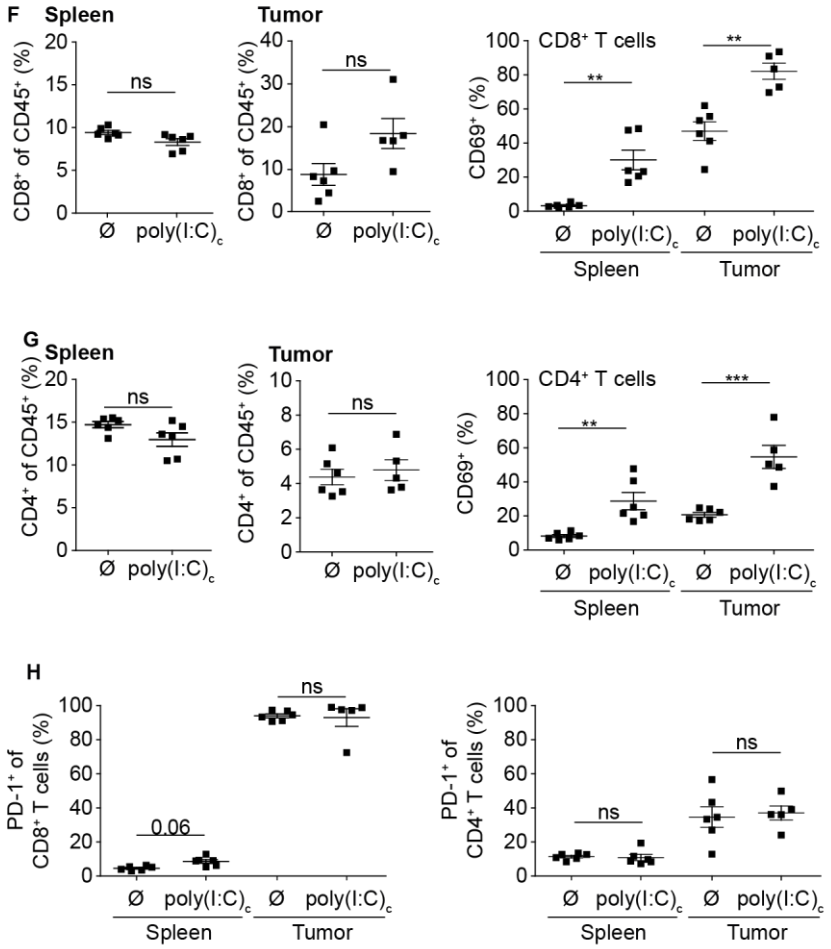

Figure 10: MDA5-targeted immunotherapy induces immune cell activation and tumor regression in PDAC-bearing mice

KPC-derived T110299 tumors were implanted orthotopically. After 18 and 20 days mice were treated with 50 µg of poly(I:C)$_c$ intravenously (A). After 21 days, tumor weight (B) was measured and immune cells were analyzed by flow cytometry (C-H). Differences between control and poly(I:C)$_c$ treatment was analyzed using Mann Whitney U test, error bars represent mean +/- SEM of n = 6, asterisks indicate * $p < 0.05$, ** $p < 0.01$, *** $p < 0.001$.

3.4.2 MDA5-targeted immunotherapy reduces suppressive capacity of MDSC

Next, the functional consequences of the poly(I:C)$_c$ treatment on MDSC was evaluated. Mice with PDAC were treated on day 18 and 20 after tumor implantation with poly(I:C)$_c$, MDSC were isolated from the spleens and tumors on day 21 and T cell suppressive capacity was assessed (Fig. 10A). As shown before, tumor-derived MDSC were more suppressive compared to splenic counterparts. Importantly, poly(I:C)$_c$ treatment reduced the suppressive capacity of both PMN-MDSC and M-MDSC from tumor as well as the spleen (Fig. 11).

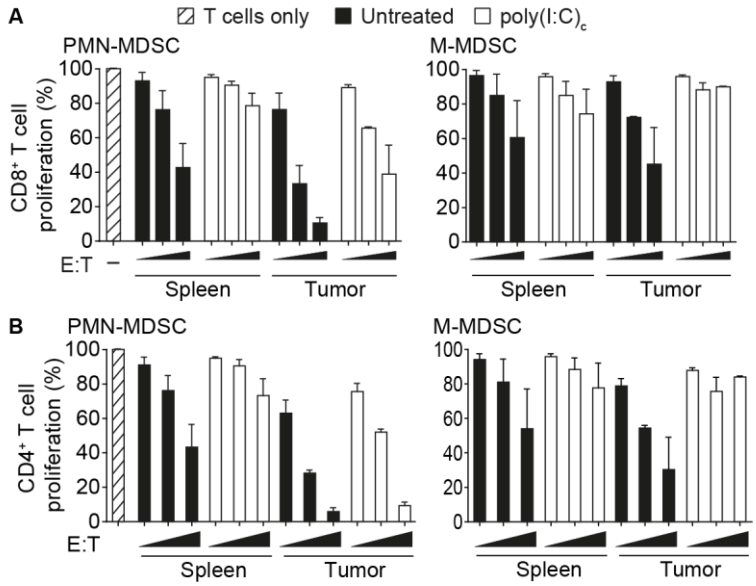

Figure 11: MDA5-targeted therapy reduces suppressive capacity of MDSC.
Mice were treated as shown in Fig. 10 A. After 21 days, MDSC were isolated, co-cultured with CFSE-labeled T cells and the proportion of proliferated CFSE^{low} CD8$^+$ (A) and CD4$^+$ (B) T cells was analyzed by flow cytometry. Representative graphs of two independent experiments are depicted, error bars represent mean +/- SEM of duplicates.

3.4.3 MDA5-targeted immunotherapy reprograms MDSC

To investigate the effects of poly(I:C)$_c$ treatment on MDSC in more depth, unbiased whole transcriptome analysis was performed. Mice with orthotopic PDAC were treated on day 18 and 20 after tumor implantation with poly(I:C)$_c$ or were left untreated (Fig. 10A). On day 21, MDSC were isolated followed by RNA extraction and next-generation sequencing. In all poly(I:C)$_c$ treated mice, CXCL10 levels in the serum were elevated after the first and second treatment, indicating good treatment response. In the spleen, MDSC purity was on average 96.8% (SD = +/- 3.7%) and in the tumor the purity was on average 93.1% (SD = +/- 6.3). RNA yield ranged from 6.8 ng to 353.8 ng. Ribosomal RNA integrity was studied by Bioanalyzer 2100 and found adequate, as indicated by a

RIN value above 7 (Fig. S3). Tumor cell contamination in the MDSC samples was evaluated by measuring the expression of tumor cell-restricted genes such as cytokeratin 8, 18 and 19. As expected, there was no tumor cell contamination in splenic MDSC. The concentration of tumor cell-restricted RNA was <1% and equally distributed in MDSC samples, indicating low tumor cell contamination (Fig. S3).

First, an unbiased principle component analysis (PCA) using the 20.000 most expressed genes was performed. For both PMN-MDSC and M-MDSC, the replicates of each condition clustered closely, confirming the high quality of the data. For both MDSC types, PCA revealed that the first principle component (PC1) distinguishes the samples based on the compartment from which they were isolated. In PMN-MDSC 35.5% (PC1) of the variance between all samples contributed to the separation between spleen and tumor. In M-MDSC 20.4% of the variance could be attributed to the compartment where the cells were isolated from. The second principle component describes the changes that were induced by the poly(I:C)$_c$ treatment (PC2 9.5% and 14.4% for PMN-MDSC and M-MDSC, respectively) (Fig. 12A).

Next, the treatment-induced transcriptomic changes were analyzed by performing a differential gene expression analysis. As the change in suppressive capacity after poly(I:C)$_c$ treatment was observed in both spleen and tumor, genes were selected that were significantly differentially expressed in both organs (adjusted $p < 0.05$, fold change > 2). As shown in Fig. 12B, 116 genes were differentially expressed in PMN-MDSC from both compartments. In M-MDSC 134 genes were differentially expressed in both spleen and tumor. Functional annotation analysis using the Database for Annotation, Visualization and Integrated Discovery (DAVID) was performed with differentially expressed genes from both spleen and tumor. Genes were found to be significantly enriched in gene ontology biological process (GO:BP) clusters related to immune system processes, virus and type I IFN response-related pathways as well as to antigen presentation gene sets (Fig. 12C).

The expression levels of the genes contributing to the functional annotation analysis from the spleen are depicted in Fig. 12D. Antigen presentation-associated genes of the H2 complex and viral sensors such as genes of the 2'-5'-oligoadenylate synthetase (OAS) and IFN-induced protein with tetratricopeptide repeats (IFIT) family were enriched. Interestingly, one of the GO:BP terms in M-MDSC was embryonic hematopoiesis with *Runx1*, *Pbx1* and *Ahr* being down-regulated upon poly(I:C)$_c$ treatment (Fig. 12D). The

expression levels of the genes contributing to the functional annotation analysis from both spleen and tumor are depicted in Fig. S4.

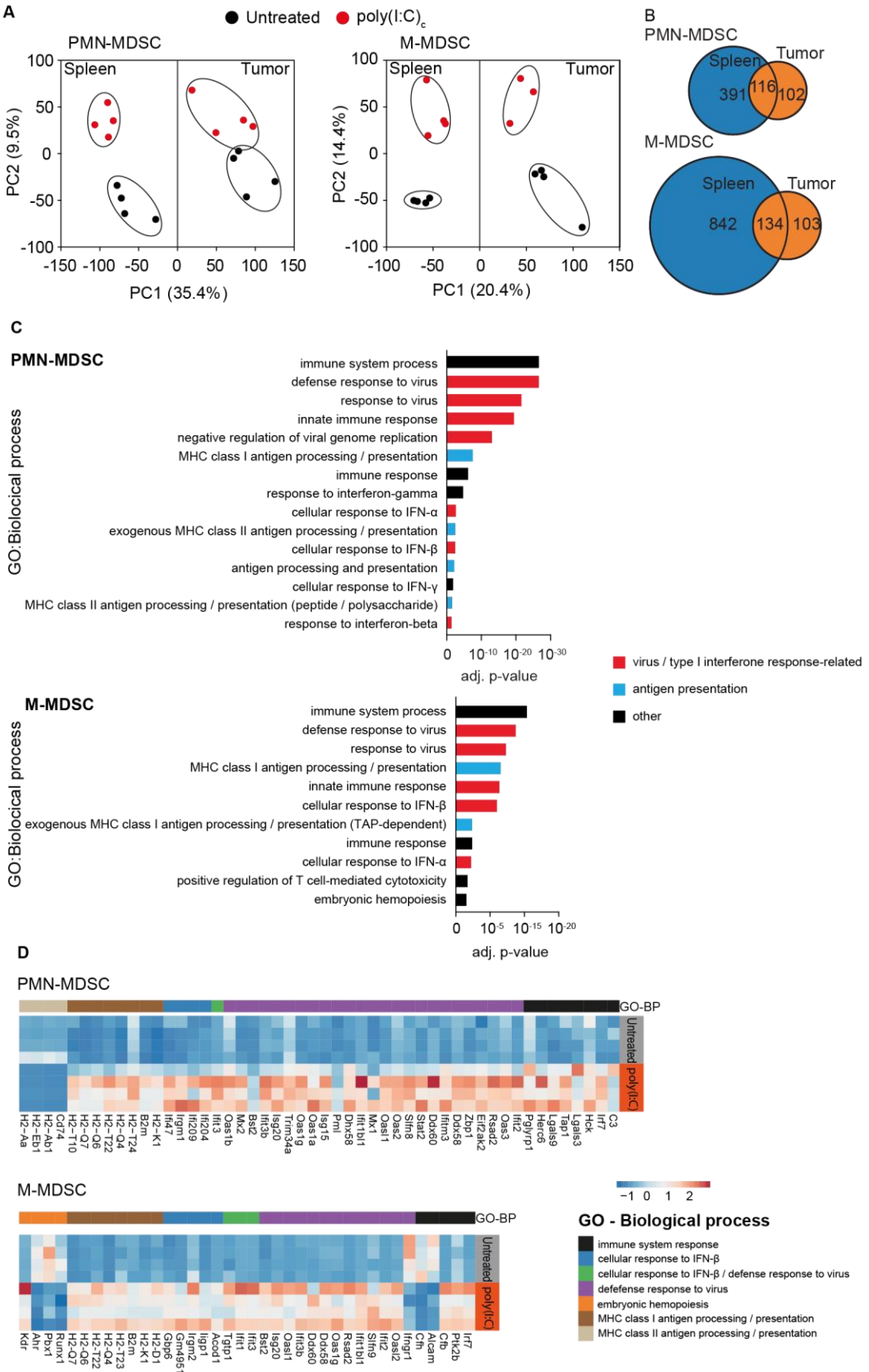

Figure 12: MDA5-targeted immunotherapy induces a type I IFN-dominated reprograming of MDSC.

Figure 12: MDA5-targeted immunotherapy induces a type I IFN-dominated reprograming of MDSC.
Mice were treated as shown in Fig. 10A. After 21 days, MDSC were isolated and the transcriptome was analyzed by RNA sequencing. A) Unbiased principal component analysis (PCA) of the 20.000 most expressed genes was performed. B) Number of differentially expressed genes in spleens and tumors from poly(I:C)$_c$ treated or untreated mice are depicted in a Venn diagram. C) DAVID functional gene annotation using the gene ontology biological processes (GO:BP) terms was performed. Significantly enriched GO:BP terms (adjusted $p < 0.05$) are depicted (C). Expression level of shared genes contributing to one of the GO:BP terms are shown in a heat map (D).

3.4.4 Immune activation induced by MDA5-targeted therapy is IFNAR-mediated

Poly(I:C)$_c$ treatment is known to induce a type I IFN response and the transcriptomic profile of MDSC in treated mice confirmed a predominant type I IFN response. Therefore, the role of type I IFN signaling upon poly(I:C)$_c$ treatment in MDSC was assessed using type I IFN receptor (IFNAR)-deficient mice. As shown in Fig. 13A, the same approach as before was used to investigate the role of type I IFN signaling.

In line with previous data, tumor weight was significantly decreased in wild-type mice after poly(I:C)$_c$ treatment ($p < 0.05$). No significant difference in tumor weight was observed in IFNAR-deficient mice, supporting the role of type I IFN in the anti-tumor effect (Fig. 13B). Both wild-type and IFNAR-deficient mice secreted similar levels of CXCL10 upon poly(I:C)$_c$ treatment. In wild-type mice serum IL-6 levels were significantly elevated upon poly(I:C)$_c$ treatment ($p < 0.01$). In contrast, there was no significant IL-6 induction upon poly(I:C)$_c$ treatment in *Ifnar*$^{-/-}$ mice, placing IL-6 production downstream of IFN signaling (Fig. 13C).

Poly(I:C)$_c$ treatment led to a significant decrease of PMN-MDSC and an increase of M-MDSC frequency in the spleen of wild-type mice ($p < 0.01$). However, there was no significant change in the frequency of PMN-MDSC or M-MDSC in *Ifnar*$^{-/-}$ mice (Fig. 13D). In contrast to wild-type mice, there was no induction of MHC class I or PD-L1 upon poly(I:C)$_c$ treatment in splenic MDSC of *Ifnar*$^{-/-}$ mice, pointing towards a critical role of type I IFN in MDA5-based therapy induced changes in MDSC numbers and phenotype (Fig. 13E, F).

Next, influence of MDA5-based therapy on the T cell frequency and expression of the activation marker CD69 was assessed. CD4$^+$ and CD8$^+$ T cell frequency in spleen and tumor was neither influenced by the genotype nor the treatment (Fig. 13G, H). As observed earlier, in wild-type mice poly(I:C)$_c$ treatment induced upregulation of CD69

expression in T cells. However, no significant increase of CD69 expression was found in $CD4^+$ or $CD8^+$ T cells in *Ifnar*$^{-/-}$ mice (Fig. 13H-J).

Next, the role of type I IFN signaling on suppressive capacity of MDSC was investigated. Interestingly, under steady state conditions the suppressive capacity of MDSC in *Ifnar*$^{-/-}$ mice was reduced (Fig. 13K, L). This points towards a role of tumor-intrinsic type I IFN in MDSC differentiation in PDAC. As seen before, T cell suppressive capacity of both MDSC subtypes was reduced upon poly(I:C)$_c$ treatment in wild-type mice. The suppressive capacity of both PMN-MDSC and M-MDSC of *Ifnar*$^{-/-}$ mice was not reduced upon poly(I:C)$_c$ treatment as seen in wild-type mice, rather a small increase was observed (Fig. 13K, L). Together these data argue for a dual role of type I IFN signaling on MDSC suppressive capacity, a suppression promoting effect in tumors under “steady state” and an inhibitory effect upon massive MDA5-induced IFN production.

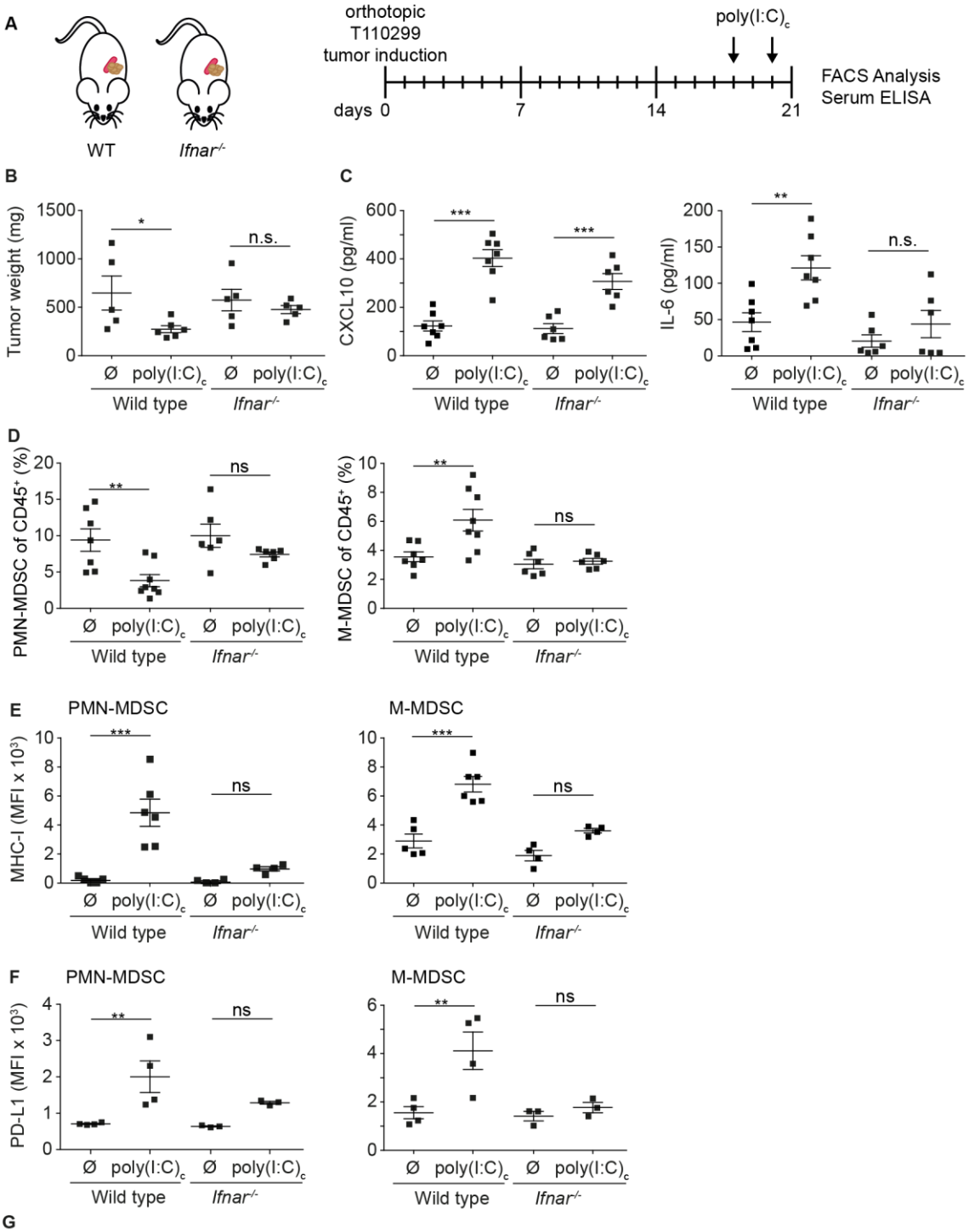

G

p value of Two-Way ANOVA

	tumor weight	CXCL10	IL6	PMN-MDSC of CD45+ in spleen	M-MDSC of CD45+ in spleen	MHC-I MFI of PMN-MDSC in spleen	MHC-I MFI of M-MDSC in spleen	PD-L1 MFI of PMN-MDSC in spleen	PD-L1 MFI of M-MDSC in spleen
genotype	0.53	0.08	0.002	0.09	0.003	0.005	0.0004	0.16	0.03
treatment	0.03	<0.0001	0.003	0.002	0.02	0.0004	<0.0001	0.003	0.02

Figure 13: Treatment efficacy and immune activation of MDA5-based immunotherapy is mediated by type I IFN signaling. (continued)

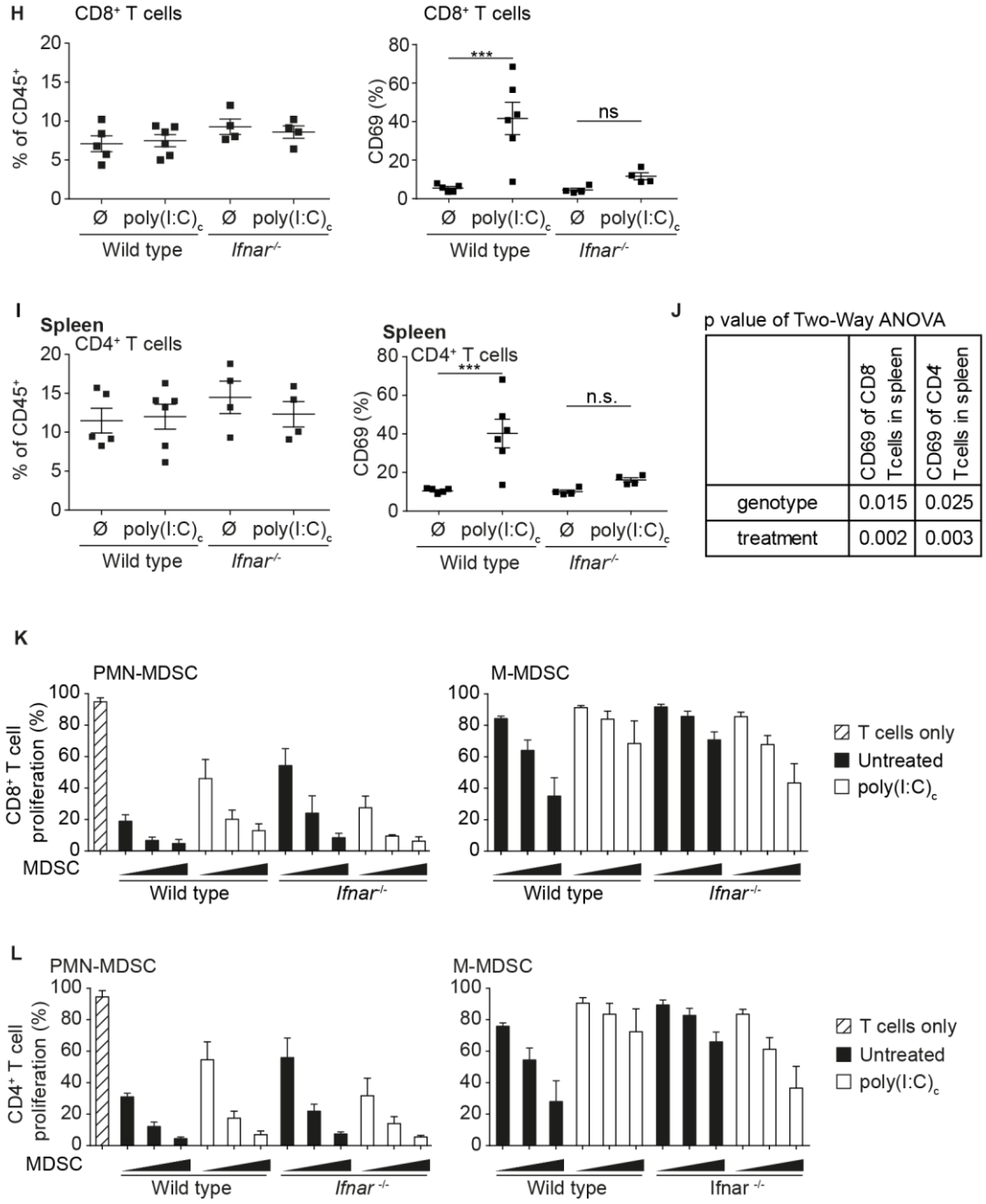

Figure 13: Treatment efficacy and immune activation of MDA5-targeted immunotherapy is mediated by type I IFN signaling.

A) KPC-derived T110299 tumors were implanted orthotopically in C57BL/6 wild-type and *Ifnar*$^{-/-}$ mice. After 18 and 20 days mice were treated with 50 µg poly(I:C)$_c$ intravenously. After 21 days, tumor weight (B) and serum levels of cytokines (C) were measured. Immune cells were analyzed by flow cytometry (C-F, H-I). MDSC were isolated, co-cultured with CFSE-labeled T cells and proportion of proliferated CFSE^{low} CD4 and CD8 T cells was analyzed by flow cytometry (K, L). A-I) Differences mediated by genotype and treatment were statistically analyzed using a 2-way ANOVA followed by a *post hoc* test between the two treatment groups (B-F, H-I). P values of 2-way ANOVA are reported in tables G and J. Results of *post hoc* tests are shown in each graph. K, L) Representative graphs of three independent experiments are depicted, error bars represent mean +/- SEM of duplicates. Asterisks indicate * $p < 0.05$, ** $p < 0.01$, *** $p < 0.001$.

3.4.5 MDSC are not capable of MHC class I antigen cross-presentation

In addition to IFN response, the second significantly enriched functional gene cluster in the RNA-Seq experiment was associated with MHC class I antigen presentation. The majority of genes annotated in the KEGG pathway of MHC class I-dependent antigen processing and presentation are up-regulated in both PMN-MDSC (Fig 14A) and M-MDSC (Fig 14B) upon poly(I:C)$_c$ treatment. To investigate the antigen processing and presentation capability of MDSC, T110299 tumors expressing the model non-self antigen ovalbumin (OVA) were used. 18 and 20 days after tumor induction mice were treated with poly(I:C)$_c$ or were left untreated and MDSC from both tumor and spleen were isolated. Tumor-derived MDSC were co-cultured with OT-I T cells that uniformly express a T cell receptor specific for the MHC class I-restricted OVA peptide SIINFEKL and T cell proliferation was measured (Fig. 14C). Both MDSC types were unable to induce antigen-dependent CD8 T cell proliferation independent of treatment (Fig. 14D).

As the amount of OVA antigen may be limiting *in vivo*, we also evaluated the capability of MDSC to process and cross-present OVA protein *ex vivo*. Splenic MDSC were isolated from T110299-OVA tumor-bearing hosts that were treated as described above. MDSC were incubated overnight with OVA protein and subsequently co-cultured with OT-I T cells. Again, no increase of T cell proliferation was measurable after 72 h of co-culture with OVA-treated MDSC, independent of *in vivo* poly(I:C)$_c$ treatment (Fig. 14E).

To rule out that lack of cross-presentation is due to T cell inhibition by MDSC, the presentation of exogenously pulsed peptide was assessed. MDSC from T110299-OVA tumor bearing hosts with and without prior poly(I:C)$_c$ treatment were isolated, MHC-I molecules were loaded with SIINFEKL peptides *in vitro*, washed and subsequently co-cultured with OT-I T cells. Peptide-loaded MDSC were able to induce vigorous OT-I T cell proliferation. No differences were observed between MDSC of untreated or poly(I:C)$_c$ treated mice (Fig. 14F). Together, these data argue for a cross-presentation defect in MDSC populations that cannot be reverted by MDA5-based immunotherapy.

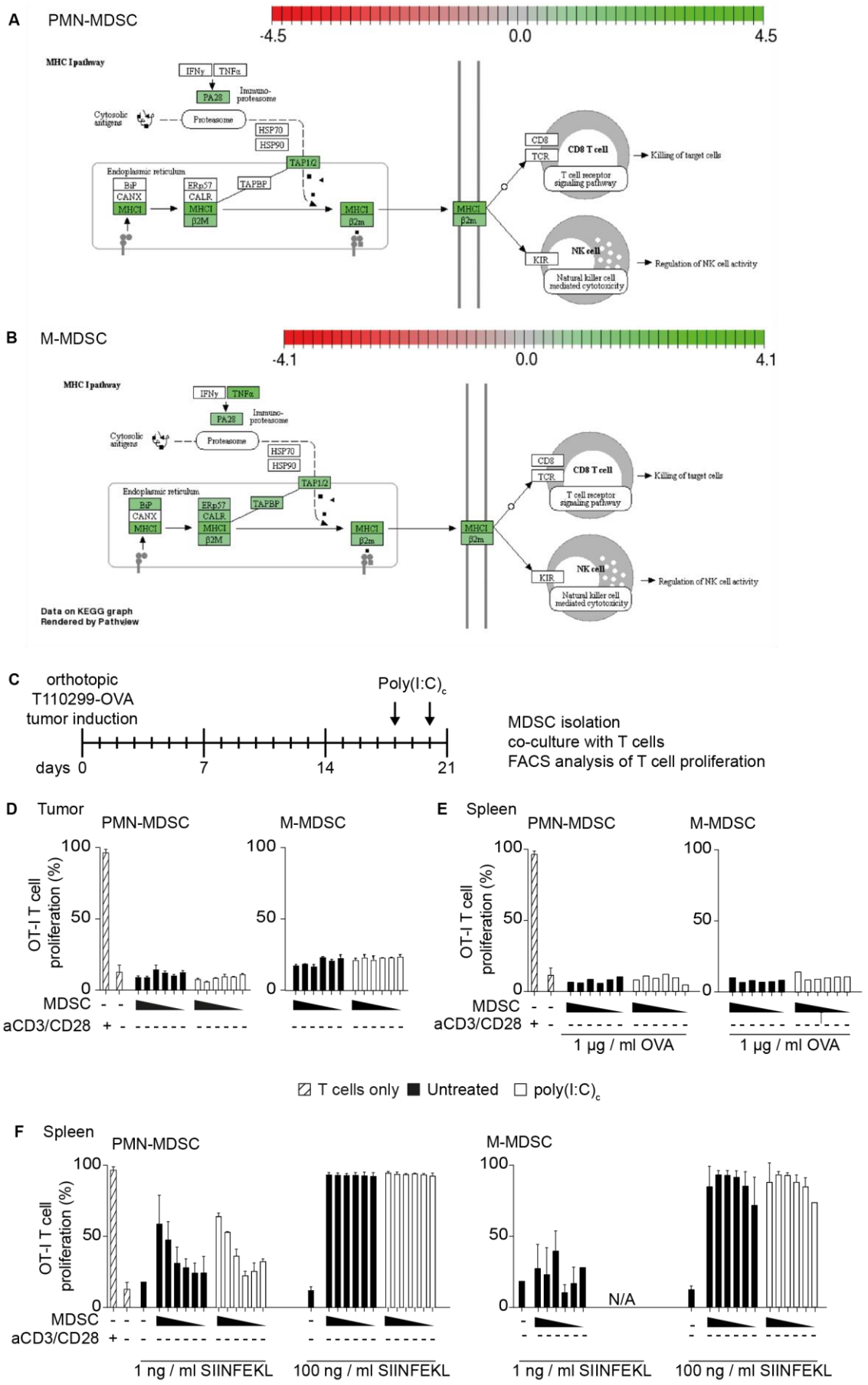

Figure 14: MDSC in mice with PDAC do not cross-present antigen to CD8 T cells.

Figure 14: MDSC in mice with PDAC do not cross-present antigen to CD8 T cells.
RNA-Seq revealed induction of genes associated with MHC-I pathway upon poly(I:C)$_c$ treatment. Genes annotated in KEGG MHC-I pathway are depicted for PMN-MDSC (A) and M-MDSC (B). Genes that are up-regulated and down-regulated upon poly(I:C)$_c$ treatment are shown in green and red, respectively (A,B). T110299-OVA tumors were implanted orthotopically in C57BL/6 mice. After 18 and 20 days mice were treated with poly(I:C)$_c$ (C). After 21 days, MDSC were isolated from tumor (D) and spleen (E, F). Tumor-derived MDSC were not manipulated *in vitro* (D). Splenic MDSC were either incubated over night with OVA protein (E) or were loaded with the SIINFEKL peptide (F). MDSC were co-cultured with CFSE-labeled TCR-transgenic OT-I T cells and the proportion of proliferated CFSE^{low} T cells was analyzed by flow cytometry (D-F). Representative graphs of two independent experiments are depicted, error bars represent mean +/- SEM of duplicates N/A = not analyzed.

3.5 Role of IRF4 in MDSC development and function

3.5.1 IRF4 is expressed by M-MDSC, but not by PMN-MDSC

Transcription factor IRF4 has been implicated to control macrophage M2 polarization and MDSC function [103, 104]. To study the role of IRF4 in MDSC in murine PDAC, IRF4 expression of PMN-MDSC as well as M-MDSC was analyzed in tumor-free and tumor-bearing mice by flow cytometry. IRF4 was expressed homogenously by M-MDSC in the blood, spleen and tumor independent of the tumor status. In contrast, IRF4 expression by PMN-MDSC in blood, spleen and tumor was close to the detection limit or absent (Fig. 15A, B).

Next, IRF4 expression of myeloid cells in the bone marrow culture was evaluated *in vitro*. IL-4 and IL-13 are known inducers of IRF4 [90]. $CD11b^+$ $CD11c^+$ BMDC expressed IRF4 and the expression could be further increased by stimulation with IL-4 and IL-13. IRF4 expression in PMN-MDSC-like cells and M-MDSC-like cells was low. IL-4 and IL-13 increased the expression of IRF4 in M-MDSC-like cells only (Fig. 15C).

3.5.2 IRF4 deficiency increases MDSC-like cell frequency *in vitro*

To evaluate the role of IRF4 in development and function of myeloid cells, bone marrow cells of wild-type and *Irf4*$^{-/-}$mice were cultured for seven days in the presence of GM-CSF and T cell suppressive capacity was measured. IRF4-deficient cells suppressed the T cell proliferation more potently compared to WT controls (Fig. 15D).

Next, the cellular composition of the bone marrow cultures was analyzed. The absolute cell count per culture dish as well as the relative frequency of MDSC-like cells was significantly increased in bone marrow cultures from *Irf4*$^{-/-}$ mice. The frequency of BMDC was significantly reduced and mature BMDC ($CD11b^+CD11c^+$MHC-II^{high}) were almost absent in cultures of *Irf4*$^{-/-}$mice (Fig. 15E). Thus, IRF4 controls proliferation and differentiation of MDSC-like cells from bone marrow precursors. As the difference in MDSC composition in the cultures may influence the outcome of the suppressive effect in T cell suppression assays, FACSorted $Gr1^{high}$MHC-II^{low} MDSC-like cells from wild-type and *Irf4*$^{-/-}$ mice were co-cultured with T cells in the presence of anti-CD3/anti-CD28 beads and T cell proliferation was measured. There was no significant difference in the T cell suppressive capacity of IRF4-deficient $Gr1^+$ MDSC-like cells compared to wild-type controls, arguing against a direct role of IRF4 in controlling the suppressive mechanism of MDSC-like cells (Fig. 15F).

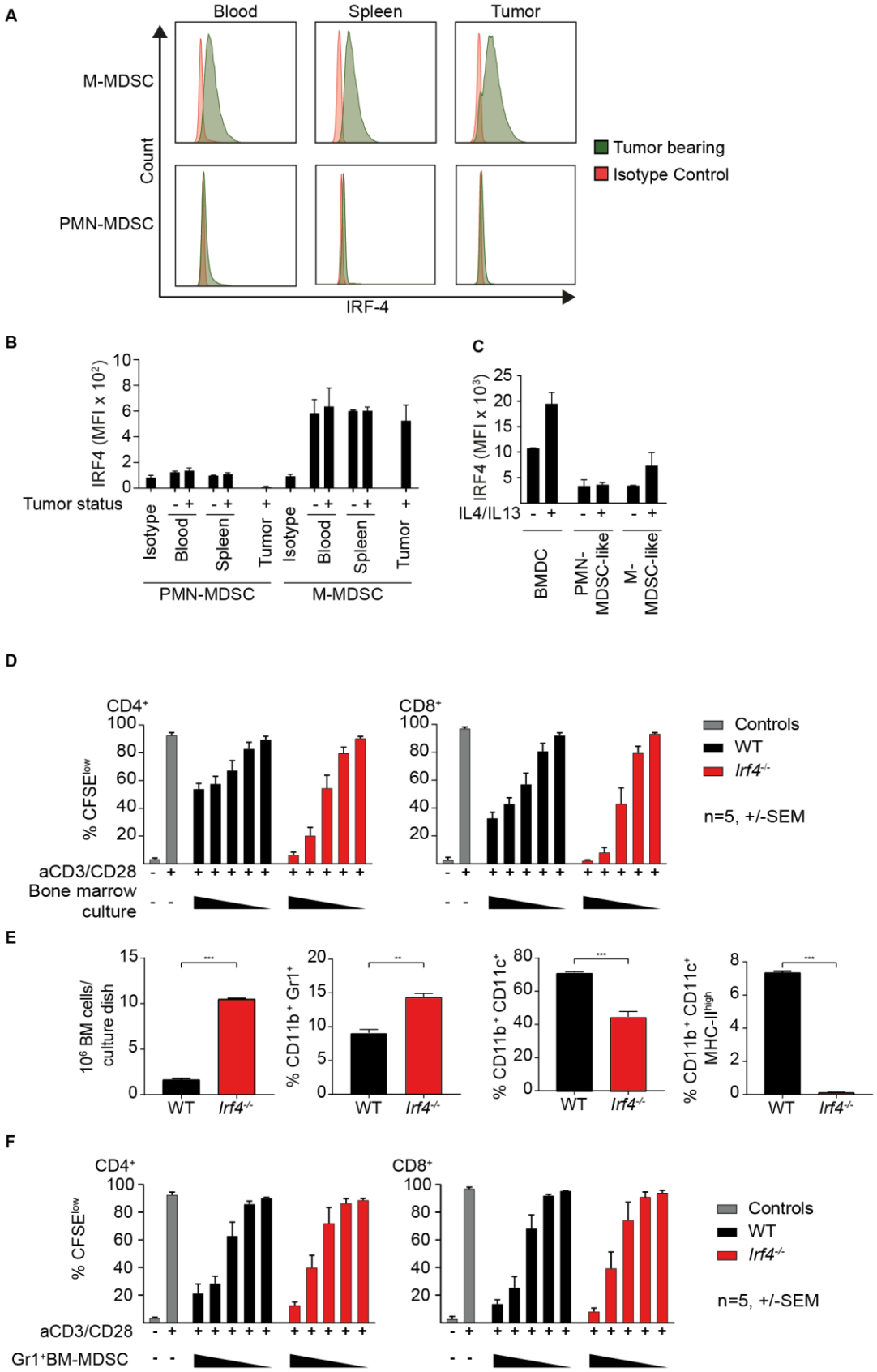

Figure 15: IRF4 deficiency leads to MDSC-like cell expansion in bone marrow cultures *in vitro* but does not influence their T cell suppressive function.

Figure 15: IRF4 deficiency leads to MDSC-like cell expansion in bone marrow cultures *in vitro* but does not influence their T cell suppressive function.
IRF4 expression of MDSC subsets from tumor-free and PDAC-bearing mice was analyzed by flow cytometry (A-B). IRF4 expression of myeloid cells from bone marrow cultures were analyzed by flow cytometry in the absence and presence of IL-4 and IL-13 (C). Bone marrow cells from wild-type (WT) and *Irf4*$^{-/-}$ mice were co-cultured with CFSE-labeled T cells and proportion of proliferated CFSE^{low} CD8^{+} and CD4^{+} (D) T cells was analyzed by flow cytometry. Absolute number of cells was counted, and relative cell frequency was analyzed by flow cytometry (E). Gr1^{high} MHC-II^{low} cell population of WT and IRF4-deficient bone marrow cultures were FACSorted, co-cultured with CFSE-labeled T cells and the proportion of proliferated CFSE^{low} CD8^{+} and CD4^{+} was determined (F). The difference between genotypes was statistically analyzed using Mann Whitney U test, error bars represent mean +/- SEM (n=3), asterisks indicate * $p < 0.05$, ** $p < 0.01$ and *** $p < 0.001$.

3.5.3 Global IRF4 deficiency accelerates PDAC tumor growth

To study the role of IRF4 *in vivo*, KPC-derived T110299 tumors were induced orthotopically in *Irf4*$^{-/-}$ mice. Three weeks after tumor induction, tumor weight in *Irf4*$^{-/-}$ mice was significantly increased compared to wild-type controls (Fig. 16A). Moreover, the survival of tumor-bearing *Irf4*$^{-/-}$ mice was significantly reduced (Fig. 16B). In both blood and spleen of *Irf4*$^{-/-}$ mice, PMN-MDSC frequency was significantly increased, with no significant change in the tumor (Fig. 16C). Similarly, M-MDSC frequency was significantly increased in the blood and spleen of *Irf4*$^{-/-}$ mice. There was no significant change in M-MDSC frequency in the tumor (Fig. 16D).

As the MDSC frequency depends on tumor weight (Fig. 6D) and both MDSC frequency and tumor weight were elevated in *Irf4*$^{-/-}$ mice, MDSC frequency was correlated to the tumor weight for both genotypes separately (Fig. S5). As observed before in wild-type mice, there was a good correlation of tumor size and MDSC frequency in blood and spleen. Thus, accelerated tumor growth may determine the MDSC phenotype observed in *Irf4*$^{-/-}$ mice.

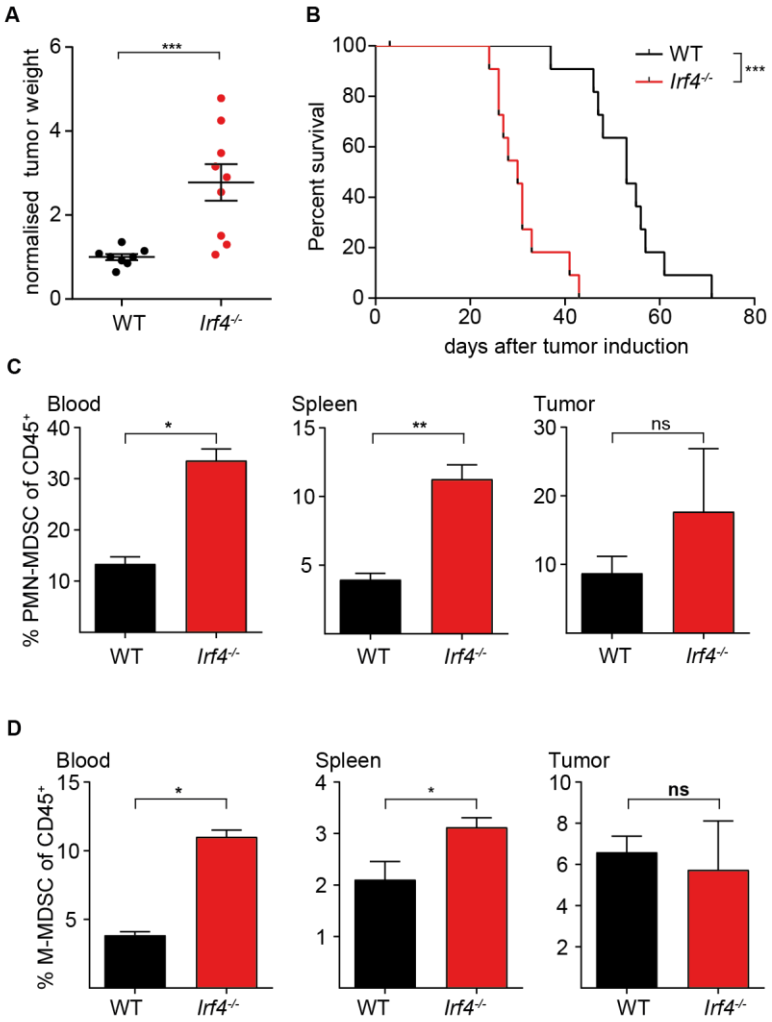

Figure 16: IRF4 deficiency accelerates PDAC tumor growth and expansion of MDSC populations in blood and spleen.
T110299-derived PDAC were induced orthotopically in *Irf4*$^{-/-}$ and wild-type (WT) mice. After 21 days, tumor weight was measured (A) and MDSC cell frequency in blood, spleen and tumor was analyzed by flow cytometry (C, D). Survival of orthotopic PDAC-bearing mice was monitored (B). Differences between genotypes were statically analyzed using the Mann Whitney U test (A, C, D) or Log rank test (B). Shown are pooled data from 2-3 independent experiments, error bars represent mean +/- SEM (n=5-8 mice/group), asterisks indicate * $p < 0.05$, ** $p < 0.01$, *** $p < 0.001$.

3.5.5 MDSC from IRF4-deficient mice show higher T cell suppressive capacity

To study the functional consequences of IRF4 deficiency on myeloid cells, PDAC were induced in both *Irf4*$^{-/-}$ and wild-type mice. Three weeks later MDSC were isolated from the spleen, co-cultured with T cells and T cell proliferation was measured. PMN-MDSC as well as M-MDSC from *Irf4*$^{-/-}$ mice showed a higher suppressive capacity compared to wild-type controls (Fig. 17).

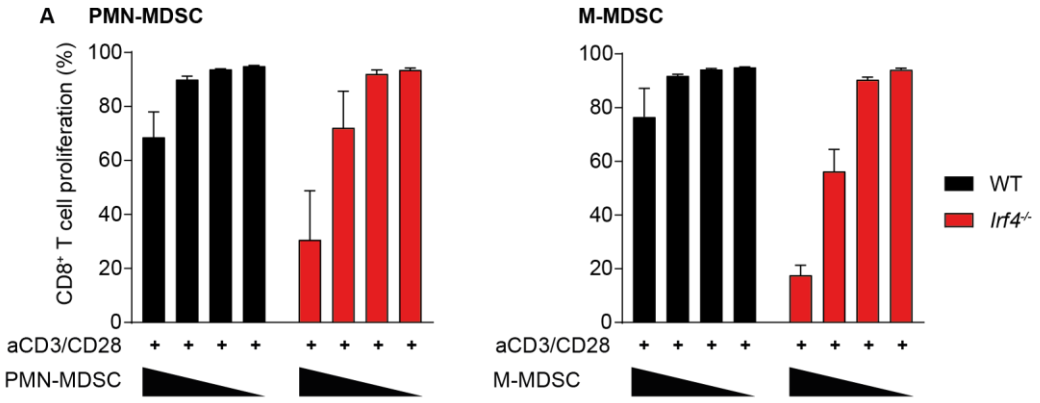

Figure 17: MDSC from IRF4-deficient mice have higher suppressive capacity 21 days after tumor induction.
T110299 tumors were induced orthotopically in *Irf4*$^{-/-}$ and wild-type (WT) mice. After 21 days, MDSC populations were isolated from the spleen, co-cultured with CFSE-labeled T cells and proportion of proliferated CFSE^{low} T cells was analyzed by flow cytometry (A). Representative graphs of three independent experiments are shown, error bars represent mean +/- SEM (n=3).

3.5.6 Myeloid-specific depletion of IRF4 accelerates PDAC growth

IRF4 is expressed by many cells of the immune system, including T cells, B cells and DC. To study the intrinsic role of IRF4 solely in myeloid cells, two conditional mouse models were established. Ly6G^{Cre} mice, in which floxed target sites are specifically deleted in polymorphonuclear cells (including PMN-MDSC) [123], and LysM^{Cre} mice, in which floxed target sites are specifically deleted in granulocytes, monocytes, macrophages and partly DC (including PMN-MDSC and M-MDSC) [124], were cross-bred with Irf4^{flox} mice. Irf4^{flox} mice were designed to express GFP instead of IRF4 upon successful Cre recombination under the same physiological control as IRF4. Therefore, the conditional IRF4 knockout mice can be used as reporter mice. First, expression of GFP was confirmed by flow cytometry. As expected, M-MDSC of the *LysM*^{Cre}*Irf4*$^{fl/fl}$ mice were positive for GFP in the blood, spleen and tumor. There was no GFP detectable in PMN-MDSC as well as M-MDSC of the *Ly6G*^{Cre}*Irf4*$^{fl/fl}$ mice (green, Fig. 18A). In contrast, in *LysM*^{Cre}*Irf4*$^{fl/fl}$ mice there was a small fraction of approximately 15 % of PMN-MDSC in blood, spleen and tumor that were positive for GFP (Fig. 18A).

Next, the impact of myeloid-targeted IRF4 deficiency on PDAC tumor growth was investigated. KPC-derived T110299 tumors were orthotopically induced in *Ly6G*^{Cre}*Irf4*$^{fl/fl}$ mice, *LysM*^{Cre}*Irf4*$^{fl/fl}$ mice as well as *Irf4*$^{fl/fl}$ control mice. There was no significant difference between *Ly6G*^{Cre}*Irf4*$^{fl/fl}$ and control mice. In contrast, tumor weight was significantly increased in *LysM*^{Cre}*Irf4*$^{fl/fl}$ mice compared to IRF4$^{fl/fl}$ control mice (Fig. 18B). For both myeloid-specific IRF4-deficient mice, there was no survival disadvantage

compared to *Irf4*$^{fl/fl}$ controls (Fig. 18C). Three weeks after tumor induction MDSC frequencies were analyzed by flow cytometry. There was no significant difference in PMN-MDSC in blood, spleen and tumor of *LysM*^{Cre}*-Irf4*$^{fl/fl}$ mice and *Ly6G*^{Cre}*Irf4*$^{fl/fl}$ mice compared to *Irf4*$^{fl/fl}$ controls. M-MDSC frequency was significantly increased in the spleen of *LysM*^{Cre}*Irf4*$^{fl/fl}$ mice. However, no difference in M-MDSC frequency was detectable in the blood or tumor of the myeloid cell-specific IRF4-deficient mice (Fig. 18D).

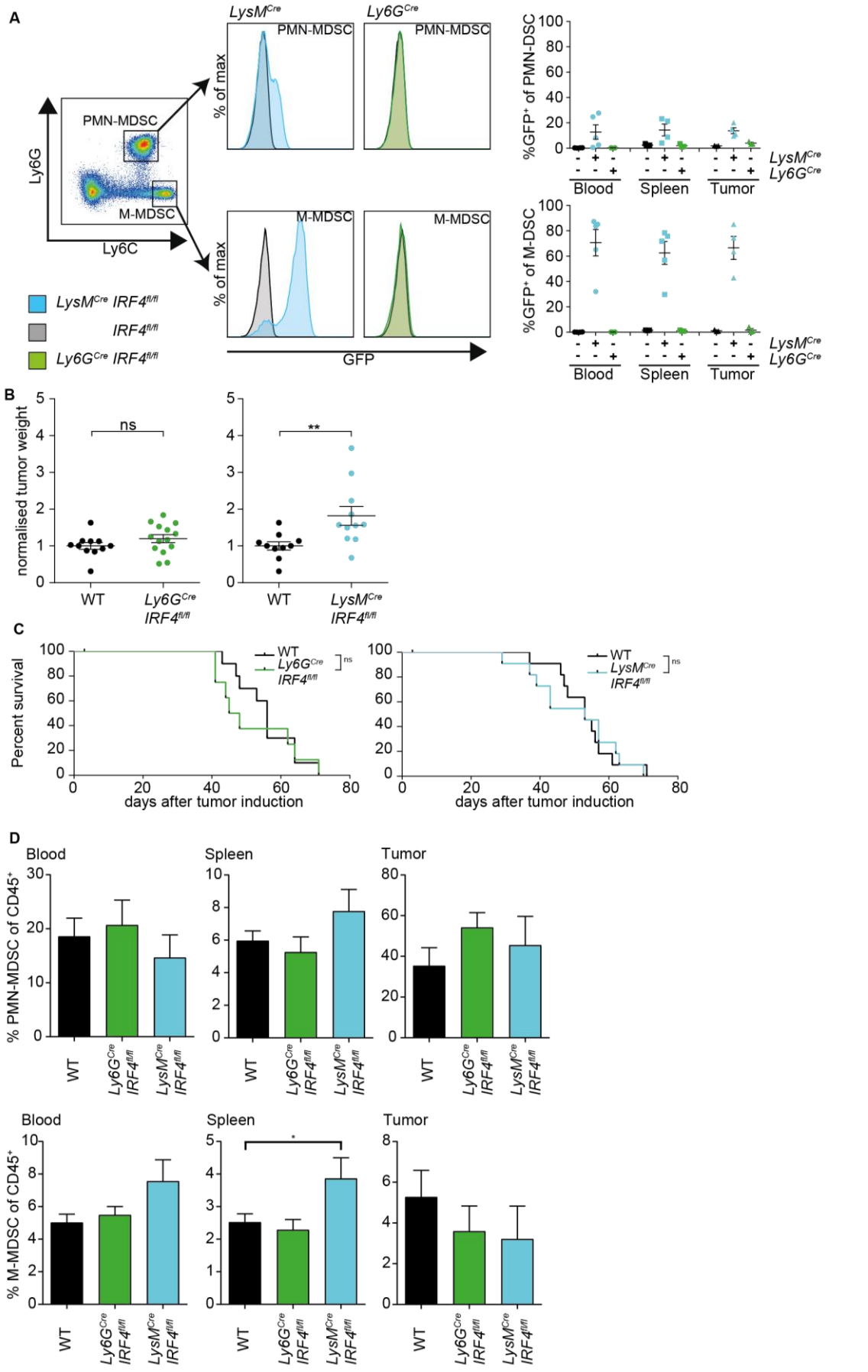

Figure 18: Targeted deletion of *Irf4* in *LysM^{Cre}* but not *Ly6G^{Cre}* mice increases tumor growth but has no influence on survival.

Figure 18: Targeted deletion of Irf4 in LysMCre but not Ly6GCre mice increases tumor growth but has no influence on survival.
KPC-derived T110299 tumors were induced orthotopically in Ly6GCre Irf4fl/fl (green), LysMCre Irf4fl/fl (blue) and Irf4fl/fl (black) mice. After 21 days, GFP expression of MDSC was analyzed by flow cytometry (A), tumor weight was measured (B) and MDSC frequency was analyzed by flow cytometry (D). Survival of PDAC-bearing mice was monitored (C). Statistical analysis was performed using Kruskal Wallis test, followed by Dunn's multiple comparisons test between controls and conditional knock-out mice. Pooled data from 3 independent experiments are depicted, error bars represent mean +/- SEM (n=8-14 mice/group), p value of Dunn's test are shown in the graph, asterisks indicate * $p < 0.05$.

4. Discussion

4.1 PDAC induce an immunosuppressive program in myeloid cells

In the first part of the study, the immune cell composition in the KPC-derived T110299 tumor model was characterized. We found that in PDAC-bearing hosts the myeloid compartment in blood, lymphoid organs and tumor is expanded and an immunosuppressive program is induced. Similar findings could be recapitulated *in vitro* using a bone marrow culture system.

In the first three weeks of tumor growth, the relative intratumoral immune cell composition changed and three waves of different immune cell infiltrates could be described: One week after tumor induction, innate immune cells such as NK cells and Ly6C$^+$ monocytes were the dominant cell type. After two weeks, the tumor stroma was dominated by CD8$^+$ and CD4$^+$ T lymphocytes. After three weeks, the relative frequency of T cells dropped and PMN-MDSC were significantly enriched. This situation closely mirrors the human situation, as myeloid cells typically densely infiltrate human PDAC tissue and T cells are rarely found [36]. Therefore, knowledge of the intratumoral immune cell composition is important when investigating immunotherapy in orthotopic PDAC models. The tumor microenvironment of advanced tumors around day 21 reflects the human situation best, however, experimental treatments in transplantable tumor models commonly start between day 5 and 10 [47]. In this early phase the tumor microenvironment is dominated by NK cells and T lymphocytes and thus may more easily respond to immunotherapy. For studying the role of poly(I:C)$_c$ on MDSC polarization and function in this study, mice were treated on day 18 and 20 and therefore, the immune cell composition should more closely mirror the human situation.

We found that CD8$^+$ T cells infiltrating T110299 tumors were strongly expressing the checkpoint molecule PD-1. Li et al. showed that the frequency of PD-1$^+$ cells among CD8$^+$ T cells in the tumor of KPC-derived models correlates with response to immunotherapy [20]. Therefore, the T110299 orthotopic tumor model is an interesting model for studying immunotherapy of PDAC.

Both, G-CSF and GM-CSF are growth factors implicated in MDSC expansion in PDAC [118, 119]. We showed that GM-CSF was not detectable in the serum of T110299 tumor-bearing mice. In contrast, G-CSF levels were highly elevated and correlated significantly

with PMN-MDSC frequency in blood and spleen. Furthermore, G-CSF levels secreted by different KPC-derived PDAC cell lines *in vitro* correlated with PMN-MDSC-like cell frequency in bone marrow cultures. Bayne et al. showed that GM-CSF levels are elevated in the tumor microenvironment of spontaneous KPC tumors. Furthermore, they showed that GM-CSF depletion reduced the recruitment of $Gr1^+$ MDSC [118]. Interestingly, they did not report on GM-CSF levels in serum. Therefore, the role of GM-CSF in inducing a systemic expansion of the myeloid compartment by acting on myeloid precursors in the bone marrow is not yet clear. Welte et al. showed that in breast cancer G-CSF regulates PMN-MDSC accumulation [125]. Li et al found that both CXCL1 and G-CSF are important regulators of MDSC recruitment in the tumor stroma in pancreatic cancer [20]. Both cytokines appear to be key hurdles for successful immunotherapy [126]. Further studies are needed to dissect the local and systemic role of GM-CSF and G-CSF in mice with PDAC.

Myeloid cells in the orthotopic T110299 model fulfill all three criteria that have been defined recently by the leading scientists in the field to classify MDSC [18]: Firstly, the myeloid compartment is expanded in T110299-bearing mice and bone marrow cultures supplemented with tumor conditioned medium. Secondly, both PMN-MDSC ($CD11b^+Ly6G^+Ly6C^{low}$) and M-MDSC ($CD11b^+Ly6G^-Ly6C^{high}$) express the surface markers for definition. Thirdly, both MDSC subtypes acquire T cell suppressive activity in tumor-bearing host or when cultured in the presence of tumor-conditioned medium [127]. The GM-CSF-driven bone marrow culture supplemented with tumor-conditioned medium resembles the characteristics of MDSC differentiation *in vivo* and could therefore be a valuable tool for studying MDSC differentiation and function *in vitro*.

In humans, it has been shown that cancer patients bear distinct subsets of granulocytes and PMN-MDSC [63]. To date, no marker has been identified to distinguish PMN-MDSC from granulocytes in mice. In renal cell carcinoma more than 17 subtypes of TAMs have been proposed by mass cytometry [128]. Recent advances in high dimensional single cell analysis methods such as mass cytometry and single cell transcriptomic analysis (scRNA-Seq), will improve the understanding of myeloid subpopulations and will facilitate the identification of additional therapeutic targets of pro-tumoral and anti-tumoral myeloid cells.

4.2 Anti-PD-1 antibodies cross-react with an unknown marker in dying cells

In this study, we showed that the anti-PD-1 antibody clone 29F1A12 cross-reacts with an antigen in cell death marker-positive MDSC, $CD4^+$ T cells and B3Z T cell hybridoma cells. In genetic deletion studies using primary cells as well as cell lines, we confirmed that this staining of dead cells with anti-PD-1 mAb is due to unspecific binding to an unknown intracellular antigen. In further experiments we were able to show that B16F10 melanoma cells that were reported to express PD-1 [129] do not express PD-1, but instead the anti-PD-1 antibody stained a distinct nuclear antigen in dead cells, characterized by low forward scatter characteristic and positive staining with cell death dyes [130]. A similar staining pattern was observed with another anti-PD-1 antibody clone, namely RMP1-14 [130]. Thus, the antibody-binding epitopes of PD-1 and the unknown nuclear antigen seem to share similar motifs.

This study is questioning the results of several other studies, describing PD-1 expression in non-T cells, such as MDSC and tumor cells [79, 129]. We conclude that flow cytometric data obtained with the anti-PD-1 antibody clones 29F1A12 and RMP1-14 have to be carefully analyzed. Small, death cell marker positive cells have to be strictly excluded to avoid false conclusions.

4.3 MDA5-based immunotherapy reprograms MDSC in PDAC-bearing mice

In this study, we showed that MDA5-based immunotherapy with poly(I:C)$_c$ reprograms MDSC leading to a reduced suppressive capacity. In this respect, type I IFN appears to be the key driver of modulated MDSC function *in vivo*. MDA5 activation is known to induce a type I IFN driven immune response [47]. Whole transcriptome sequencing of poly(I:C)$_c$ treated MDSC and experiments with poly(I:C)$_c$ treated IFNAR-deficient mice confirmed the pivotal role of type I IFN in MDSC biology and the role in poly(I:C)$_c$ treatment.

Here, we showed that poly(I:C)$_c$ treatment reduced the number of splenic PMN-MDSC whereas the M-MDSC frequency in spleen and tumor were increased upon treatment. The changes in immune cell frequency were strictly dependent on IFNAR signaling, as shown in IFNAR-deficient hosts. In line with these findings, Dangi et al. recently reported that $CD11b^+Ly6C^{high}$ M-MDSC were increased whereas $CD11b^+Gr1^{high}$ PMN-MDSC

were reduced in an acute type I IFN-driven virus infection model [131]. IFN-α is reported to act on bone marrow myeloid progenitor cells to shift the development from granulocytic to monocytic cells [131]. This suggests that systemic RLH activation might interfere with the development of MDSC in the bone marrow.

On both MDSC subtypes in spleen, activation markers such as MHC-I and PD-L1 were upregulated upon poly(I:C)$_c$ treatment. The induction was less pronounced in the tumor tissue. The upregulation of MHC-I and PD-L1 upon poly(I:C)$_c$ treatment was strictly dependent on type I IFN signaling, as demonstrated with IFNAR-deficient mice. Xiao et at. found that autocrine type I IFN stimulation through constant JAK-STAT signaling in MDSC induces the expression of PD-L1 [76]. Interestingly, in steady state PD-L1 expression was not decreased in *Ifnar-/-* mice in the T110299 tumor model, arguing for other potential mechanisms leading to PD-L1 upregulation in intratumoral MDSC. Analysis of T cells in our model revealed induction of the early activation marker CD69 in both CD4$^+$ and CD8$^+$ T cells, which was also type I IFN mediated. These findings are in line with previous reports [132].

Importantly, we demonstrated that poly(I:C)$_c$ treatment reduced the suppressive capacity of both MDSC subtypes, suggesting that MDSC function may play a role in the anti-tumor effect of poly(I:C)$_c$-based therapy, which has been shown to be CD8$^+$ T cell-dependent [47]. In line with our data on poly(I:C)$_c$ treatment, Zoglmeier et al. showed that TLR9-based therapy reduces PMN-MDSC frequency and diminishes the suppressive capacity of MDSC [133]. Type I IFN induction is a shared down-stream effect of both RLH and TLR9 signaling [134].

Interestingly, the role of type I IFN signaling in the suppressive function of MDSC appears to have two opposing sides: The suppressive capacity of MDSC in *Ifnar-/-* mice was lower compared to wild-type controls, arguing for an important role of tumor autochthonous type I IFN in MDSC differentiation. Surprisingly, in contrast to wild-type mice, the suppressive capacity of MDSC in *Ifnar-/-* mice increased upon poly(I:C)$_c$ treatment from poor suppressors to moderate suppressors. These differences in the suppressive capacity point toward opposing roles of type I IFN, which cannot be separated in *Ifnar-/-* mice, as both effects are lacking. 1) Tumors including PDAC induce a chronic inflammation, which is accompanied by type I IFN production. It has been shown in other tumor models that DNA release by dying tumor cells triggers STING activation leading to a low-grade type I IFN induction [77]. 2) In contrast, poly(I:C)$_c$ treatment mimics an acute viral infection leading to high levels of type I IFN in a temporal

limited manner. Taleb et al. showed that chronic administration of recombinant IFN-α at a dose characteristic for a chronic viral infection induced T cell suppressive activity in Ly6C^{high} monocytes. In contrast, short high-dose treatment with IFN-α - mimicking an acute viral infection - did not induce T cell suppressive potential in Ly6C^{high} monocytes [135]. In this line, Zoglmeier et al. showed that high levels of recombinant IFN-α is sufficient to reduce the immunosuppressive function of MDSC from C26 tumor bearing mice [133].

Thus, based on our data and published reports, one can hypothesize that tumor autochthonous, low-dose type I IFN stimulation initiates a suppressive program in MDSC, which is particularly pronounced in the tumor microenvironment. In contrast, RLH-based therapy induces high-dose type I IFN, mimicking an acute viral infection, which leads to a reduction of suppressive capacity. RNA sequencing of untreated T110299 tumors could confirm upregulation of genes associated with a type I IFN response, when compared to normal pancreas (unpublished data). Recent analysis of human pancreatic resections identified a subtype of PDAC with a predominant type I IFN signature [136]. Further studies are needed to understand the functional status of MDSC from IFNAR-deficient hosts. This may provide further insights in type I IFN-independent mechanisms influencing the suppressive capacity of MDSC upon RLH-based immunotherapy.

Whole transcriptome analysis revealed potential antigen cross-presentation function of MDSC, which has been described for professional antigen presenting cells such as DC in the context of RLH-based therapy [46]. Furthermore, Lee et al. demonstrated that MDSC isolated from 4T1 breast tumor-bearing mice can be differentiated in macrophages and DC *in vitro* using the TLR7/8 agonist resiquimod [137]. Spinetti et al showed in a TLR7-targeting therapy that MDSC upregulated antigen presenting markers *in vivo* and that bone marrow generated MDSC-like cells presented antigens on MHC-II and stimulated CD4$^+$ T cell proliferation upon TLR7 activation [138]. In our model, MHC-II was downregulated upon poly(I:C)$_c$ treatment whereas the MHC class I-dependent antigen processing and presentation machinery was upregulated on transcriptomic level. Furthermore, upregulation of MHC-I and the costimulatory molecule CD86 was confirmed on protein level by flow cytometry. This led us to investigate cross-presenting capacity of MDSC both *in vitro* and *in vivo* using the model antigen OVA. These experiments clearly showed that MDSC isolated from OVA-expressing T110299 tumor-bearing hosts are unable to activate CD8$^+$ OT-1 T cells, irrespective of treatment with poly(I:C)$_c$ or not. Furthermore, MDSC loaded *ex vivo* with OVA protein did not activate

OT-I T cells, indicative of lacking cross-presenting function. To rule out that lack of OT-I T cell stimulation was due to T cell suppression by MDSC, MHC-I molecules of MDSC were externally loaded with SIINFEKL peptide, which resulted in efficient OT-I T cell proliferation. Taken together, no evidence was found that MDSC can present tumor-associated antigen in the T110299 tumor model, irrespective of poly(I:C)$_c$ treatment. Upregulation of MHC-I expression is more likely reflecting an indirect response to IFNAR signaling.

Another gene set that was identified in the RNA-Seq experiment was the GO:BP term embryonic hematopoiesis, which was significantly enriched in M-MDSC. One of the genes contributing to enrichment is *Runx1*, a crucial regulator of early hematopoiesis [139]. Recently, RUNX1 has been linked to MDSC differentiation and function. Controversially, Tian et al. showed that gene silencing of RUNX1 increased the suppressive capacity of both PMN-MDSC and M-MDSC. However, according to our RNA-Seq data, *Runx1* is down-regulated upon poly(I:C)$_c$ treatment, correlating with reduced suppressive activity. Further studies are needed to dissect the role of RUNX1 in MDSC function in the setting of RLH-based immunotherapy [140].

The precise mechanism of MDSC-mediated T cell suppression in the PDAC model was not addressed in this study. Several genes defined by Bronte et al. have been implicated to mediate suppressive capacity in MDSC, such as *Arg1, Nos2, Cebpb, Pdl1* and *S100a8/9* [18]. Of note, in the differential gene expression analysis between untreated and poly(I:C)$_c$ treated MDSC, none of these genes were significantly altered.

CCL5 is a type I IFN-inducible gene that is upregulated upon poly(I:C)$_c$ treatment. In melanoma, MDSC are recruited to the tumor in a CCL5-CCR5-dependent manner. Therapeutic blockade of CCL5 in a melanoma mouse model reduced the migration of MDSC into the tumor and improved survival [141]. One can therefore speculate that CCL5 blockade is a potential combination partner for RLH ligands or in general type I IFN-inducing therapies. Another promising combination partner of RLH-targeting therapy is checkpoint blockade as PD-L1 expression is induced upon type I IFN signaling and intratumoral T cells are highly positive for PD-1. Current projects in our working group address this question in several murine tumor models.

Taken together, these data suggest that RLH-based immunotherapy in the T110299 PDAC model induces a systemic immune activation and a reprograming of MDSC leading to a reduction of their suppressive function. In this respect, type I IFN play an

important role in modulating MDSC function, similar to an acute viral infection. For many other treatment strategies in preclinical and clinical development type I IFN play an important role. For example, radiation therapy can induce type I IFN via the cGAS-STING pathway [142]. Moreover, oncolytic viruses, which are potent inducers of type I IFN, are currently investigated in clinical trials [143]. RLH ligands broaden the repertoire of potent type I IFN inducers leading to enhanced immune-mediated tumor control. RLH-based immunotherapy therefore holds promise to improve outcomes for patients with cancer [144].

4.4 IRF4 deficiency accelerates pancreatic tumor growth and expands MDSC

During the course of this study, Nam et al reported that IRF4 is expressed by MDSC, particularly PMN-MDSC. Moreover, the group showed that IRF4-defciency increases MDSC frequency and induces suppressive function [104].

In contrast to Nam et al., this study showed by anti-IRF4 antibody staining as well as using GFP reporter mice that IRF4 is not expressed by PMN-MDSC or granulocytes, but instead by M-MDSC. Nam et al. studied the role of IRF4 in two mouse models: the BALB/c-derived 4T1 breast cancer model and the C57BL/6-derived B16F10 melanoma model. However, expression data were only presented for BALB/c mice, whereas in this study C57BL/6 mice were used. The difference between Nam et al. and the findings of this study could possibly be explained by the usage of different mouse strains [104].

As reported by Nam et al., IRF4 deficiency expands the frequency of MDSC-like cells in bone marrow cultures and increases the suppressive capacity of the whole bone marrow culture. The increase of MDSC-like cells in IRF4-deficient cultures could be confirmed in this study. However, the GM-CSF-driven culture contains, besides MDSC-like cells with suppressive capacity also BMDC which are less suppressive or even stimulatory in a mature stage. To study the suppressive activity of MDSC-like cells alone, MDSC-like cells were isolated from the bone marrow culture in this study. This strategy revealed that isolated MDSC-like cells do not differ in their suppressive capacity in wild-type and IRF4-deficient mice. These findings lead to the conclusion that in C57BL/6 mice IRF4 deficiency increases the proportion of suppressive MDSC-like cells *in vitro* but does not influence their suppressive capacity.

GM-CSF-driven bone marrow cultures are a common model to generate DC *in vitro*, however, Helft et al. showed through comprehensive analysis that GM-CSF-driven bone marrow culture consists of a heterogeneous mix of myeloid cells. Generally, all $CD11c^{+}MHC\text{-}II^{+}$ cells are considered as BMDC. However, Helft et al. defined two distinct populations within the BMDC population: GM-macrophages ($CD11c^{+}MHCII^{int}$ $CD115^{+}MerTK^{+}$) and GM-dendritic cells ($CD11c^{+}MHC\text{-}II^{hi}CD115^{-}CD135^{+}$) [122]. In IRF4-deficient cultures, the frequency of $CD11c^{+}MHC\text{-}II^{high}$ dendritic cells was dramatically reduced indicating that GM-dendritic cells are the main population affected by IRF4. Vander Lugt et al. showed that IRF4-deficient dendritic cells failed to induce MHC-II-dependent $CD4^{+}$ T cell proliferation and that IRF4 regulates the MHC-II peptide loading machinery transcriptionally [145].

Global deletion of IRF4 led to accelerated T110299 pancreatic tumor growth and reduced survival accompanied by a systemic increase of both PMN-MDSC and M-MDSC frequencies in the peripheral organs. Of note, selective IRF4 deletion in $Ly6G^{+}$ cells had no effect on tumor growth, survival or MDSC frequency. This is in line with the above discussed expression data with lack of IRF4 expression in $Ly6G^{+}$ cells. In contrast, myeloid deletion of IRF4 in the $LysM^{Cre}IRF4^{flox}$ mouse model led to increased tumor weight and M-MDSC frequency, but no significant change in survival.

The role of IRF4 in myeloid cells is difficult to dissect. On the one hand, IRF4 deficiency increased the frequency of MDSC-like cells *in vitro* and led to a dramatic expansion of both MDSC subtypes *in vivo*. On the other hand, myeloid-specific depletion of IRF4 *in vivo* increased the frequency of M-MDSC in the spleen only, whereas PMN-MDSC frequency and M-MDSC frequency in the blood were not significantly altered. There are two possible explanations for this discrepancy: Firstly, IRF4 might regulate the differentiation of MDSC at an early progenitor state that is not yet sufficiently targeted in the $LysM^{Cre}$ conditional mouse model. Lineage tracing experiments using the LysM-GFP reporter mice showed that LysM is already expressed in a proportion of hematopoietic stem cells. The Cre recombinase activity increased in the common myeloid precursor (CMP) and granulocyte-macrophage precursor (GMP) [146]. The targeting efficiency in macrophages and granulocytes is described to be almost 100% [124, 147]. However, in our model, the recombination efficiency for IRF4 in M-MDSC was on average only around 70% ranging from 30 to 90% (Fig. 18A).

Secondly, the deletion of IRF4 in T cells, B cells and DC could contribute to the accelerated tumor growth and the reduced survival in global IRF4-deficient mice.

Although there is increasing evidence of regulatory function of B cells, the role of B cells in the murine pancreatic cancer model remains unclear [148]. IRF4 controls the function of cDC2 cells, however it is dispensable for cDC1 development and function. The role of cDC2 in tumor immunology is still a matter of debate. In contrast to cDC1, cDC2 are not required for the induction of antigen-specific T cell responses. There is increasing evidence that IRF4 is pivotal for an effective, sustained $CD8^+$ T cell response. T110299 tumor cells are susceptible to $CD8^+$ T cell killing *in vivo,* and one could postulate that accelerated tumor growth in IRF4-deficient hosts is at least partially due to T cell dysfunction. As shown in Fig. 6I, PMN-MDSC frequency in tumor, blood and spleen, as well as M-MDSC frequency in the blood correlated with the tumor weight. Therefore, the increase in MDSC frequency in IRF4-deficient hosts could be a secondary effect due to the increased tumor size. The sample size in this study was too small to perform a regression analysis of the connection between tumor size and MDSC frequency depending on the genotype. However, preliminary correlation analysis suggests that tumor size has a greater influence on MDSC frequency than the IRF4 genotype (Fig. S5). Further studies are needed to dissect the role of IRF4 in different immune cell subsets.

The suppressive activity of MDSC from IRF4-deficient mice was higher compared to wild-type controls. This is in contrast to the suppressive capacity of *in vitro* generated MDSC-like cells. Again, tumor size influences the suppressive capacity of MDSC. The inter-assay variability makes it difficult to compare the absolute suppressive capacity of many samples. A correlation analysis of the tumor weight and the suppressive capacity is not feasible due to the low number of replicates. Further studies with comparable tumor sizes in both groups are required to better understand to role of IRF4 in the suppressive capacity of MDSC *in vivo*.

Taken together, these data demonstrate that IRF4 plays an important role in the immune control of T110299 tumor development. Polymorphonuclear cells do not express IRF4 in T110299 tumor bearing mice and in line with that, deletion of IRF4 in $Ly6G^+$ cells did not alter T110299 tumor development. In the *in vitro* bone marrow culture, the differentiation of MDSC-like cells from precursor cells was dramatically accelerated, but the suppressive capacity was not affected. The role of IRF4 in myeloid cells *in vivo* is still not fully understood and further studies are needed to dissect the role of IRF4 in immune cells in PDCA.

5. Summary

Despite recent advances in the understanding of the molecular pathology and thereof resulting targeted therapies of PDAC, the prognosis of affected patients remains very poor, pointing out the need for developing new treatment modalities. Immunotherapy has shown remarkable success in several tumor types, however, immunotherapeutic approaches explored in patients with PDCA have shown no clinical benefit. A major hurdle for immunotherapy is the immunosuppressive tumor microenvironment with MDSC being a key component. The aim of this study was to characterize the immune cell composition in a murine PDCA model with a special focus on MDSC and to investigate the effect of RLH-based immunotherapy on the differentiation and function of MDSC. Additionally, the role of the transcription factor IRF4 in MDSC development and function was assessed.

We found that MDSC frequency and suppressive capacity are significantly increased in PDAC tumor-bearing mice, accompanied by a decrease of infiltrating T cells. The expansion of MDSC and the induction of a suppressive program could be modeled *in vitro* using bone marrow cell cultures in the presence of tumor-derived factors. G-CSF was identified as a key factor driving the expansion of PMN-MDSC *in vivo* and *in vitro*. Additional tumor-derived factors enhance suppressive programming.

The PD-1/PD-L1 axis has been identified as a potent tumor-induced immune suppressive mechanism. In contrast to previous reports, we could rule out PD-1 expression by MDSC and several tumor cell lines tested. Commonly used anti-PD-1 antibody clones were found to bind unspecifically to an intracellular antigen in dead cells. Using wild-type and PD-1 deficient cell lines clearly demonstrated that when dead cell exclusion is strictly applied, PD-1 expression is restricted to T cells in tumor-bearing hosts.

Our group previously reported that RLH-based immunotherapy mediates a systemic type I IFN response, immunogenic cell death and effective T cell-mediated antitumor immunity [46, 47, 72]. In the present work systemic and intratumoral immune activation was further assessed with a special focus on MDSC. Treatment of PDAC tumor-bearing mice with the MDA5 ligand poly(I:C)$_c$ reduced PMN-MDSC frequency whereas M-MDSC frequency was increased. This effect was type I IFN-dependent. Interestingly, the suppressive capacity of MDSC in treated mice was strongly reduced. Whole transcriptomic profiling of isolated MDSC populations from spleen and tumor revealed functional reprograming.

Altered gene sets included type I IFN signaling and upregulation of genes associated with antigen presentation, such as MHC-I, *B2m* and CD86. However, functional assays did not detect MHC-I-restricted antigen presenting function in MDSC using an OVA-expressing PDCA model, ruling out professional APC function in MDSC.

IRF4 has been reported to play an important role in myelopoiesis, however the precise impact of IRF4 in MDSC in the context of PDAC has not been defined. The role of IRF4 on MDSC populations in PDAC-bearing hosts was studied in global and conditional knockout mouse models that were generated for this study. IRF4 expression was only found in M-MDSC but not PMN-MDSC. In bone marrow cultures, IRF4 deficiency increased MDSC-like cell frequency, but the suppressive capacity of MDSC-like cells was not influenced. *In vivo*, global IRF4 deficiency accelerated PDAC tumor growth, which was associated with an increased MDSC frequency. Myeloid-specific deletion of IRF4 using Ly6G-Cre and LysM-Cre mice did not influence survival and the changes in MDSC frequency were less pronounced. Interestingly, the suppressive capacity of IRF4-deficient MDSC from global knockout mice was increased three weeks after PDAC tumor induction, which is possibly linked to increased tumor size in these mice. Taken together, IRF4 deficiency accelerates myelopoiesis and MDSC differentiation *in vitro* and *in vivo*. Further studies are needed to unravel the role of IRF4 in the suppressive function.

In summary, tumor-derived factors such as G-CSF induce emergency myelopoiesis in PDAC bearing hosts leading to enhanced MDSC numbers and T cell suppression. MDSC are promising targets for novel immune therapeutic interventions. RLH-based immunotherapy leads to functional reprograming of MDSC with reduced suppressive capacity, largely depending on type I IFN signaling. Drugs targeting MDSC development have the potential to improve anti-tumor immunotherapy.

6. References

1. Siegel, R.L., K.D. Miller, and A. Jemal, *Cancer statistics, 2018.* CA Cancer J Clin, 2018. **68**(1): p. 7-30.
2. Rahib, L., et al., *Projecting cancer incidence and deaths to 2030: the unexpected burden of thyroid, liver, and pancreas cancers in the United States.* Cancer Res, 2014. **74**(11): p. 2913-21.
3. Quante, A.S., et al., *Projections of cancer incidence and cancer-related deaths in Germany by 2020 and 2030.* Cancer Med, 2016. **5**(9): p. 2649-56.
4. el-Kamar, F.G., M.L. Grossbard, and P.S. Kozuch, *Metastatic pancreatic cancer: emerging strategies in chemotherapy and palliative care.* Oncologist, 2003. **8**(1): p. 18-34.
5. Teague, A., K.H. Lim, and A. Wang-Gillam, *Advanced pancreatic adenocarcinoma: a review of current treatment strategies and developing therapies.* Ther Adv Med Oncol, 2015. **7**(2): p. 68-84.
6. Aune, D., et al., *Body mass index, abdominal fatness and pancreatic cancer risk: a systematic review and non-linear dose-response meta-analysis of prospective studies.* Ann Oncol, 2012. **23**(4): p. 843-52.
7. Anderson, M.A., et al., *Alcohol and tobacco lower the age of presentation in sporadic pancreatic cancer in a dose-dependent manner: a multicenter study.* Am J Gastroenterol, 2012. **107**(11): p. 1730-9.
8. Pihlak, R., J.W. Valle, and M.G. McNamara, *Germline mutations in pancreatic cancer and potential new therapeutic options.* Oncotarget, 2017. **8**(42): p. 73240-73257.
9. Mueller, S., et al., *Evolutionary routes and KRAS dosage define pancreatic cancer phenotypes.* Nature, 2018. **554**(7690): p. 62-68.
10. Bailey, P., et al., *Genomic analyses identify molecular subtypes of pancreatic cancer.* Nature, 2016. **531**(7592): p. 47-52.
11. Waddell, N., et al., *Whole genomes redefine the mutational landscape of pancreatic cancer.* Nature, 2015. **518**(7540): p. 495-501.
12. Witkiewicz, A.K., et al., *Whole-exome sequencing of pancreatic cancer defines genetic diversity and therapeutic targets.* Nat Commun, 2015. **6**: p. 6744.
13. Muckenhuber, A., et al., *Pancreatic ductal adenocarcinoma subtyping using the biomarkers hepatocyte nuclear factor-1a and cytokeratin-81 correlates with outcome and treatment response.* Clin Cancer Res, 2018. **24**(2): p. 351-359.
14. Masamune, A., et al., *Roles of pancreatic stellate cells in pancreatic inflammation and fibrosis.* Clin Gastroenterol Hepatol, 2009. **7**(11 Suppl): p. S48-54.
15. Jiang, H., et al., *Targeting focal adhesion kinase renders pancreatic cancers responsive to checkpoint immunotherapy.* Nat Med, 2016. **22**(8): p. 851-60.
16. Neesse, A., et al., *Stromal biology and therapy in pancreatic cancer: ready for clinical translation?* Gut, 2019. **68**(1): p. 159-171.
17. Mitchem, J.B., et al., *Targeting tumor-infiltrating macrophages decreases tumor-initiating cells, relieves immunosuppression, and improves chemotherapeutic responses.* Cancer Res, 2013. **73**(3): p. 1128-41.
18. Bronte, V., et al., *Recommendations for myeloid-derived suppressor cell nomenclature and characterization standards.* Nat Commun, 2016. **7**: p. 12150.
19. Nywening, T.M., et al., *Targeting both tumour-associated CXCR2(+) neutrophils and CCR2(+) macrophages disrupts myeloid recruitment and improves*

chemotherapeutic responses in pancreatic ductal adenocarcinoma. Gut, 2018. **67**(6): p. 1112-1123.

20. Li, J., et al., *Tumor cell-intrinsic factors underlie heterogeneity of immune cell infiltration and response to immunotherapy.* Immunity, 2018. **49**(1): p. 178-193.
21. Stromnes, I.M., et al., *Targeted depletion of an MDSC subset unmasks pancreatic ductal adenocarcinoma to adaptive immunity.* Gut, 2014. **63**(11): p. 1769-81.
22. Neoptolemos, J.P., et al., *Therapeutic developments in pancreatic cancer: current and future perspectives.* Nat Rev Gastroenterol Hepatol, 2018. **15**(6): p. 333-348.
23. Conroy, T., et al., *FOLFIRINOX versus gemcitabine for metastatic pancreatic cancer.* N Engl J Med, 2011. **364**(19): p. 1817-25.
24. Von Hoff, D.D., et al., *Increased survival in pancreatic cancer with nab-paclitaxel plus gemcitabine.* N Engl J Med, 2013. **369**(18): p. 1691-703.
25. Rougier, P., et al., *Randomised, placebo-controlled, double-blind, parallel-group phase III study evaluating aflibercept in patients receiving first-line treatment with gemcitabine for metastatic pancreatic cancer.* Eur J Cancer, 2013. **49**(12): p. 2633-42.
26. Kindler, H.L., et al., *Axitinib plus gemcitabine versus placebo plus gemcitabine in patients with advanced pancreatic adenocarcinoma: a double-blind randomised phase 3 study.* Lancet Oncol, 2011. **12**(3): p. 256-62.
27. Moore, M.J., et al., *Erlotinib plus gemcitabine compared with gemcitabine alone in patients with advanced pancreatic cancer: a phase III trial of the National Cancer Institute of Canada Clinical Trials Group.* J Clin Oncol, 2007. **25**(15): p. 1960-6.
28. Balachandran, V.P., et al., *Identification of unique neoantigen qualities in long-term survivors of pancreatic cancer.* Nature, 2017. **551**(7681): p. 512-516.
29. Connor, A.A., et al., *Association of Distinct Mutational Signatures With Correlates of Increased Immune Activity in Pancreatic Ductal Adenocarcinoma.* JAMA Oncol, 2017. **3**(6): p. 774-783.
30. Hodi, F.S., et al., *Improved survival with ipilimumab in patients with metastatic melanoma.* N Engl J Med, 2010. **363**(8): p. 711-23.
31. Borghaei, H., et al., *Nivolumab versus docetaxel in advanced nonsquamous non-small-cell lung cancer.* N Engl J Med, 2015. **373**(17): p. 1627-39.
32. Gong, J., et al., *Development of PD-1 and PD-L1 inhibitors as a form of cancer immunotherapy: a comprehensive review of registration trials and future considerations.* J Immunother Cancer, 2018. **6**(1): p. 8.
33. Brahmer, J.R., et al., *Safety and activity of anti-PD-L1 antibody in patients with advanced cancer.* N Engl J Med, 2012. **366**(26): p. 2455-65.
34. Royal, R.E., et al., *Phase 2 trial of single agent Ipilimumab (anti-CTLA-4) for locally advanced or metastatic pancreatic adenocarcinoma.* J Immunother, 2010. **33**(8): p. 828-33.
35. Yan, X., et al., *Prognostic factors for checkpoint inhibitor based immunotherapy: An update with new evidences.* Front Pharmacol, 2018. **9**: p. 1050.
36. Stromnes, I.M., et al., *T-cell localization, activation, and clonal expansion in human pancreatic ductal adenocarcinoma.* Cancer Immunol Res, 2017. **5**(11): p. 978-991.
37. Le, D.T., et al., *Mismatch repair deficiency predicts response of solid tumors to PD-1 blockade.* Science, 2017. **357**(6349): p. 409-413.

38. Yu, Y., *Molecular classification and precision therapy of cancer: immune checkpoint inhibitors.* Front Med, 2018. **12**(2): p. 229-235.
39. Rizvi, N.A., et al., *Cancer immunology. Mutational landscape determines sensitivity to PD-1 blockade in non-small cell lung cancer.* Science, 2015. **348**(6230): p. 124-8.
40. Corporation, N.G. *NewLink genetics announces results from phase 3 IMPRESS trial of Algenpantucel-L for patients with resected pancreatic cancer*. 2016 [cited 2018 02.08.2018]; Available from: https://globenewswire.com/news-release/2016/05/09/837878/0/en/NewLink-Genetics-Announces-Results-from-Phase-3-IMPRESS-Trial-of-Algenpantucel-L-for-Patients-with-Resected-Pancreatic-Cancer.html.
41. Middleton, G., et al., *Gemcitabine and capecitabine with or without telomerase peptide vaccine GV1001 in patients with locally advanced or metastatic pancreatic cancer (TeloVac): an open-label, randomised, phase 3 trial.* Lancet Oncol, 2014. **15**(8): p. 829-40.
42. Hardacre, J.M., et al., *Addition of algenpantucel-L immunotherapy to standard adjuvant therapy for pancreatic cancer: a phase 2 study.* J Gastrointest Surg, 2013. **17**(1): p. 94-100; discussion p. 100-1.
43. Wang-Gillam, A., et al., *A Phase IIb, randomized, multicenter study of the efficacy of GVAX pancreas vaccine and CRS-207 compared to chemotherapy or to CRS-207 alone in adults with previously-treated metastatic pancreatic adenocarcinoma (eclipse study).* J Immunotherap Canc, 2014. **2**(Suppl 3): p. P68-P68.
44. Beatty, G.L., et al., *CD40 agonists alter tumor stroma and show efficacy against pancreatic carcinoma in mice and human.* Science, 2011. **331**(6024): p. 1612-6.
45. Morrison, A.H., K.T. Byrne, and R.H. Vonderheide, *Immunotherapy and prevention of pancreatic cancer.* Trends Cancer, 2018. **4**(6): p. 418-428.
46. Duewell, P., et al., *RIG-I-like helicases induce immunogenic cell death of pancreatic cancer cells and sensitize tumors toward killing by CD8(+) T cells.* Cell Death Differ, 2014. **21**(12): p. 1825-37.
47. Duewell, P., et al., *Targeted activation of melanoma differentiation-associated protein 5 (MDA5) for immunotherapy of pancreatic carcinoma.* Oncoimmunology, 2015. **4**(10): p. e1029698.
48. Mahalingam, D., et al., *A phase II study of pelareorep (REOLYSIN®) in combination with gemcitabine for patients with advanced pancreatic adenocarcinoma.* Cancers (Basel), 2018. **10**(6).
49. Chao, T., E.E. Furth, and R.H. Vonderheide, *CXCR2-dependent accumulation of tumor-associated neutrophils regulates T-cell immunity in pancreatic ductal adenocarcinoma.* Cancer Immunol Res, 2016. **4**(11): p. 968-982.
50. Nywening, T.M., et al., *Targeting tumour-associated macrophages with CCR2 inhibition in combination with FOLFIRINOX in patients with borderline resectable and locally advanced pancreatic cancer: a single-centre, open-label, dose-finding, non-randomised, phase 1b trial.* Lancet Oncol, 2016. **17**(5): p. 651-62.
51. Linehan, D., et al., *Overall survival in a trial of orally administered CCR2 inhibitor CCX872 in locally advanced/metastatic pancreatic cancer: Correlation with blood monocyte counts.* J Clin Oncol, 2018. **36**(5_suppl): p. 92-92.
52. Hingorani, S.R., et al., *HALO 202: randomized phase II study of PEGPH20 plus nab-paclitaxel/gemcitabine versus nab-paclitaxel/gemcitabine in patients with untreated, metastatic pancreatic ductal adenocarcinoma.* J Clin Oncol, 2018. **36**(4): p. 359-366.

53. Rhim, A.D., et al., *Stromal elements act to restrain, rather than support, pancreatic ductal adenocarcinoma.* Cancer Cell, 2014. **25**(6): p. 735-47.
54. Ozdemir, B.C., et al., *Depletion of carcinoma-associated fibroblasts and fibrosis induces immunosuppression and accelerates pancreas cancer with reduced survival.* Cancer Cell, 2014. **25**(6): p. 719-34.
55. Hingorani, S.R., et al., *Trp53R172H and KrasG12D cooperate to promote chromosomal instability and widely metastatic pancreatic ductal adenocarcinoma in mice.* Cancer Cell, 2005. **7**(5): p. 469-83.
56. Adunka, T., *Characterization of murine pancreatic carcinoma models regarding immunosuppressive mechanisms and therapy with bifunctional siRNA targeting galectin-1.* Dissertation, LMU München: Medizinische Fakultät 2014.
57. Gabrilovich, D.I., et al., *The terminology issue for myeloid-derived suppressor cells.* Cancer Res, 2007. **67**(1): p. 425; author reply 426.
58. Gentles, A.J., et al., *The prognostic landscape of genes and infiltrating immune cells across human cancers.* Nat Med, 2015. **21**(8): p. 938-945.
59. Mowbray, N.G., et al., *A meta-analysis of the utility of the neutrophil-to-lymphocyte ratio in predicting survival after pancreatic cancer resection.* HPB (Oxford), 2018. **20**(5): p. 379-384.
60. Gabrilovich, D.I., *Myeloid-Derived Suppressor Cells.* Cancer Immunol Res, 2017. **5**(1): p. 3-8.
61. Kumar, V., et al., *The nature of myeloid-derived suppressor cells in the tumor microenvironment.* Trends Immunol, 2016. **37**(3): p. 208-220.
62. Condamine, T., J. Mastio, and D.I. Gabrilovich, *Transcriptional regulation of myeloid-derived suppressor cells.* J Leukoc Biol, 2015. **98**(6): p. 913-22.
63. Condamine, T., et al., *Lectin-type oxidized LDL receptor-1 distinguishes population of human polymorphonuclear myeloid-derived suppressor cells in cancer patients.* Sci Immunol, 2016. **1**(2).
64. Mondanelli, G., et al., *The immune regulation in cancer by the amino acid metabolizing enzymes ARG and IDO.* Curr Opin Pharmacol, 2017. **35**: p. 30-39.
65. Park, M.J., et al., *Interleukin-10 produced by myeloid-derived suppressor cells is critical for the induction of Tregs and attenuation of rheumatoid inflammation in mice.* Sci Rep, 2018. **8**(1): p. 3753.
66. Gabrilovich, D.I. and S. Nagaraj, *Myeloid-derived suppressor cells as regulators of the immune system.* Nat Rev Immunol, 2009. **9**(3): p. 162-74.
67. Noman, M.Z., et al., *PD-L1 is a novel direct target of HIF-1alpha, and its blockade under hypoxia enhanced MDSC-mediated T cell activation.* J Exp Med, 2014. **211**(5): p. 781-90.
68. de Haas, N., et al., *Improving cancer immunotherapy by targeting the STATe of MDSCs.* Oncoimmunology, 2016. **5**(7): p. e1196312.
69. Hornung, V., et al., *5'-Triphosphate RNA is the ligand for RIG-I.* Science, 2006. **314**(5801): p. 994-7.
70. Kato, H., et al., *Differential roles of MDA5 and RIG-I helicases in the recognition of RNA viruses.* Nature, 2006. **441**(7089): p. 101-5.
71. Reikine, S., J.B. Nguyen, and Y. Modis, *Pattern Recognition and Signaling Mechanisms of RIG-I and MDA5.* Front Immunol, 2014. **5**: p. 342.
72. Ellermeier, J., et al., *Therapeutic efficacy of bifunctional siRNA combining TGF-beta1 silencing with RIG-I activation in pancreatic cancer.* Cancer Res, 2013. **73**(6): p. 1709-20.

73. Musella, M., et al., *Type-I-interferons in infection and cancer: Unanticipated dynamics with therapeutic implications.* Oncoimmunology, 2017. **6**(5): p. e1314424.
74. Dunn, I.S., et al., *Enhancement of human melanoma antigen expression by IFN-beta.* J Immunol, 2007. **179**(4): p. 2134-42.
75. Zhu, Y., et al., *Influence of interferon-alpha on the expression of the cancer stem cell markers in pancreatic carcinoma cells.* Exp Cell Res, 2014. **324**(2): p. 146-56.
76. Xiao, W., et al., *IFNAR1 controls autocrine type I IFN regulation of PD-L1 expression in myeloid-derived suppressor cells.* J Immunol, 2018. **201**(1): p. 264-277.
77. Snell, L.M., T.L. McGaha, and D.G. Brooks, *Type I interferon in chronic virus infection and cancer.* Trends Immunol, 2017. **38**(8): p. 542-557.
78. Huang, A., et al., *Myeloid-derived suppressor cells regulate immune response in patients with chronic hepatitis B virus infection through PD-1-induced IL-10.* J Immunol, 2014. **193**(11): p. 5461-9.
79. Lei, G.S., C. Zhang, and C.H. Lee, *Myeloid-derived suppressor cells impair alveolar macrophages through PD-1 receptor ligation during Pneumocystis pneumonia.* Infect Immun, 2015. **83**(2): p. 572-82.
80. Zhao, G.N., D.S. Jiang, and H. Li, *Interferon regulatory factors: at the crossroads of immunity, metabolism, and disease.* Biochim Biophys Acta, 2015. **1852**(2): p. 365-78.
81. Negishi, H., et al., *Negative regulation of Toll-like-receptor signaling by IRF-4.* Proc Natl Acad Sci U S A, 2005. **102**(44): p. 15989-94.
82. Yee, A.A., et al., *Cooperative interaction between the DNA-binding domains of PU.1 and IRF4.* J Mol Biol, 1998. **279**(5): p. 1075-83.
83. Klein, U., et al., *Transcription factor IRF4 controls plasma cell differentiation and class-switch recombination.* Nat Immunol, 2006. **7**(7): p. 773-82.
84. Sciammas, R., et al., *Graded expression of interferon regulatory factor-4 coordinates isotype switching with plasma cell differentiation.* Immunity, 2006. **25**(2): p. 225-36.
85. Raczkowski, F., et al., *The transcription factor Interferon Regulatory Factor 4 is required for the generation of protective effector CD8+ T cells.* Proc Natl Acad Sci U S A, 2013. **110**(37): p. 15019-24.
86. Man, K., et al., *The transcription factor IRF4 is essential for TCR affinity–mediated metabolic programming and clonal expansion of T cells.* Nature Immunology, 2013. **14**: p. 1155.
87. Yao, S., et al., *Interferon regulatory factor 4 sustains CD8+ T cell expansion and effector differentiation.* Immunity, 2013. **39**(5): p. 833-845.
88. Nayar, R., et al., *Graded levels of IRF4 regulate CD8+ T cell differentiation and expansion, but not attrition, in response to acute virus infection.* J Immunol, 2014. **192**(12): p. 5881-93.
89. Reiner, S.L., *Decision making during the conception and career of CD4+ T cells.* Nat Rev Immunol, 2009. **9**(2): p. 81-2.
90. Honma, K., et al., *Interferon regulatory factor 4 differentially regulates the production of Th2 cytokines in naive vs. effector/memory CD4+ T cells.* Proc Natl Acad Sci U S A, 2008. **105**(41): p. 15890-5.
91. Lohoff, M., et al., *Dysregulated T helper cell differentiation in the absence of interferon regulatory factor 4.* Proc Natl Acad Sci USA, 2002. **99**(18): p. 11808-12.

92. Staudt, V., et al., *Interferon-regulatory factor 4 is essential for the developmental program of T helper 9 cells.* Immunity, 2010. **33**(2): p. 192-202.

93. Brustle, A., et al., *The development of inflammatory T(H)-17 cells requires interferon-regulatory factor 4.* Nat Immunol, 2007. **8**(9): p. 958-66.

94. Biswas, P.S., et al., *Phosphorylation of IRF4 by ROCK2 regulates IL-17 and IL-21 production and the development of autoimmunity in mice.* J Clin Invest, 2010. **120**(9): p. 3280-95.

95. Huber, M., et al., *IL-17A secretion by CD8+ T cells supports Th17-mediated autoimmune encephalomyelitis.* J Clin Invest, 2013. **123**(1): p. 247-60.

96. Cretney, E., et al., *The transcription factors Blimp-1 and IRF4 jointly control the differentiation and function of effector regulatory T cells.* Nat Immunol, 2011. **12**(4): p. 304-11.

97. Yamamoto, M., et al., *Shared and distinct functions of the transcription factors IRF4 and IRF8 in myeloid cell development.* PLoS One, 2011. **6**(10): p. e25812.

98. Kurotaki, D., et al., *Transcription factor IRF8 governs enhancer landscape dynamics in mononuclear phagocyte progenitors.* Cell Rep, 2018. **22**(10): p. 2628-2641.

99. Guilliams, M., et al., *Unsupervised high-dimensional analysis aligns dendritic cells across tissues and species.* Immunity, 2016. **45**(3): p. 669-684.

100. Gardner, A. and B. Ruffell, *Dendritic Cells and Cancer Immunity.* Trends Immunol, 2016. **37**(12): p. 855-865.

101. Bajana, S., et al., *IRF4 and IRF8 act in CD11c+ cells to regulate terminal differentiation of lung tissue dendritic cells.* J Immunol, 2016. **196**(4): p. 1666-77.

102. Briseno, C.G., et al., *Distinct transcriptional programs control cross-priming in classical and monocyte-derived dendritic cells.* Cell Rep, 2016. **15**(11): p. 2462-74.

103. Satoh, T., et al., *The Jmjd3-Irf4 axis regulates M2 macrophage polarization and host responses against helminth infection.* Nat Immunol, 2010. **11**(10): p. 936-44.

104. Nam, S., et al., *Interferon regulatory factor 4 (IRF4) controls myeloid-derived suppressor cell (MDSC) differentiation and function.* J Leukoc Biol, 2016. **100**(6): p. 1273-1284.

105. Moore, M.W., F.R. Carbone, and M.J. Bevan, *Introduction of soluble protein into the class I pathway of antigen processing and presentation.* Cell, 1988. **54**(6): p. 777-85.

106. Sanjana, N.E., O. Shalem, and F. Zhang, *Improved vectors and genome-wide libraries for CRISPR screening.* Nat Methods, 2014. **11**(8): p. 783-784.

107. Shalem, O., et al., *Genome-scale CRISPR-Cas9 knockout screening in human cells.* Science, 2014. **343**(6166): p. 84-87.

108. Truett, G.E., et al., *Preparation of PCR-quality mouse genomic DNA with hot sodium hydroxide and tris (HotSHOT).* Biotechniques, 2000. **29**(1): p. 52, 54.

109. Andrews, S. *FastQC: a quality control tool for high throughput sequence data*. 2010; Available from: http://www.bioinformatics.babraham.ac.uk/projects/fastqc.

110. Bonfert, T., et al., *ContextMap 2: fast and accurate context-based RNA-seq mapping.* BMC Bioinformatics, 2015. **16**: p. 122.

111. Li, H. and R. Durbin, *Fast and accurate long-read alignment with Burrows-Wheeler transform.* Bioinformatics, 2010. **26**(5): p. 589-95.

112. Liao, Y., G.K. Smyth, and W. Shi, *featureCounts: an efficient general purpose program for assigning sequence reads to genomic features.* Bioinformatics, 2014. **30**(7): p. 923-30.

113. Love, M.I., W. Huber, and S. Anders, *Moderated estimation of fold change and dispersion for RNA-seq data with DESeq2.* Genome Biol, 2014. **15**(12): p. 550.

114. Benjamini, Y. and Y. Hochberg, *Controlling the false discovery rate: A practical and powerful approach to multiple testing.* Journal of the Royal Statistical Society. Series B (Methodological), 1995. **57**(1): p. 289-300.

115. Kluge, M. and C.C. Friedel, *Watchdog - a workflow management system for the distributed analysis of large-scale experimental data.* BMC Bioinformatics, 2018. **19**(1): p. 97.

116. Metsalu, T. and J. Vilo, *ClustVis: a web tool for visualizing clustering of multivariate data using Principal Component Analysis and heatmap.* Nucleic Acids Res, 2015. **43**(W1): p. W566-70.

117. Huang da, W., B.T. Sherman, and R.A. Lempicki, *Systematic and integrative analysis of large gene lists using DAVID bioinformatics resources.* Nat Protoc, 2009. **4**(1): p. 44-57.

118. Bayne, L.J., et al., *Tumor-derived granulocyte-macrophage colony-stimulating factor regulates myeloid inflammation and T cell immunity in pancreatic cancer.* Cancer Cell, 2012. **21**(6): p. 822-35.

119. Li, W., et al., *G-CSF is a key modulator of MDSC and could be a potential therapeutic target in colitis-associated colorectal cancers.* Protein Cell, 2016. **7**(2): p. 130-40.

120. Alsaab, H.O., et al., *PD-1 and PD-L1 checkpoint signaling inhibition for cancer immunotherapy: mechanism, combinations, and clinical outcome.* Front Pharmacol, 2017. **8**: p. 561.

121. Liu, Y., et al., *Regulation of arginase I activity and expression by both PD-1 and CTLA-4 on the myeloid-derived suppressor cells.* Cancer Immunol Immunother, 2009. **58**(5): p. 687-97.

122. Helft, J., et al., *GM-CSF mouse bone marrow cultures comprise a heterogeneous population of CD11c(+)MHCII(+) macrophages and dendritic cells.* Immunity, 2015. **42**(6): p. 1197-211.

123. Hasenberg, A., et al., *Catchup: a mouse model for imaging-based tracking and modulation of neutrophil granulocytes.* Nat Methods, 2015. **12**(5): p. 445-52.

124. Abram, C.L., et al., *Comparative analysis of the efficiency and specificity of myeloid-Cre deleting strains using ROSA-EYFP reporter mice.* J Immunol Methods, 2014. **408**: p. 89-100.

125. Welte, T., et al., *Oncogenic mTOR signalling recruits myeloid-derived suppressor cells to promote tumour initiation.* Nat Cell Biol, 2016. **18**(6): p. 632-44.

126. Sharma, P. and J.P. Allison, *The future of immune checkpoint therapy.* Science, 2015. **348**(6230): p. 56-61.

127. Teng, M.W., et al., *Classifying Cancers Based on T-cell Infiltration and PD-L1.* Cancer Res, 2015. **75**(11): p. 2139-45.

128. Chevrier, S., et al., *An immune atlas of clear cell renal cell carcinoma.* Cell, 2017. **169**(4): p. 736-749.e18.

129. Kleffel, S., et al., *Melanoma cell-intrinsic PD-1 receptor functions promote tumor growth.* Cell, 2015. **162**(6): p. 1242-56.

130. Metzger, P., et al., *Dying cells expose a nuclear antigen cross-reacting with anti-PD-1 monoclonal antibodies.* Sci Rep, 2018. **8**(1): p. 8810.

131. Dangi, A., et al., *Murine CMV induces type 1 IFN that impairs differentiation of MDSCs critical for transplantation tolerance.* Blood Adv, 2018. **2**(6): p. 669-680.

132. Urban, S.L., L.J. Berg, and R.M. Welsh, *Type 1 interferon licenses naive CD8 T cells to mediate anti-viral cytotoxicity.* Virology, 2016. **493**: p. 52-9.

133. Zoglmeier, C., et al., *CpG blocks immunosuppression by myeloid-derived suppressor cells in tumor-bearing mice.* Clin Cancer Res, 2011. **17**(7): p. 1765-75.

134. Kawai, T. and S. Akira, *Toll-like receptor and RIG-I-like receptor signaling.* Ann N Y Acad Sci, 2008. **1143**: p. 1-20.

135. Taleb, K., et al., *Chronic type I IFN is sufficient to promote immunosuppression through accumulation of myeloid-derived suppressor cells.* J Immunol, 2017. **198**(3): p. 1156-1163.

136. Dijk, F., et al., *PO-521 Gene expression-based subtypes of pancreatic ductal adenocarcinoma offer leads for targeted therapy.* ESMO Open, 2018. **3**: p. A227-A227.

137. Lee, M., et al., *Resiquimod, a TLR7/8 agonist, promotes differentiation of myeloid-derived suppressor cells into macrophages and dendritic cells.* Arch Pharm Res, 2014. **37**(9): p. 1234-40.

138. Spinetti, T., et al., *TLR7-based cancer immunotherapy decreases intratumoral myeloid-derived suppressor cells and blocks their immunosuppressive function.* Oncoimmunology, 2016. **5**(11): p. e1230578.

139. Chen, M.J., et al., *Runx1 is required for the endothelial to haematopoietic cell transition but not thereafter.* Nature, 2009. **457**(7231): p. 887-91.

140. Tian, J., et al., *MicroRNA-9 regulates the differentiation and function of myeloid-derived suppressor cells via targeting Runx1.* J Immunol, 2015. **195**(3): p. 1301-11.

141. Blattner, C., et al., *CCR5(+) myeloid-derived suppressor cells are enriched and activated in melanoma lesions.* Cancer Res, 2018. **78**(1): p. 157-167.

142. Deng, L., et al., *STING-dependent cytosolic DNA sensing promotes radiation-induced type I interferon-dependent antitumor immunity in immunogenic tumors.* Immunity, 2014. **41**(5): p. 843-52.

143. Lundstrom, K., *New frontiers in oncolytic viruses: optimizing and selecting for virus strains with improved efficacy.* Biologics, 2018. **12**: p. 43-60.

144. Benci, J.L., et al., *Tumor interferon signaling regulates a multigenic resistance program to immune checkpoint blockade.* Cell, 2016. **167**(6): p. 1540-1554.e12.

145. Vander Lugt, B., et al., *Transcriptional programming of dendritic cells for enhanced MHC class II antigen presentation.* Nat Immunol, 2013. **15**: p. 161.

146. Ye, M., et al., *Hematopoietic stem cells expressing the myeloid lysozyme gene retain long-term, multilineage repopulation potential.* Immunity, 2003. **19**(5): p. 689-699.

147. Clausen, B.E., et al., *Conditional gene targeting in macrophages and granulocytes using LysMcre mice.* Transgenic Res, 1999. **8**(4): p. 265-77.

148. Yuen, G.J., E. Demissie, and S. Pillai, *B lymphocytes and cancer: a love-hate relationship.* Trends Cancer, 2016. **2**(12): p. 747-757.

7. Appendix

7.1 Supplementary figures

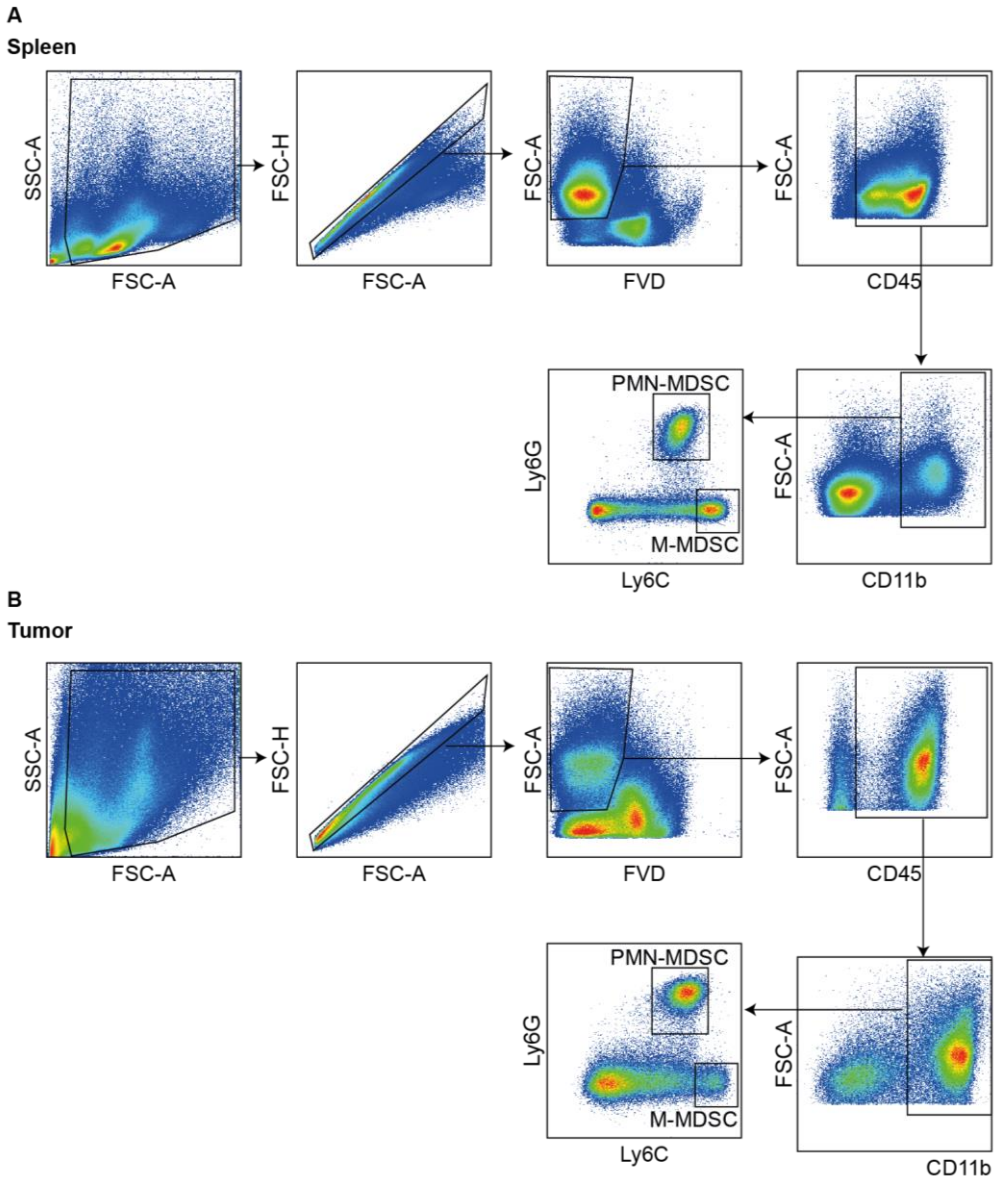

Figure S1: Gating strategy for flow cytometric analysis and FACSorting of splenic and tumor MDSC populations.
Representative FACS plots of single cell suspensions generated from spleen and tumor. Arrows indicate which events were used for the subsequent gating strategy.

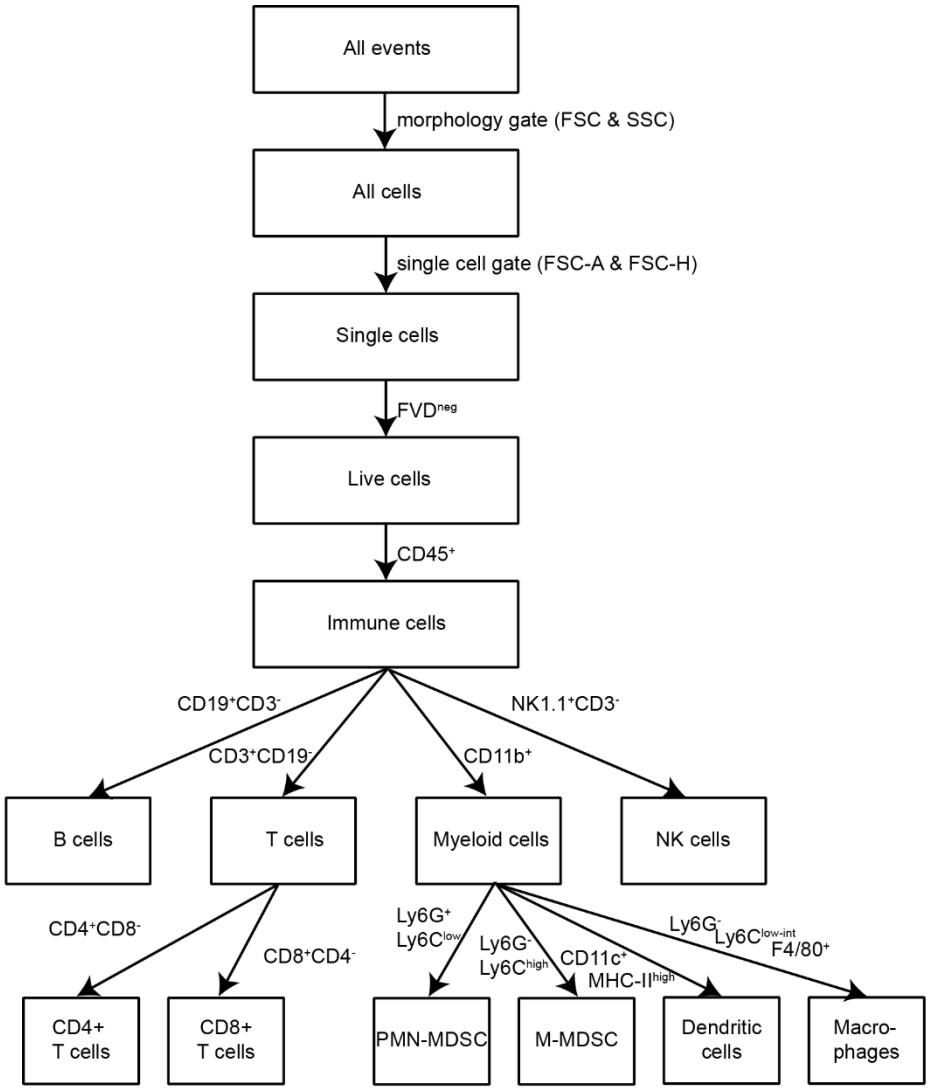

Figure S2: Gating strategy for flow cytometric analysis of different immune cell populations in tumor, spleen and blood.

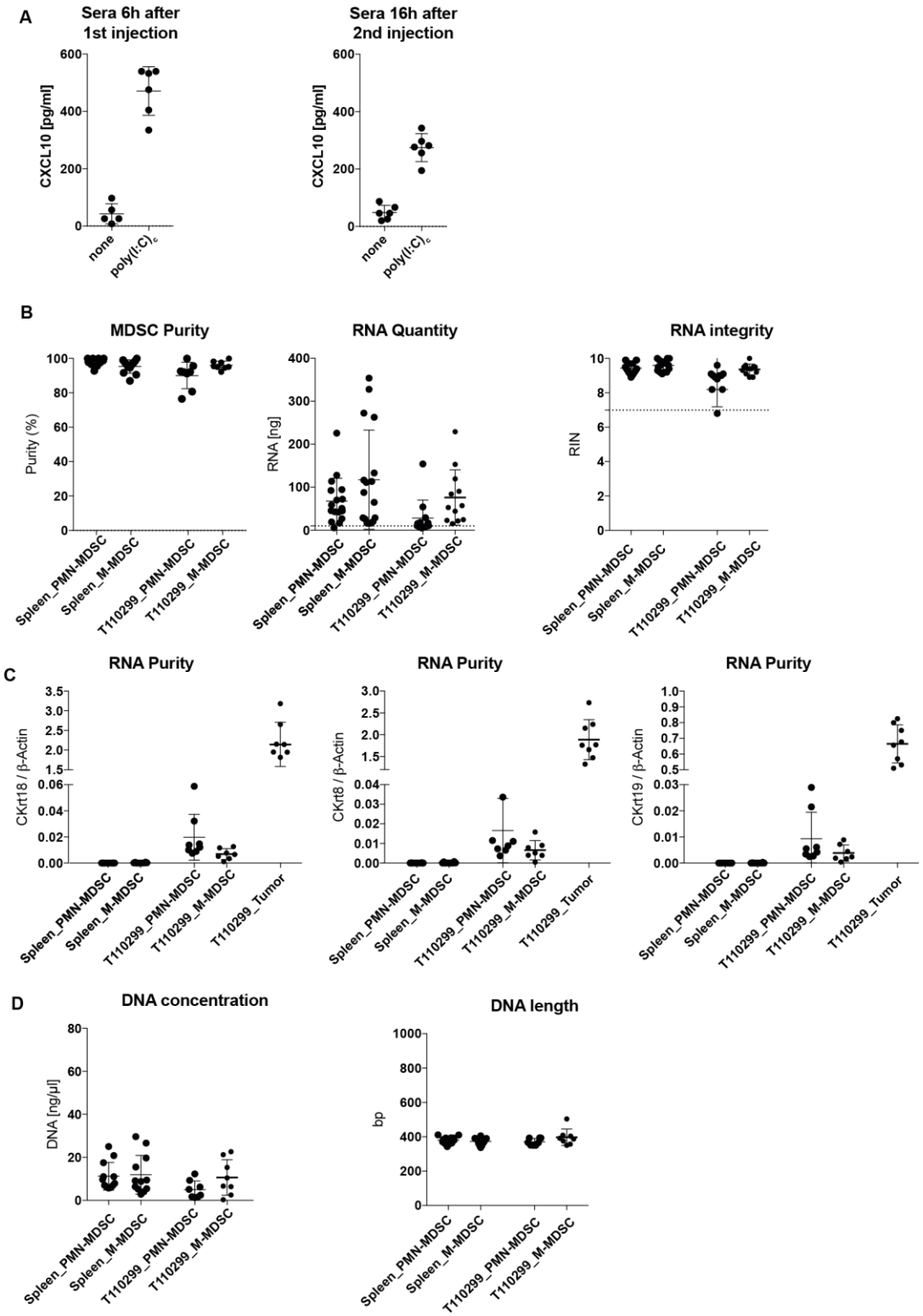

Figure S3: Quality controls of RNA sequencing samples

Mice were treated as shown in Fig. 5A. A) 6 hours after the first and 16 hours after the second poly(I:C)$_c$ treatment, CXCL10 concentration in serum was measured by ELISA. B) FACSorting purity of MDSC was analyzed by flow cytometry. RNA quantity, RNA quality and integrity after isolation was analyzed using Bioanalyzer. C) RNA purity was analyzed quantifying tumor-specific cytokeratin expression levels by qRT-PCR. T110299 tumor samples were used as positive controls. D) After library preparation for RNA sequencing, DNA concentration and length were analyzed using the Bioanalyzer, n=4/group.

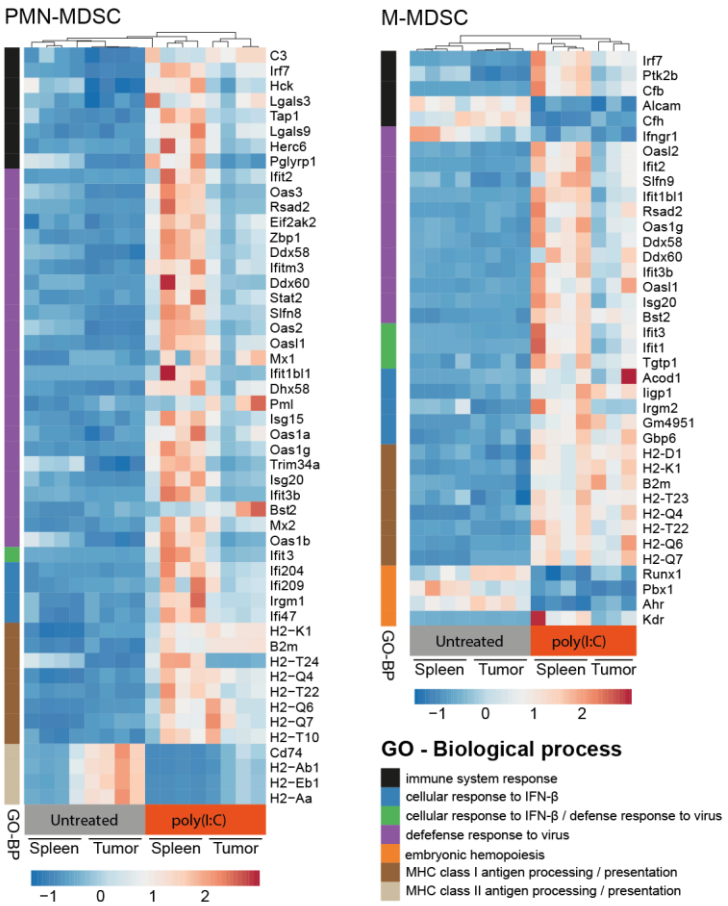

Figure S4: Expression of genes contributing to one of the GO:BP terms
Heatmap showing the expression of genes contributing to one of the GO:BP terms in both spleen and tumor of M-MDSC and PMN-MDSC. Samples were arranged unbiased using the Euclidean clustering.

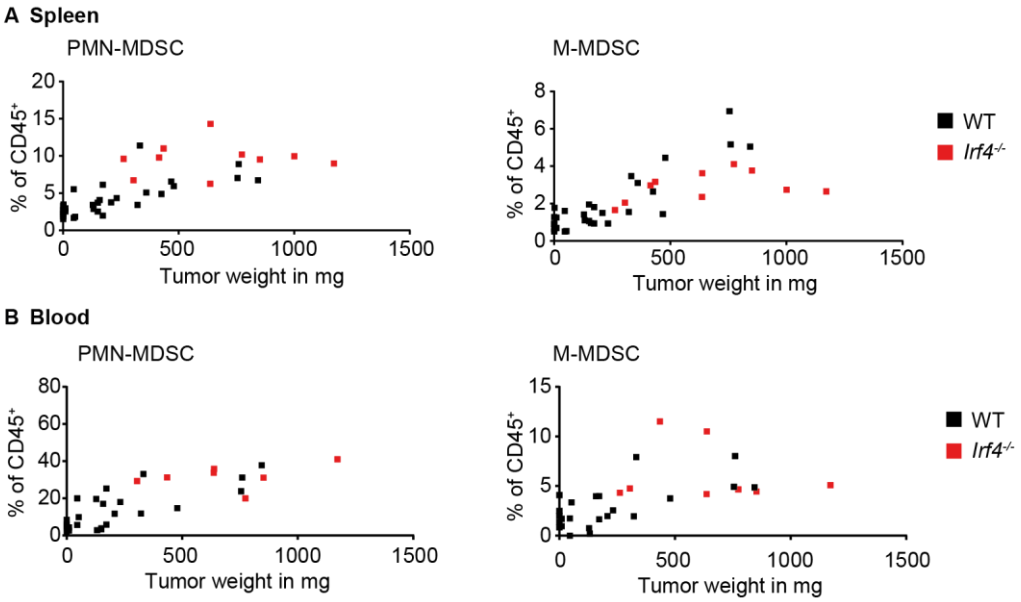

Figure S5: Correlation of MDSC frequency with tumor weight in wild-type and *Irf4*$^{-/-}$ mice.

Frequency of MDSC populations from spleen (A) and blood (B) were correlated with the tumor weight.

7.2 Abbreviations

3-MCA	3-Methylcholanthrene
4T1	Murine breast tumor model
ACM	Acinar-to-ductal metaplasia
ADEX	Aberrantly differentiated endocrine/exocrine subtype
AID	Activation-induced cytidine deaminase
AF	Alexa Fluor™
APC	Antigen presenting cell
ARG1	Arginase 1
Blimp1	Protein gene coded by the *Prdm1* gene
BRCA	Breast Cancer, early-onset
BSA	Bovine Serum-Albumin
C57BL/6	Inbred mouse strain
CAF	Cancer-associated fibroblasts
CCL	CC-chemokine ligand
CD	Cluster of differentiation
cDC	Conventional type dendritric cell
CDKN2A	Cyclin dependent kinase inhibitor 2A
cDNA	Copy desoxyribonucleic acid
CFSE	5-(6-)-Carboxyfluorescein diacetate succinimidyl ester
CM	Conditioned medium
CMP	Common myeloid progenitor
CRISPR	Clustered Regularly Interspaced Short Palindromic Repeats
CTLA4	Cytotoxic T-lymphocyte-associated protein 4
Cy7	Cyanine 7
CXCL	CXC-chemokine ligand
DC	Dendritic cell
DMSO	Dimethylsulfoxid
DNA	Desoxyribonucleic acid
ECM	Extracellular matrix
EDTA	Ethylendiamintetraacetic acid
ELISA	Enzyme-linked immunosorbent assay
FACS	Fluorescence-activated cell sorting
FAK1	Focal adhesion kinase 1
FBS	Fetal bovine serum
FDA	Food and Drug Administration
FITC	Fluorescein isothiocyanate

GM-CSF	Granulocyte-macrophage colony-stimulating factor
GMP	Granulocyte macrophage progenitor
G-CSF	Granulocyte colony-stimulating factor
G-MDSC	Granulocytic MDSC
HA	Hyaluronic acid
HNF1A	Hepatocyte nuclear factor 1A
HSC	Hematopoetic stem cell
IDO1	Indoleamine 2,3-dioxygenase 1
IFN	Interferon
IFNAR	Interferon-alpha receptor
Ig	Immunglobulin
IL	Interleukin
iNOS	Inducible nitric oxide synthases
IRF	IFN regulatory factor
ISRE	IFN-stimulated response elements
JMJD3	Jumonji domain containing protein D3
KPC model	Genetically engineered mouse model of pancreatic cancer with $kras^{G12D}$ mutation and p53 inactivation
KRAS	Rat sarcoma (proto-oncogene)
KRT81	Keratin 81
LOX1	Lectin-type oxidized LDL receptor-1
Ly6C	Lymphocyte antigen 6 complex, locus C
Ly6G	Lymphocyte antigen 6 complex, locus G
MACS	Magnetic-activated cell sorting
MAVS	Mitochondrial antiviral-signaling protein
M-MDSC	Monocytic myeloid-derived suppressor cells
MDA5	Melanoma differentiation-associated antigen 5
MDSC	Myeloid-derived suppressor cells
MFI	Mean fluorescence intensity
MHC	Major histocompatibility complex
Min	Minute(s)
moDC	Monocyte-derived DC
mRNA	Messenger RNA
MSI	Microsatellite instability
Myd88	Myeloid differentiation primary response 88
NK cell	Natural killer cell

NLR	Neutrophil-to-lymphocyte ratio
NOS	Nitrogen species
NOX	Nicotinamide adenine dinucleotide phosphate oxidase
OVA	Ovalbumin
PBS	Phosphate-buffered saline
PD-1	Programmed cell death protein 1
PDAC	Pancreatic ductal adenocarcinoma
pDC	Plasmacytoid DC
PDCD1	Gene coding for PD-1
PD-L1	Programmed cell death 1 ligand 1
PE	Phycoerythrin
PerCP	Peridinin-chlorophyll-protein complex
Poly(I:C)	Polyinosinic:polycytidylic acid
PMN-MDSC	Polymorphonuclear MDSC
Prdm1	PR domain zinc finger protein 1
PRR	Pattern recognition receptor
RIG-I	Retinoic acid-inducible gene I
RLH	RIG-I-like helicases
RNA	Ribonucleic acid
RNA-Seq	RNA sequencing
RORγt	RAR-related orphan receptor
ROS	Reactive oxygen
RPMI	Roswell Park Memorial Institute
RT	Room temperature
SEM	Standard error of mean
SMAD4	MAD-Homolog 4
STAT3	Signal transducer and activator of transcription 3
T110299	KPC-derived PDAC cell line
TAM	Tumor-associated macrophages
TCR	T cell receptor
TGF	Transforming growth factor
Th cell	T helper cell
TLR	Toll-like receptor
TNF	Tumor necrosis factor
TP53	Gene coding for protein 53 (tumor suppressor)
Treg	Regulatory T cell

7.3 List of figures

7.4 List of tables

7.5 Publications

The results of this study have been presented on the following conferences:

1. P. Metzger, S.V. Kirchleitner, I. Ritter, S. Endres, P. Duewell and M. Schnurr.
   Surface staining of PD-1 discriminates viable cell populations
   Cancer Immunotherapy conference (CIMT) 2016, Mainz, Germany

2. P. Metzger, S.V. Kirchleitner, I. Ritter, S. Endres, P. Duewell and M. Schnurr.
   Anti-PD-1 monoclonal antibodies stain unrecognized marker on myeloid and tumor cells
   Myeloid Suppressors Conference 2016, Philadelphia, USA

3. P. Metzger, S.V. Kirchleitner, P. Duewell and M. Schnurr.
   Melanoma differentiation-associated protein 5 (MDA5)-mediated reprograming of myeloid-derived suppressor cells (MDSC) as novel therapeutic strategy for pancreatic cancer
   1st i-Target Kubus Conference 2016, München, Germany

4. P. Metzger, S.V. Kirchleitner, M Zukowska, D Saur, S. Endres, P. Duewell and M. Schnurr.
   Pancreatic tumor cell line-derived factors inhibit dendritic cell differentiation and induce a T cell suppressive program in myeloid cells
   Cancer Immunotherapy Conference (CIMT), 2018, Mainz, Germany

5. P. Metzger, S.V. Kirchleitner, C. Hörth, S. Endres, L. König, M. Schnurr and P. Duewell
   Activation of RIG-I-like helicases improves anti-tumor therapy and reduces suppressive capacity of myeloid-derived suppressor cells
   3rd Immunoradiation Conference (Immunorad), 2018, Paris, France

6. P. Metzger, S.V. Kirchleitner, C. Hörth, L. König, S. Endres, P. Duewell and M. Schnurr
   Irf4-deficiency expands myeloid cells and accelerates tumor growth in an orthotopic pancreatic cancer model
   1st European Symposium on Myeloid Regulatory Cells in Health and Disease, 2018, Essen, Germany

Some results of this study have been published in the following international peer-reviewed journal:

1. P. Metzger, S. V. Kirchleitner, L. M. Koenig, C. Hörth, S. Kobold, S. Endres, M. Schnurr & P. Duewell.
   Dying cells expose a nuclear antigen cross-reacting with anti-PD-1 monoclonal antibodies.
   Scientific Reports 2018; (8) 8810. doi: 10.1038/s41598-018-27125-6.

7.6. Curriculum Vitae

7.7 Acknowledgement

First of all, I thank my supervisors Prof. Max Schnurr and PD Peter Düwell for giving me the opportunity to work on this interesting and challenging project. I especially appreciate their valuable advice and support and that they always encouraged me to develop new ideas.

I would like to thank my colleagues in the Division of Clinical Pharmacology. Particularly, I express my thanks to Sabrina Kirchleitner for being a great colleague. I cannot thank Christine Hörth enough for her help with many experiments, for doing all the genotyping of the mice and creating a nice working atmosphere. I would like to thank Daniel Böhmer and Dr. Lars König for their help with the CRISPR/Cas9 method, critical advice and inspiring discussions.

I am grateful to Prof. Stefan Endres for creating an enjoyable and productive environment in the division and for being supportive throughout my PhD.

I would like to express my thanks to Michael Kluge and Prof. Caroline Friedel for performing the bioinformatic analysis. I would like to thank the staff from both animal facilities ZVH and THZ: Dr. Katharina Ebert, PD Maciej Lech, Jonas Standt, Bettina Spillmann, Ira Mordhorst, Marcel Grießhammer, Barbara Lukas and Christian Kollmer. I appreciate their support with the mouse breeding and their valuable advice.

I thank the members of my thesis advisory committee Prof. Marion Subklewe and PD Maciej Lech for giving me useful advice and guiding me through the PhD.

I would like to express my gratitude to the elite network Bavaria for funding the PhD program i-Target and giving me the possibility to participate in national and international conferences as well as workshops. I thank the coordinators of the program Dr. Anne Averdam, Dr. Inga Gerlach and Dr. Katharina Dennemarck for their support and Prof. Wolfgang Zimmermann for mentoring and critical proof-reading of my PhD thesis.

Last but not least, I would like to thank my parents, Angelika Eisele and my siblings for supporting me throughout my diploma studies in Freiburg and my PhD studies. They were very understanding in difficult parts of my thesis. In particular, I would like to thank Angelika Eisele for her patience in listening to all the lab stories, giving valuable advice and for proof-reading my PhD thesis.

7.8 Erklärung zu Daten in zwei Dissertationen

Die Daten in folgendem Teil der vorliegenden Dissertation wurden in Kooperation mit Sabrina V. Kirchleitner generiert und werden auch in ihrer Dissertation veröffentlicht werden:

- Kapitel 3.1.2 KPC-derived PDAC induce suppressive capacity in MDSC
- Kapitel 3.4 Therapeutic reprograming of MDSC via MDA5-based immunotherapy
- Kapitel 7.1 Supplementary figures

Folgende Abbildungen wurden initial von Sabrina V. Kirchleitner erstellt und von Philipp Metzger adaptiert:

- Figure 5: Working model
- Figure 7C-D: KPC-derived PDAC induce T cell suppressive function in MDSC
- Figure 10A: MDA5-targeted immunotherapy induces immune cell activation and tumor regression in PDAC-bearing mice
- Figure 11: MDA5-targeted therapy reduces suppressive capacity of MDSC
- Figure 13K-L: Treatment efficacy and immune activation of MDA5-targeted immunotherapy is mediated by type I IFN signaling
- Figure 14D-F: MDSC in mice with PDAC do not cross-present antigen to CD8 T cells
- Figure S3: Quality controls of RNA sequencing samples

Es ist geplant die Daten im Rahmen einer gemeinsamen Veröffentlichung mit geteilter Erstautorenschaft zu publizieren.

Hiermit wird bestätigt, dass die obenstehenden Daten in Zusammenarbeit entstanden sind:

Sabrina V. Kirchleitner

Philipp Metzger

7.9 Affidavit

Philipp Metzger

I hereby declare, that the submitted thesis entitled

“Myeloid-derived suppressor cells (MDSC) in murine pancreatic cancer: Role of IRF4 in development and function of MDSC in RIG-I-like helicase-based immunotherapy”

is my own work. I have only used the sources indicated and have not made unauthorised use of services of a third party. Where the work of others has been quoted or reproduced, the source is always given.

I further declare that the submitted thesis or parts thereof have not been presented as part of an examination degree to any other university.

Munich, 17.07.2019

Philipp Metzger

7.10 Declaration of conformity of bound and electronic versions

Philipp Metzger

I hereby declare, that the electronic version of the submitted thesis, entitled

**“Myeloid-derived suppressor cells (MDSC) in murine pancreatic cancer:
Role of IRF4 in development and
function of MDSC in RIG-I-like helicase-based immunotherapy”**

is congruent with the printed version both in content and format.

Munich, 17.07.2019

Philipp Metzger